

Spring 5-6-2022

Development and Testing of a 1:70 Scale Model Wind Turbine of the IEA Reference 15 MW Floating Offshore System

Amber Parker
University of Maine, amber.delaney@maine.edu

Follow this and additional works at: <https://digitalcommons.library.umaine.edu/etd>

 Part of the [Aerodynamics and Fluid Mechanics Commons](#), [Energy Systems Commons](#), [Manufacturing Commons](#), and the [Ocean Engineering Commons](#)

Recommended Citation

Parker, Amber, "Development and Testing of a 1:70 Scale Model Wind Turbine of the IEA Reference 15 MW Floating Offshore System" (2022). *Electronic Theses and Dissertations*. 3548.
<https://digitalcommons.library.umaine.edu/etd/3548>

This Open-Access Thesis is brought to you for free and open access by DigitalCommons@UMaine. It has been accepted for inclusion in Electronic Theses and Dissertations by an authorized administrator of DigitalCommons@UMaine. For more information, please contact um.library.technical.services@maine.edu.

**DEVELOPMENT AND TESTING OF A 1:70 SCALE MODEL WIND TURBINE OF THE IEA
REFERENCE 15 MW FLOATING OFFSHORE SYSTEM**

By

Amber Frances Delaney Parker

B.S. University of Maine, 2020

A THESIS

Submitted in Partial Fulfillment of the

Requirements for the Degree of

Master of Science

(in Mechanical Engineering)

The Graduate School

The University of Maine

May 2022

Advisory Committee:

Richard Kimball, Presidential Professor in Ocean Engineering and Energy, Advisor

Andrew Goupee, Associate Professor of Mechanical Engineering

Lauren Ross, Assistant Professor of Civil and Environmental Engineering

© 2022 Amber Parker

All Rights Reserved

**DEVELOPMENT AND TESTING OF A 1:70 SCALE MODEL WIND TURBINE OF THE IEA
REFERENCE 15 MW FLOATING OFFSHORE SYSTEM**

By Amber Frances Delaney Parker

Thesis Advisor: Dr. Richard Kimball

An Abstract of the Thesis Presented
in Partial Fulfillment of the Requirements for the
Degree of Master of Science
(in Mechanical Engineering)
May 2022

This thesis presents the development of a 1/70th scale performance-matched wind turbine intended for wind and wave basin model testing of commercially viable floating wind turbine structures based off of the International Energy Agency (IEA) Wind 15 MW design. The focus of this demonstration is to test active blade pitch response controls and to provide an experimental dataset for use by modelers and industry for future turbine improvements. Future research is planned to test the turbine in conjunction with an actively damping hull to test the interactions between the two control systems.

Outlined in this thesis are the methods of scaling, designing, manufacturing, and testing the scale model. A discussion of the scaling methodology for aerodynamic properties of the blade at model scale Reynolds number is included, as is the Froude scaling methodology used for most other turbine properties. The performance-match target properties are met by scaling the turbine rotational speed following the Froude scaled method, and increasing the test wind speed by approximately 20%, resulting in a mismatch of the tip speed ratio (TSR) between full and model scale in order to preserve the rotor rotation speed Froude scaling, ensuring proper frequency of the turbine forces felt by the hull in comparison to the waves. Scaled mass targets for the nacelle and blades necessitated the incorporation of alternative materials such as carbon fiber and foam into the component designs to lower the weight of the system.

Design of turbine components focused on the integration of all needed sensing equipment into the tower top nacelle as well as designing mechanisms to allow for individual active blade control, entirely housed in the hub. High-density foam molds were manufactured for the production of carbon fiber blades through a vacuum infusion process using a modified butterfly blade construction method designed to accommodate the size and complexity of the geometry. A process was created to align and assemble the blade flanges, foam spars, and the two-part carbon fiber skins. Additional manufacturing was done to produce and assemble parts for the nacelle and hub.

Testing of the scale model turbine structural properties included blade deflection testing, dynamic inertia testing of blades, and free-decay testing of the tower's natural frequency. Testing of the turbine performance was conducted in a uniform wind environment over a range of rotor speeds and blade pitches to measure the thrust and torque reactions in each case. This information was used to produce coefficient of power and coefficient of thrust curves versus the rotor tip speed ratio. Additional controller tests were performed to validate the rotor controller's response to torque feedback in order to optimize the rotor performance in dynamic-wind environments.

ACKNOWLEDGEMENTS

I would like to express my sincere gratitude to the US Department of Energy (DOE), Advanced Research Program Agency - Energy (ARPA-e) for recognizing the importance of this continuing research and their funding of the ATLANTIS Floating Offshore-wind and Controls Advanced Laboratory (FOCAL) Experimental Program, Contract No. DE-AC36-08GO28308. I would also like to recognize the guidance of the National Renewable Energy Laboratory (NREL) and those that worked closely with the team to organize the data for use by modelers to further develop this field of research.

I would like to recognize the guidance of the offshore energy team at the University of Maine Advanced Structures and Composites Center (ASCC), as well as Dr. Habib Dagher for his continued enthusiasm and advocacy for the continuation of offshore wind research and development. Special thanks to Dr. Richard Kimball, my graduate thesis advisor and graduate committee chair for his advice and support throughout my research. I am very grateful for the mentorship of my ASCC supervisor, Matt Fowler, and all of the practical knowledge I have gained from him while working on this program. Thank you to Dr. Anthony Viselli for your insights and advice on the especially challenging aspects of the research, and to Dr. Andrew Goupee for his detailed engineering advice and expertise. To Peter Jalbert, Chris Urquart, Walter Morris, and Quest Teichman for their technical and composites expertise. To Sam Heathcote, Curtis Libby, and Kelsey Kunich for their instrumentation expertise. And to Lauren Dickson, Casey Borque, Lora Lindyburg, Alyssa McGlynn, and Summer Camire for their blade fabrication and characterization efforts.

In regards to those that have assisted outside of academia, I would like to thank those from the University of Maine Advanced Manufacturing Center (AMC) and Lyman-Morse Boatbuilding Inc. From the AMC, I am very grateful for the help of Kyle Forsythe with machining and 3D scanning. I would like to thank those at Lyman-Morse who assisted in the machining of blade molds when we were in a pinch.

I also would be remiss if I did not include a heartfelt thank you to my husband, Michael Beau Parker, and my family for their support throughout my academic career. As well as my high school robotics team advisors, Robert Taylor and Dan Lemieux for introducing me to the fields of offshore energy and mechanical engineering.

TABLE OF CONTENTS

ACKNOWLEDGEMENTS	iii
LIST OF TABLES	vii
LIST OF FIGURES	viii
LIST OF ABREVIATIONS	xi
LIST OF DEFINITIONS	xii
CHAPTER 1: INTRODUCTION	1
1.1. Motivation.....	1
1.2. Background.....	2
1.3. Objectives	4
CHAPTER 2: SCALING METHODOLOGY AND APPLICATION	6
2.1. Methodology	6
2.1.1. Froude Scaling Relationships and Parameters	6
2.1.3. Performance Match Scaling	8
2.2. Scale Model Parameters.....	10
CHAPTER 3: MODEL SCALE WIND TURBINE DESIGN AND FABRICATION	11
3.1. Nacelle and Hub.....	11
3.1.1. Instrumentation	12
3.1.2. Pitch Control	14
3.2. Blade Design.....	15
3.2.1. Geometry.....	16
3.2.2. Blade Mold Design	23
3.2.3. Blade Manufacturing Process	27
3.3. Tower Design.....	30
3.4. Full Assembly	31
CHAPTER 4: MODEL CHARACTERIZATION AND PERFORMANCE RESULTS	32
4.1. Physical Characterization.....	32
4.2. Blade Characterization.....	32
4.2.1. Blade Dynamic Testing.....	32
4.2.2. Blade Structural Testing.....	35
4.2.3. Blade Surface Scanning	38

4.3. Data Acquisition and Controls	39
4.4. Wind Turbine Performance.....	40
4.4.1. Uniform Wind Environment Testing	40
4.4.2. Turbine Response Validation.....	47
CHAPTER 5: CONCLUSIONS	53
5.1. Overview of Design and Results.....	53
5.2. Future Work.....	54
5.3. Contributions.....	56
BIBLIOGRAPHY	57
APPENDIX A: SHOP DRAWINGS OF THE FOCAL TURBINE ASSEMBLY	59
APPENDIX B: AIRFOIL GEOMETRY DATASETS.....	100
APPENDIX C: VACUUM INFUSION OF CARBON-FIBER REINFORCED THERMOSET LAMINA	108
APPENDIX D: TENSILE TESTING OF CARBON-FIBER REINFORCED THERMOSET LAMINA	110
APPENDIX E: BLADE INERTIAL CALCULATIONS	119
APPENDIX F: BLADE SCAN PROCEDURE.....	124
APPENDIX G: FIGURE REPUBLICATION PERMISSIONS	127
BIOGRAPHY OF THE AUTHOR	128

LIST OF TABLES

Table 2.1	Table of Froude scaling values	8
Table 2.2	Important turbine properties table.....	10
Table 3.1	Blade geometric properties table.....	22
Table 4.1	Individual blade properties.....	35
Table D.1	3K Plain Weave Carbon Fiber Fabric Properties	110
Table D.2	Derakane 8084 Epoxy Vinyl Ester Resin Properties	111
Table D.3	Measured tension specimen properties	113
Table D.4	Calculate predicted lamina properties	113
Table D.5	Actual strain values used for calculations	117
Table D.6	Tensile Modulus, Tensile Strength and Poisson's Ratio for all specimens.....	117
Table D.7	Failure modes of each test specimen.....	118

LIST OF FIGURES

Figure 1.1	Rendering of IEA 15MW.....	1
Figure 1.2	Geo-sim (a) and Performance-Match (b) Turbine Model	4
Figure 2.1	W2 basin and wind machine	7
Figure 3.1	As-build turbine side-view	11
Figure 3.2	RNA Instrumentation	13
Figure 3.3	Front view of hub instrumentation.....	14
Figure 3.4	Cross-sectional view of pitch assembly	15
Figure 3.5	Full scale (IEA15MW) vs. Model scale (FOCAL) airfoil cross-section	16
Figure 3.6	Cl (a) and Cd (b) Xfoil plot comparisons of airfoils at full scale and model scale operating conditions	18
Figure 3.7	Thickened and unmodified SD7032 airfoil geometry	19
Figure 3.8	Cl (a) and Cd (b) Xfoil plot comparisons of standard and thickened SD7032 airfoils at scale operating conditions.....	20
Figure 3.9	Matlab generated blade section distribution.....	21
Figure 3.10	SolidWorks blade model after geometry modifications.....	21
Figure 3.11	Blade Flange	23
Figure 3.12	Cross-sectional view of blade molds.....	24
Figure 3.13	Blade flange assembly jig	25
Figure 3.14	Mold Machining at Lyman-Morse Boatbuilding Inc.	26
Figure 3.15	Full set of Blade Molds	26
Figure 3.16	Blade Infusion Set-up.....	27
Figure 3.17	Blade Assembly (a) Adhesion of spars (b) Adhesion of skin (c) Adhesion of flange	29
Figure 3.18	Finished Blade.....	29

Figure 3.19	Tower Hammer Test Free Decay Graph	30
Figure 3.20	Fully assembled turbine	31
Figure 4.1	Blade Inertia Testing Setup.....	33
Figure 4.2	Blade Inertia Testing Encoder Voltage vs. Time test plot	35
Figure 4.3	Blade deflection testing (edgewise configuration shown)	36
Figure 4.4	Blade Deflection chart for Flap wise (a) and Edge wise (b) tests	37
Figure 4.5	Scan and SolidWorks data for the 70% span station with estimated mid-lines	38
Figure 4.6	Turbine configuration during basin testing	39
Figure 4.7	Labview dashboard for basin testing.....	40
Figure 4.8	Rotor Speed Step File at 0 degree AOA and Uniform Wind Environment	41
Figure 4.9	Response to rotor speed step file at 0 degree AOA.....	41
Figure 4.10	Torque (a) and Thrust (b) response to rotor speed step file at 0 degree AOA	43
Figure 4.11	C_p (a) and C_t (b) curves at 0 degree AOA.....	45
Figure 4.12	C_p (a) and C_t (b) surface plots over range of TSR and Blade Pitch	46
Figure 4.13	Full-scale experimental and theoretical Torque (a) and Thrust (b) performance curves of as-built scale model compared to IEA 15 MW performance	48
Figure 4.14	Full-scale experimental and theoretical Blade Pitch (a) and RPM (b) response curves of as-built scale model compared to IEA 15 MW response	49
Figure 4.15	Turbine response to sustained gust	51
Figure 5.1	Turbine/Hull assembly for combination wind and wave testing.....	55
Figure D.1	Partial Blade Infusion.....	111
Figure D.2	Portions of part cut on waterjet for eight specimens	112
Figure D.3	Tension test setup on the MTS test frame with DIC	114
Figure D.4	ARAMIS data processing for longitudinal and lateral strain	115

Figure D.5	Force applied to specimen vs. load-head deflection for both tension specimens	115
Figure D.6	Stress vs. strain in the longitudinal direction over range of data collection.....	116
Figure D.7	Stress vs. strain in the longitudinal direction over range of data collection.....	116
Figure D.8	Tension specimen failure modes	118
Figure F.1	Blade Alignment	124
Figure F.2	Blade Mounting.....	124
Figure F.3	Scanning of Blade	125

LIST OF ABBREVIATIONS

AOA = angle of attack	u = inflow fluid velocity
A = area	U = wind speed
C = chord length	V = volt
Cd = drag coefficient	v = kinematic viscosity of fluid
C _l = lift coefficient	α = angle of attack
C _p = power coefficient	λ = scale factor
C _t = thrust coefficient	ϕ = salt to fresh water factor
D = diameter	ω = angular velocity of rotor
Fr = Froude number	ρ = density
g = acceleration due to gravity	σ = stress
Hz = hertz	
kg = kilograms	Subscripts
L = length	m = denotes scale model
m = meter	p = denotes full-scale prototype
M = mass	Unit Prefixes
N = Newton	μ = micro ($\times 10^{-6}$)
P = Power	m = milli ($\times 10^{-3}$)
Pa = Pascal	c = centi ($\times 10^{-1}$)
R = radius	k = kilo ($\times 10^3$)
Re = Reynolds number	M = mega ($\times 10^6$)
T = Thrust	G = giga ($\times 10^9$)
t = time unit	

LIST OF DEFINITIONS

3D:	Three Dimensional
AMC:	University of Maine Advanced Manufacturing Center
ARPA-e:	Advanced Research Program Agency - Energy
ASCC:	University of Maine Advanced Structures and Composites Center
CG:	Center of gravity
CML:	ASCC Composites Manufacturing Laboratory
DAQ:	Data Acquisition System
DNV-GL:	Det Norske Veritas (Norway) and Germanischer Lloyd (Germany)
DOE:	Department of Energy
DOF:	Degree of Freedom
FARO:	Frasier and Raab Orthopedics
FOCAL:	Floating Offshore-wind and Controls Advanced Laboratory Research Program
FOWT:	Floating offshore wind turbine
HDPE:	High-density polyethylene
IEA:	International Energy Agency
LHEEA:	Ecole Centrale de Nantes/France
MARIN:	Maritime Research Institute Netherlands
NREL:	National Renewable Energy Lab
OpenFAST:	An aeroelastic design code for horizontal axis wind turbines
POLIMI:	Politecnico di Milano
RMP:	Rotations per minute
RNA:	Rotor Nacelle Assembly
ROSCO:	Reference OpenSource Controller
SD7032:	Selig/Donovan 7032 airfoil
TMD:	Tuned mass damper
TSR:	Tip speed ratio
TTE:	Thickened trailing edge
UMaine:	University of Maine
VIP:	Vacuum infusion process
W2:	University of Maine's Alfond Wind/Wave Ocean Laboratory

CHAPTER 1: INTRODUCTION

1.1. Motivation

Offshore floating wind is an industry developing to meet the need for large clean energy generation facilities harnessing readily available natural resources. The wind is a solar-driven natural process that has historically been harnessed for mechanical and electrical power generation mainly on land. Locations best suited for harnessing wind energy are largely determined by natural patterns of wind intensity, elevation, and the topography of a location. Offshore wind power places turbines on foundations and floating platforms in the ocean. Placing turbines in the ocean greatly increases the area the wind resource can be extracted from. A depiction of a floating offshore wind platform is shown in Figure 1.1, and is the focus of this project.



Figure 1.1: Rendering of IEA 15 MW [2] *Reprinted with Permission*

The quality of offshore wind resources in the United States is well suited for the production of offshore wind energy production, this is true particularly off of the Northeast coast and around coastal northern California, where the average measured wind speed at 90 meters is in the 9.5-10 m/s range, close to rated conditions of modern wind turbines. [1] The floating offshore wind industry is still currently in the early stages of development and testing of full-scale models with continuous research and development being conducted in the validation of new larger designs. The FOCAL campaign focuses on the testing of technology to be deployed on full-scale models in a controlled lab environment applied to small-scale test systems. The purpose of this research was to develop a 1:70 scale model of the IEA 15 MW reference wind turbine [2, 3] shown in Figure 1.1. This scale model was then tested at the University of Maine's Alfond Wind/Wave Ocean Laboratory (W2) basin at the ASCC to test the entire Floating Offshore Wind Turbine (FOWT) system in the scaled wind and wave environments to measure model performance and to estimate full-scale performance.

1.2. Background

FOWT scale model testing is an active field of research aimed at supporting the development of a sustainable industry of power generation from wind at deep water offshore locations. The idea for the generation of wind power from turbines mounted on floating platforms was first envisioned by Professor William E. Heronemus of the University of Massachusetts in the year of 1972 [4]. Model-scale research into floating offshore wind turbines was not done until the mid-1990, after commercial fixed-based offshore wind turbines had been established [5]. Early research focused on the development of basic floating turbine platforms without sophisticated turbines, tested in wave basins such as the Maritime Research Institute Netherlands (MARIN) in Trondheim, Norway. As the hull technology began to develop, more work was done to create accurate turbine models that could provide thrust forces to the floating system.

One of the first publicly available campaigns that attempted to test the response of a fully coupled floating wind turbine system at proper scaling was conducted at the University of Maine (UMaine) in 2011. [6,7] This turbine was a 1/50th geo-sim scale model of an NREL 5 MW turbine which utilized fully

Froude scaled geometric properties and wind conditions. The data from this test was used to further develop simulation modeling tools to estimate turbine performances. In 2013, Politecnico di Milano (POLIMI) in Italy built a 1/45th scale model of a 3 MW turbine which underwent wind tunnel testing at their facility. [8] Their design preserved the TSR from full scale resulting in a Froude and Reynolds mismatch which was slightly compensated for by using a low-Reynolds number airfoil. This turbine was capable of active blade pitch and torque controls with a range of controllers used. In the following years a 1/60th scale model of the 10 MW INNWIND.EU turbine design was built by POLIMI and tested along with a semi-submersible platform at Ecole Centrale de Nantes/France (LHEEA). [9] This test utilized a similar turbine design and controls as the 2013 testing but used a Froude-scaled rotor with a RG-14 airfoil which was rated for good low-Reynolds number performance. The next campaign launched by Politecnico di Milano was the LIFES50+ tests in 2016 which fully documented the design and testing of a 1/75th scale model of a 10MW turbine. [10,11,12,13] This test included detailed airfoil characterization of the low-Reynolds number airfoil, Selig/Donovan 7032 airfoil (SD7032) and included an iterative blade design to match the thrust and torque while preserving the TSR range from full scale by increasing the rotor rotational speed and wind speed from the Froude scaled values. This turbine had active pitch control capabilities and was controlled by a torque feedback control. This test was used as a launching point for the FOCAL research by using the same airfoil, but implementing a different performance-matching scaling method, resulting in the 1:70 scale model of the IEA 15 MW turbine as pictured in Figure 1.2. This test also begins a next chapter in FOWT research of turbines with power ratings about 10 MW, introducing another suite of scaling challenges.



Figure 1.2: Performance-Match FOCAL Turbine Model

1.3. Objectives

The objective of this thesis research is to support continued research in the field of FOWT hull development by designing an accurately scaled 1:70 model of a 15 MW turbine. The turbine is based on the IEA 15 MW reference turbine and is capable of active pitch controls in response to torque feedback using a reference open-source controller (ROSCO) [14,15].

Parameters first had to be properly scaled down from the full-scale design, using Froude scaling and performance match adjustments. The parameters were then used as target values for the as-built turbine. The turbine was constructed using lightweight materials and incorporated all needed sensing equipment for the data collection into the rotor nacelle assembly (RNA) and tower. Once all components

of the turbine were constructed, they were assembled then weighed and measured to obtain proper final as-built properties. The turbine blades were weighed, the center of gravity (CG) was found, as well as the moment of inertia (I) and the blade deflection performance.

After final assembly and system checks, the turbine was mounted in the ASCC W2, attached to rigid supports above the basin with the tower braced. The turbine performance was measured over a range of rotational speeds and blade pitches in a uniform wind environment, and the resulting torque and thrust were collected. The data was used to calculate the power coefficient (C_p) and thrust coefficient (C_t) surface plots which were used as inputs for ROSCO. The rotor performance in a dynamic wind environment was tested under the control of ROSCO to measure how well the response followed the target control values. This was done to validate the rotor performance accomplished the goal of being a performance-matched scale model of a full-scale system that is capable of being controlled by a full-scale controller.

CHAPTER 2: SCALING METHODOLOGY AND APPLICATION

2.1. Methodology

The IEA 15 MW reference wind turbine design, outlined in its definition document [3] was used as the model turbine for this research. The reference turbine was originally designed for saltwater applications, therefore changes need to be made to all parameters involving mass or force to allow the floating system to perform correctly in a freshwater environment. The density of saltwater is approximately 2.5% higher than freshwater, meaning there needed to be a 2.5% reduction in properties that impacted draft and hull movement, which are mass, moments of inertia, rotor thrust, and moments. This change is represented in the scaling methodology below as the Salt to Fresh Water Factor, ϕ which equals 1.0256.

2.1.1. Froude Scaling Relationships and Parameters

To keep the relationship between inertia and gravitational forces constant between the full and model scale turbines, the Froude number was used.

$$Fr = \frac{u}{\sqrt{gD}} \quad (2.1)$$

Where u is the inflow fluid velocity, D is the characteristic length (in this case, turbine diameter), and g is the gravitational acceleration constant. In this relationship, length is scaled linearly. Therefore, in order to determine the proper target scaling value of the system, the limiting dimension needed to be identified.

This was found to be the height of the wind field available in the W2 basin, as shown in Figure 2.1 below. The full-scale rotor diameter is 240 meters, therefore a scaling factor of 70 was chosen to keep the rotor diameter smaller than the 3.5 meters of the wind machine height, resulting in a scaled rotor diameter target of 3.43 meters.

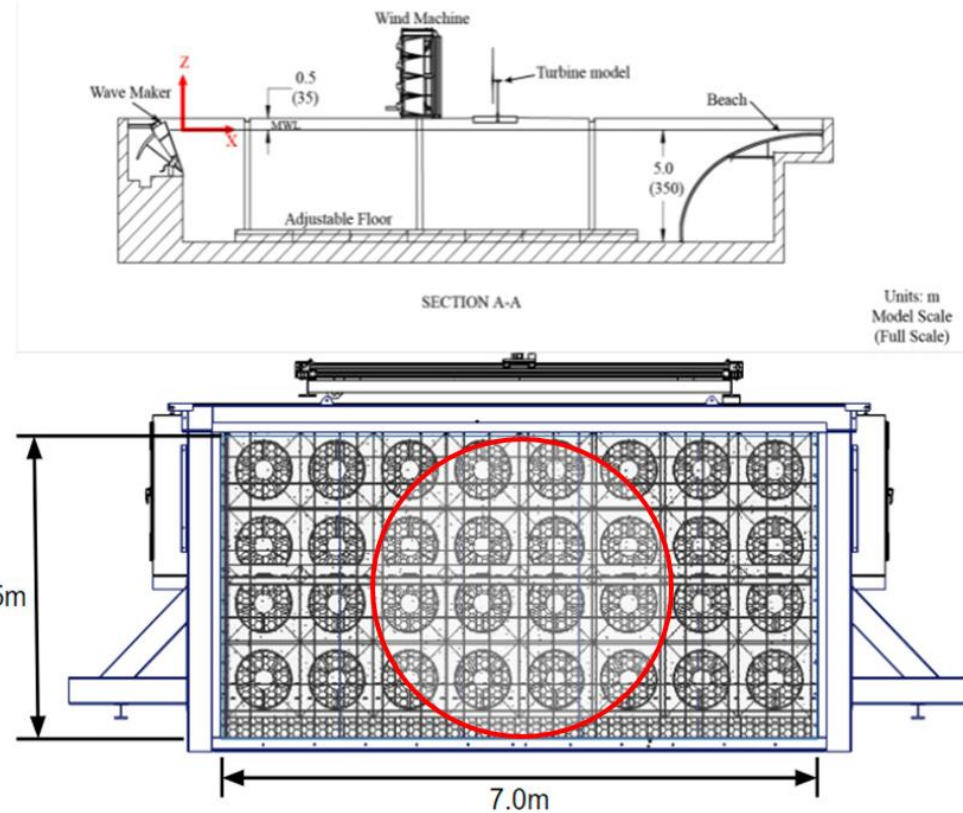


Figure 2.1: W2 basin and wind machine

Historically, scale turbines built for basin tests have been geo-sims that adhere to Froude scaling for all parameters as shown in Table 2.1 to ensure that all rotor forcing frequencies are properly scaled. This is important when testing on a floating hull structure due to the presence of waves, and the need to properly capture the stability response of the hull and turbine as a system.

Table 2.1: Table of Froude scaling values

Quantity	Analytic Scale Factor
<i>Scale Factor</i>	λ
<i>Salt to Fresh Water Factor</i>	ϕ
<i>Length/Position</i>	λ
<i>Velocity</i>	$\lambda^{0.5}$
<i>Acceleration</i>	1
<i>Angle</i>	1
<i>Angular Velocity</i>	$\lambda^{-0.5}$
<i>Angular Acceleration</i>	λ^{-1}
<i>Time</i>	$\lambda^{0.5}$
<i>Frequency</i>	$\lambda^{-0.5}$
<i>Mass</i>	$\lambda^3 \phi$
<i>Mass Moment of Inertia</i>	$\lambda^5 \phi$
<i>Force</i>	$\lambda^3 \phi$
<i>Moment/Torque</i>	$\lambda^4 \phi$

2.1.3. Performance Match Scaling

The problem with this approach is in order to keep all rotor dimensional parameters consistently Froude scaled, the resulting thrust and torque response would not be as scaled from the reference turbine. This is due to the difference in the performance of the same airfoil at different Reynolds numbers. Reynolds numbers represent the relationship between inertial and viscous forces and is characterized by the equation below.

$$Re = \frac{uC}{\nu} \quad (2.2)$$

Where u is the inflow fluid velocity, C is the characteristic length (in this case, chord length), and ν is the kinematic viscosity of the air. The same airfoil in a lower Reynolds number environment will produce less lift and will have more drag acting on it. In order to resolve this mismatch, a different type of turbine

has been proposed by (Kimball et. al) [16], which does not adhere to all dimensional Froude scaled parameters in the rotor, but instead finds a blade design with a chord and twist distribution using a low Reynolds number airfoil with an additional boost in wind speed to match the Froude scaled performance targets while preserving the scaled forcing frequencies. This specialized turbine design has been termed a performance-matched turbine.

In the case of this turbine, in order to meet the performance match requirements, the low Reynolds number airfoil that was selected was the Segil-Donovan 7032 (SD7032) airfoil. This foil was shown in wind tunnel studies conducted by POLIMI to have a good lift vs. drag response at low Reynolds numbers which correspond to the rated operating range of the turbine for most of the blade. [13] In addition to this change, a Blade Element Momentum (BEM) design method was used to determine the optimal distribution of chord length and twist angle over the length of the blade [17]. Even with these changes, limitations were still met in obtaining the correct thrust outputs from the wind field at rated conditions. Therefore, the rated wind speed value was increased by ~20% to bring the theoretical rotor performance up the rest of the way to match the target values. One side effect of this change is that it induces a shift in the Tip Speed Ratio (TSR) from the full scale range. TSR is determined by the equation:

$$TSR = \frac{\omega R}{u} \quad (2.3)$$

Where ω is the rotor rotational speed, R is the radius of the rotor plane, and u is the inflow wind speed. Because it is important to preserve the scaled rotor rotational speed to ensure proper forcing frequencies, the result is an overall lower TSR than full scale. This was not too much of a concern regarding the control of the turbine because the goal was to characterize the as-built system and use those performance curves as input to the control as opposed to using the full scale performance at a specific TSR. Ultimately, these changes brought the rated conditions to a Froude scaled match with the full scale turbine.

2.2. Scale Model Parameters

The full scale turbine parameters for the IEA 15 MW turbine can be found in its definition document [3].

To account for the difference in density of salt water vs. fresh water, a set of target parameters had to be specified to reflect those compensations and are shown in the first column of Table 2.2. Following the Froude scaling relationships and performance- matching methods discussed in section 2.1.1, a set of target values were found, which were used as a guide when designing and building the turbine. As will be shown in the next sections, not all targets could be completely matched due to limitations in material or instrumentation characteristics. The as-built properties were measured using methods to be outlined in following sections, and are presented in column three of Table 2.2. To show the relationship between the target full scale values, and the scaled-up as-built values, the properties of the as-built model were scaled up using the Froude scaling relationships, and are presented in column 2 of Table 2.2. The full as-built properties of the FOCAL turbine are outlined in the FOCAL Campaign 1 Validation Definition Document. [18]

Table 2.2: Important turbine properties table

Properties	Full Scale IEA 15-MW Freshwater*	Full Scale of As-built	Model Scale As-built	Percent Difference (%)
<i>Hub Height (m)</i>	150	149.8	2.14	0.13
<i>Rotor Diameter (m)</i>	240	242.8	3.468	1.17
<i>Hub Overhang (m)</i>	11.35	10.86	0.155	4.32
<i>Shaft Tilt (deg)</i>	6	6	6	-
<i>Coning Angle (deg)</i>	4	0	0	-
<i>Wind Speeds (m/s)</i>	3-35	3.6-30	0.4-3.6	-
<i>Rated Rotor RPM (rmp)</i>	7.56	7.56	63	0.00
<i>Total RNA Mass (kg)</i>	9.91e+05	1.16e+06	3.396	17.1
<i>Rated Thrust (N)</i>	2.45e+06	2.42e+06	7.06	1.22
<i>Rated Torque (N-m)</i>	1.91e+07	1.93e+07	0.804	0.87
<i>Blade Length (m)</i>	117	115.9	1.655	0.94
<i>Blade Mass (kg)</i>	6.362e+04	8.081e+04	0.236	27.0
<i>Blade CG (w.r.t. Root) (m)</i>	26.89	37.73	0.539	40.3
<i>Blade 2nd Mass MOI (w.r.t. Root) (kg-m²)</i>	9.03e+07	1.95e+08	0.116	116

*2.5% reduction in properties specified in section 2.1. due to water density difference

CHAPTER 3: MODEL SCALE WIND TURBINE DESIGN AND FABRICATION

3.1. Nacelle and Hub

One of the areas where mass scaling caused the most constraints was in the nacelle and hub. Normal turbines have a nacelle to house the gearbox and generator, but for the model testing, the focus is on measuring the response of the rotor to the wind environment rather than generating electricity. Therefore, the purpose of the nacelle was to house instrumentation, the drive motor, and the driveshaft support bearings. The hub contained individual pitch control actuators as well as their control boards. To limit the amount of RNA mass from the frame, lightweight materials such as aluminum and carbon fiber were used for most of the structural components. For this test, in order to most accurately capture the performance of the rotor as scaled from the full-scale design, the six degree shaft tilt was preserved. This was accomplished by mounting the nacelle on two wedges with a six degree angle between their upper and lower surfaces. These wedges also assisted in stiffening the carbon fiber nacelle baseplate in addition to the threaded rod stiffeners used to connect the top of the vertical nacelle members. The final as-built assembly can be seen below in Figure 3.1 and a copy of the full FOCAL turbine drawing package can be found in Appendix A.

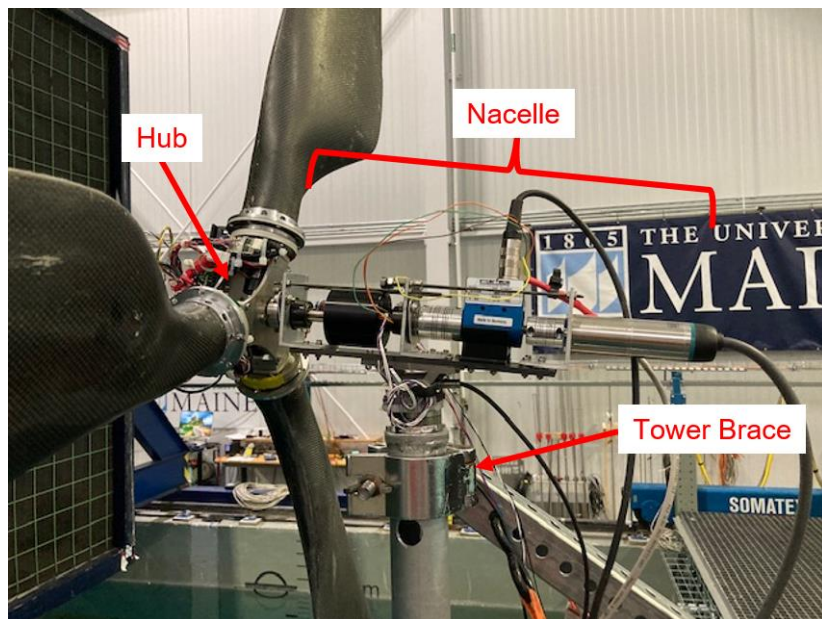


Figure 3.1: As-build turbine side-view

3.1.1. Instrumentation

Instrumentation was used to control the turbine and to collect data while the turbine was in operation. Considerations were made to choose models that were adequate for the operating range of the turbine, while being light enough to keep the RNA close to the mass targets. Figure 3.2 shows a side view of the RNA with each instrument labeled. The rotor motor was a Wittenstein ARSQ030B-020C-3V1BS-HI0GSN-FUN CyberDynamic servo motor with a 3 stage gearbox and was used to drive the rotation of the turbine during operation. The motor included an encoder and torque sensor that was used to measure the RPM and Torque during operation. The motor was also equipped with a brake to control the speed of the motor. The rotor motor was attached to the nacelle frame and was connected to the in-line torque sensor by a spring coupling. The torque sensor was an Interface T4-5-A3A rotary torque transducer and was used as the primary torque sensor in the torque-control mode of operation. The torque sensor was connected to the main driveshaft with a second spring coupling, and was restrained from rotating by a yoke which allowed for movement in all other degrees of freedom (DOF) to ensure accurate torque measurements. The main driveshaft was supported by two roller bearings mounted to the vertical frame of the nacelle. Additionally thrust bearings were used to prevent excess wear due to dynamic loading of the turbine. Between the bearing supports, a MOOG AC6438-12 slip ring was mounted to the shaft and was connected to the hub control wires which were fed through the drive shaft via a hole in front of the slip ring. This slip ring allowed for etherCAT signal and power to be passed from the stationary nacelle to the rotating hub to control the pitch actuation of each blade.

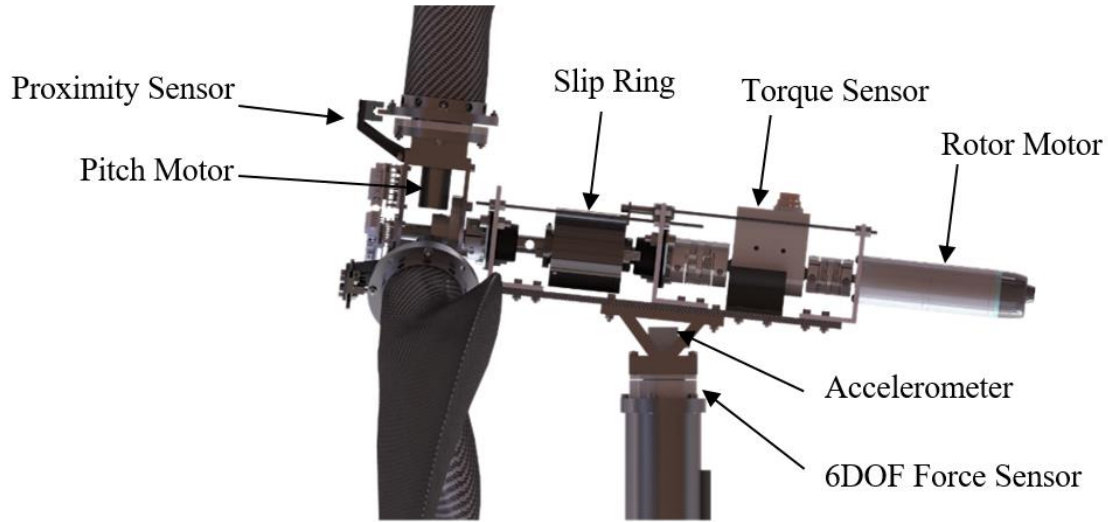


Figure 3.2: RNA Instrumentation

On the hub, which was clamped to the drive shaft, the power wires were fed to the power bus board, shown in Figure 3.3. Power was then distributed to the Pitch Motor Control Boards, which also received the etherCAT control wires, allowing for a two way communication of pitch information between the controller and the pitch assemblies. The RSF-5B-100-US050-BC pitch transducers were connected to the control boards, and were used in the active pitch of the blades during operation. Homing of the blades was assisted by Omron EE-SX951-W 1M proximity sensors which were mounted to the front of each pitch assembly, and were tripped by a tab attached to the mounting plate of the pitch assembly to indicate when the blades were at a zero degree pitch.

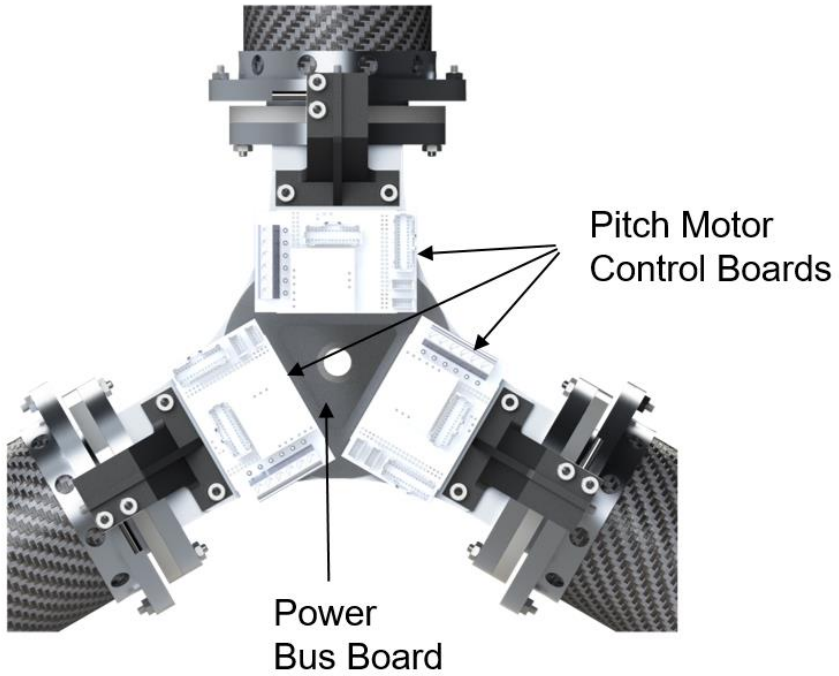


Figure 3.3: Front view of hub instrumentation

Within the six degree tilt connection between the nacelle and the tower, was a PCB 3713F112G accelerometer which measured the movement of the tower top during operation. This was used to measure the frequency of forcing and to monitor for any unwanted frequency interactions. The base plate of the six degree tilt connection was attached to the top of the ATI 9105-TW-MINI45TI-R-5 tower top 6 DOF load cell. This was the primary measure of the thrust force induced by the lift of the rotating rotor blades in a wind environment.

3.1.2. Pitch Control

The pitch control subassemblies are built around pitch actuators capable of very fine and repeatable rotation. A cross roller bearing is used to provide support for the blade and actuator to prevent binding when the blade is being rotated under load. The sub-assembly was designed to make use of the front and rear hub support plates used in a previous hub assembly, meaning that the supports of the pitch assembly made up the cross support frame of the hub. A cross-sectional view of the pitch assembly is shown in Figure 3.4. All of the plates in the subassembly were designed to be cut on the waterjet and are made out

of aluminum to decrease the weight. A flag was designed into the top plate of the pitch assembly to act as a homing indicator for the blade. This tab is located at 4 degrees from the 0-degree location of the blade, in order to allow for the homing sequence to take place even if the blade is close to 0 degrees at the initiation. This is detailed in the pitch assembly drawing on sheet 19 of Appendix A. Due to the length of the actuator and the use of the large support bearing, the stack-up of components required a larger hub diameter than scaled from the full scale, accounting for a slightly larger rotor diameter than the scaled target parameter.

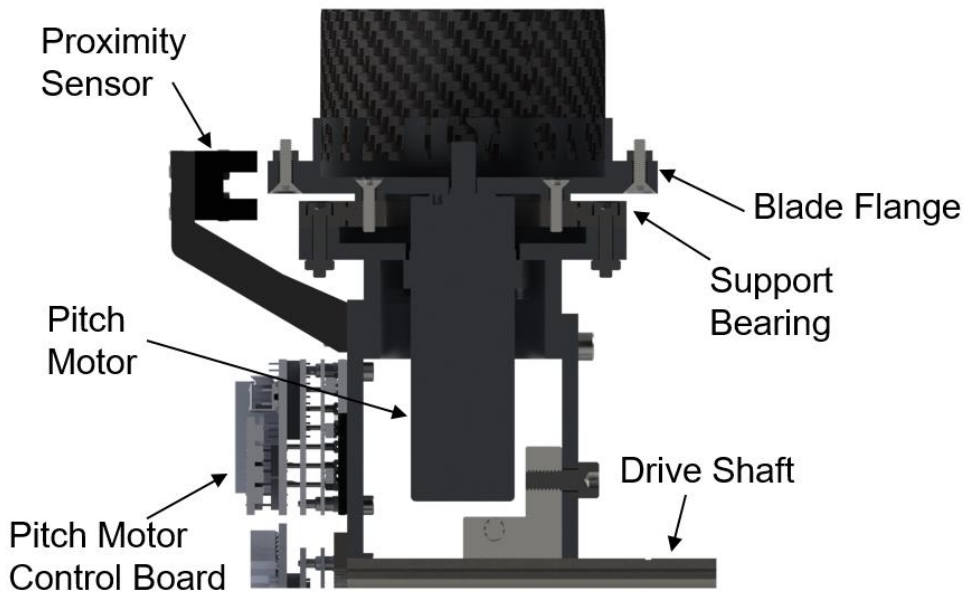


Figure 3.4: Cross-sectional view of pitch assembly

3.2. Blade Design

The target for the FOCAL blade design was to create a blade that provided a more characteristic thrust response at the rated wind conditions than a Froude scaled blade. The differences from a traditional Froude scaled turbine blade are, a different low Reynolds number airfoil, chord distribution, and twist. These allowed the blade to generate more lift at rated, resulting in a higher thrust force from the rotor. The blade distribution properties were found by following a process to determine the “Betz optimal rotor”. This method assumes no wake rotation, no drag, no tip loss, and a decrease in wind velocity

between the freestream and turbine rotor of 33%. This process is outlined in more detail in the TORQUE paper [19] as this process was performed by another member of the FOCAL team and will not be outlined in detail in this report. Airfoil sections were generated using a Matlab code, which handled the thickening of the trailing edge of the blade as well as basic fairing of the root and tip sections of the blade. Those blade sections were then imported into SolidWorks and a loft was created to generate a smooth blade skin. Additional adjustments were made to the root and tip sections to decrease drag and material of the blade. This surface file was used to design a three part blade mold which was machined out of high density foam board. These molds were used in a vacuum infusion process (VIP) to create stiff one-layer carbon fiber blade skins which were then assembled with the inclusion of light-weight foam spares and adhered to a mounting flange. This manufacturing process was repeated for a set of four blades resulting in a set of three blades used in testing with one spare.

3.2.1. Geometry

The SD7032 airfoil was selected for use because of its low Reynolds number performance. This is due to its lower thickness to chord length ratio than the full scale airfoils, which results in a more favorable camber for wind field where viscous effects are prevalent. The differences in non-dimensional cross-sectional properties can be seen below in Figure 3.5. The airfoil selected for the comparison is FFA-W3-211, and is the airfoil geometry used at 70% of the blade length for the IEA 15 MW turbine blades. [20]

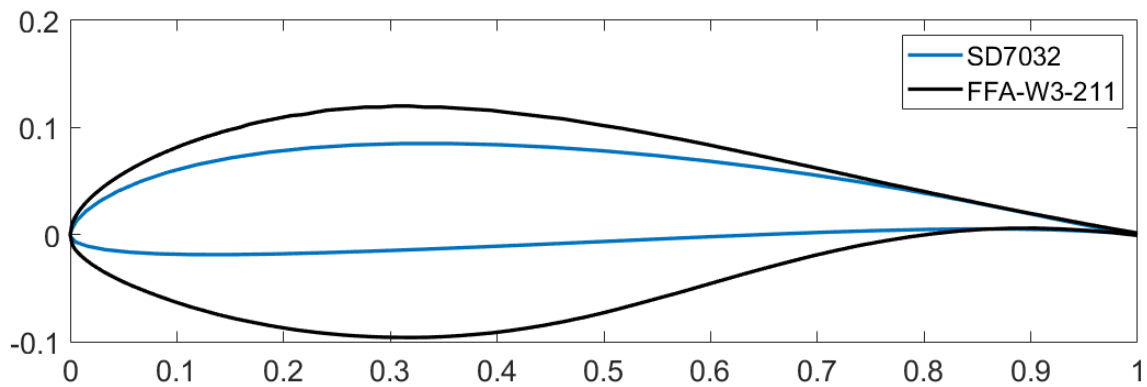
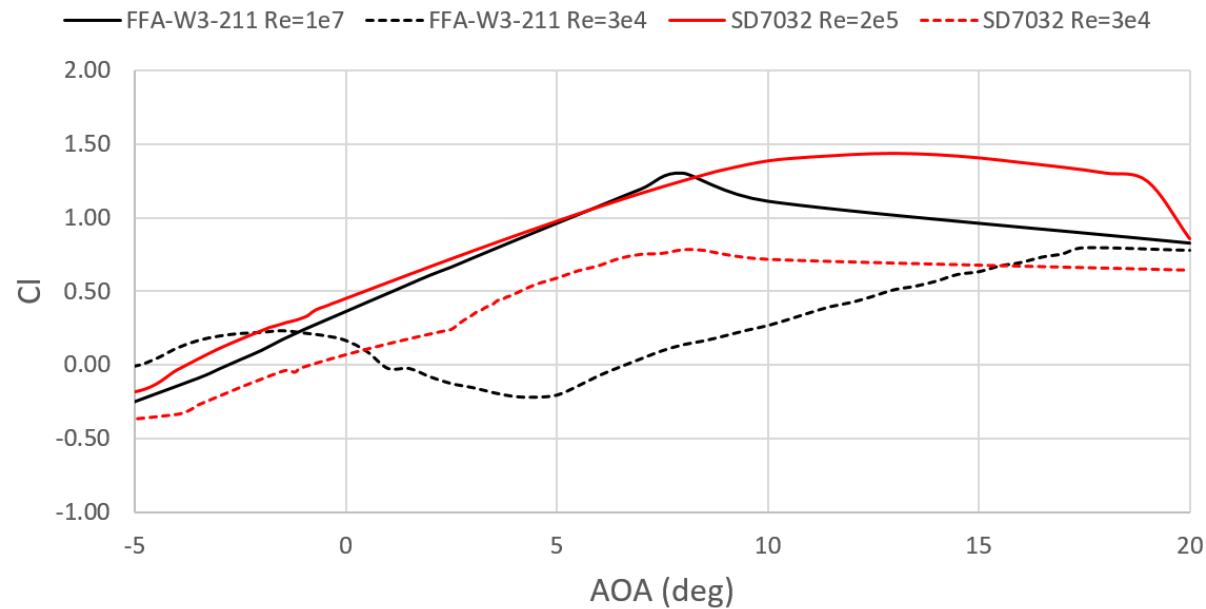
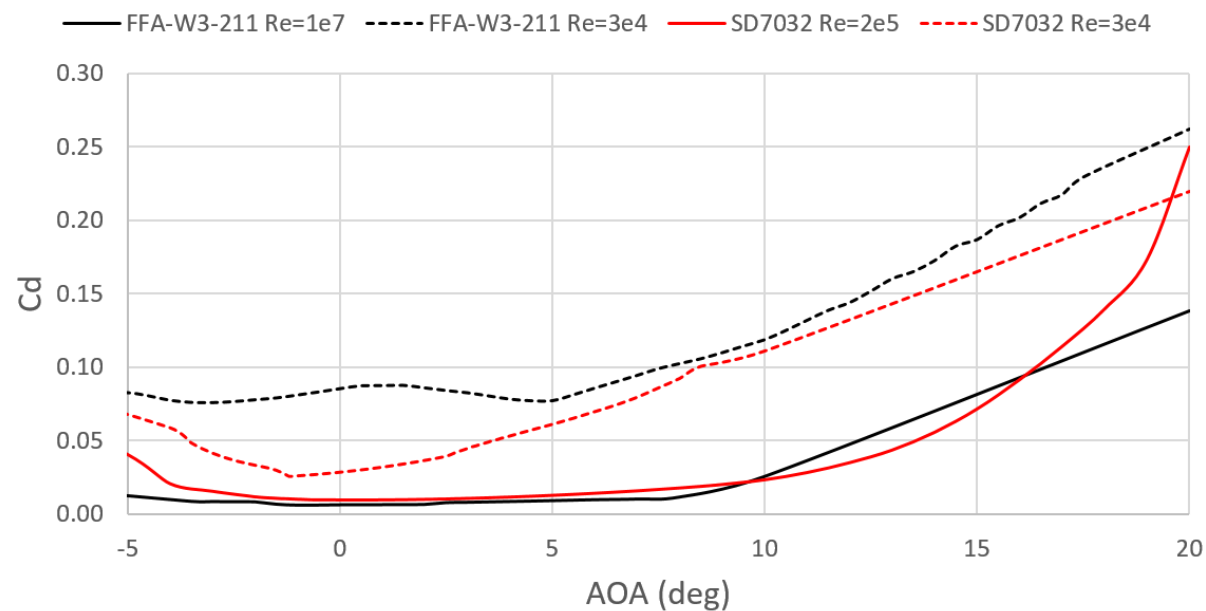


Figure 3.5: Full scale (IEA15MW) vs. Model scale (FOCAL) airfoil cross-section

Because the goal of the performance matched turbine was to match the response of the system to rated conditions, it was important to keep a similar Cl and Cd response in the operating range. Xfoil was used to perform an analysis of the performance of both airfoils at the full-scale and model-scale operating conditions, using the airfoil data files in Appendix B. This tool uses a non-turbulent wind inflow at any AOA specified, meaning that in the region past stall, or in negative lift cases, the program will continue to converge, even if the airfoil would have passed the flow separation point in real operating condition. Plots (a) and (b) of Figure 3.6 show a comparison of the full-scale airfoil at 70% blade length, FFA-W3-211, at a full-scale operating Reynolds number, 1×10^7 , which was used as the performance target. The performance of FFA-W3-211 is also shown at a lower Reynolds number, 3×10^4 , which is within the operating range of the 1:70 scale model turbine. The graphs show that the full-scale airfoil lift performance decreases and the drag experienced increases. Alternatively, the SD7032 airfoil performance is shown around its optimal operating range, 2×10^5 , and for the low Reynolds number case. The analysis shows a comparable performance of both airfoils in their optimal range, and an increased performance of the SD7032 airfoil over the FFA-W3-211 airfoil at the model scale operating condition for most of the operating range. It was also shown that the SD7032 airfoil produced significantly less drag at the same Reynold's number over the main operating range.



(a)



(b)

Figure 3.6: C_l (a) and C_d (b) Xfoil plot comparisons of airfoils at full scale and model scale operating conditions

Airfoil geometries are idealized profiles that do not account for manufacturing limitations encountered while constructing wind blades. Therefore a slight modification was made to the SD7032 geometry to add a 0.1-inch trailing edge thickness along the blade. This was done by running a program to create a wedge on the upper and lower surfaces of the blade, therefore preserving the chord and midline of the airfoil. An example of the differences in the resulting geometry can be seen below in Figure 3.7.

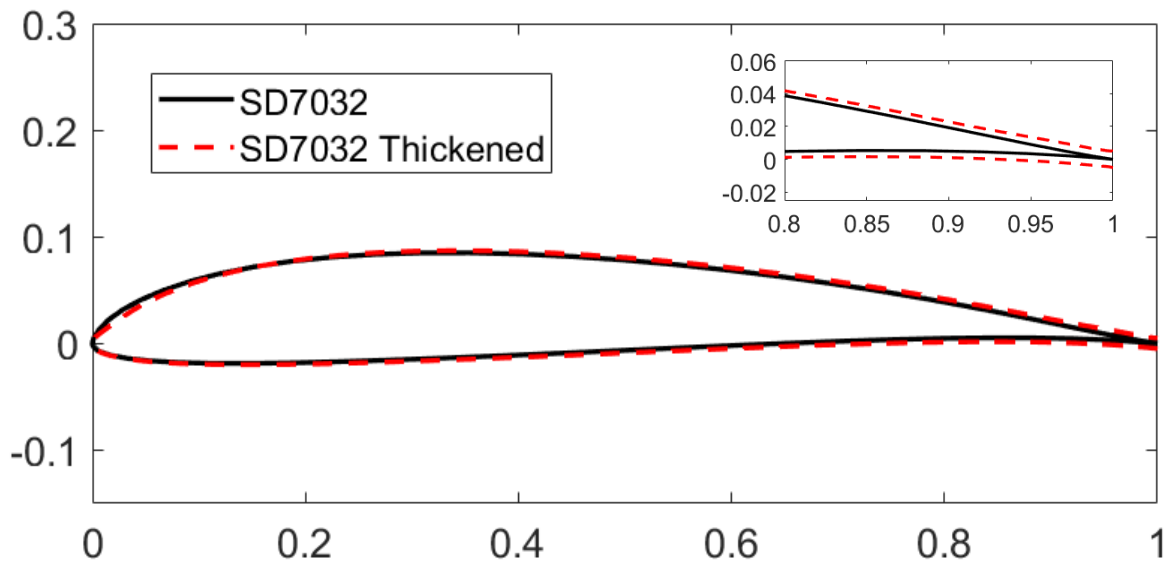
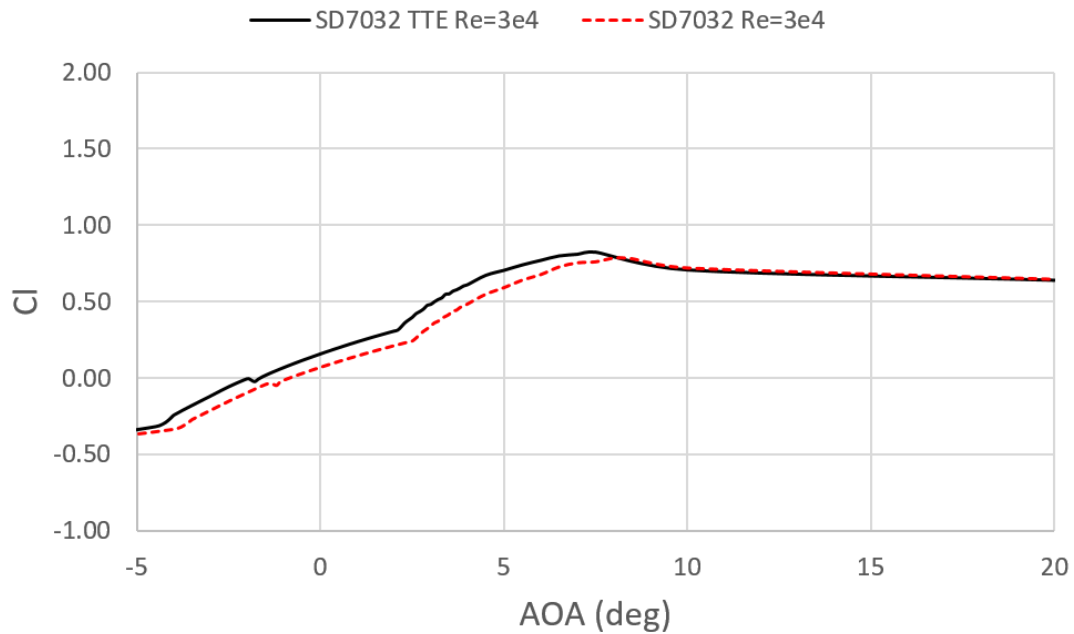
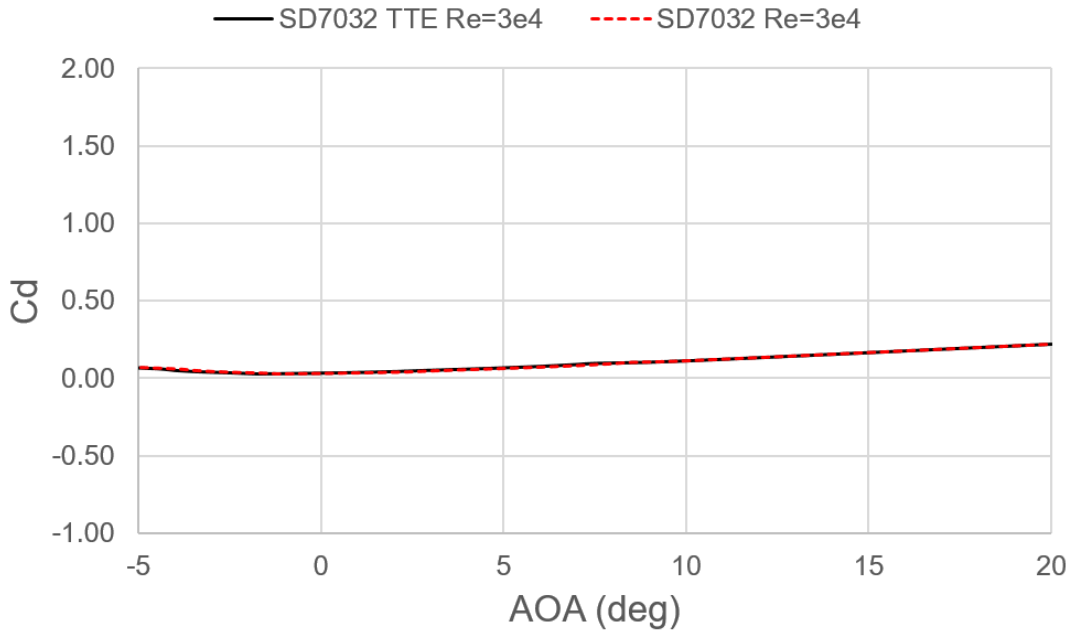


Figure 3.7: Thickened and unmodified SD7032 airfoil geometry

After the change in geometry, Xfoil analysis was performed on the new SD7032 TTE (Thickened Trailing Edge) airfoil, of which the airfoil data file is also included in Appendix B. The results are shown below in Figure 3.8 (a) and (b). As can be seen in the figure, the Xfoil analysis showed a slight increase in lift performance of the thickened airfoil over the unmodified profile, as well as no real change in drag between the two. The slight increase in performance is hypothesized to be the result of a change in the camber of pressure and suction faces, which would change the separation point of the flow. This analysis was important because it gives a better idea of the actual performance of the chosen airfoil during operation.



(a)



(b)

Figure 3.8: Cl (a) and Cd (b) Xfoil plot comparisons of standard and thickened SD7032 airfoils at scale operating conditions

After the twist and chord distribution was generated for the blade through the BEM process, the table of properties was imported into Matlab. A script was used to generate airfoil profiles along radial stations using the SD7032 airfoil with the thickened trailing edge. Additionally fairing was done starting with a cylindrical hub connection and transition to the maximum chord section. This process was also done with the last radial station to transition to a rounded tip. Figure 3.9 below shows the general shape of the blade built in Matlab using a straight loft between the sections. Those airfoil profiles were exported as x, y, z datasets. To assist in the process of lofting, three guide curves were generated, (1) a spline connecting all of the leading edge points of the airfoil sections, (2) a spline connecting all of the top surface trailing edge points, and (3) a spline connecting all of the bottom surface trailing edge points.

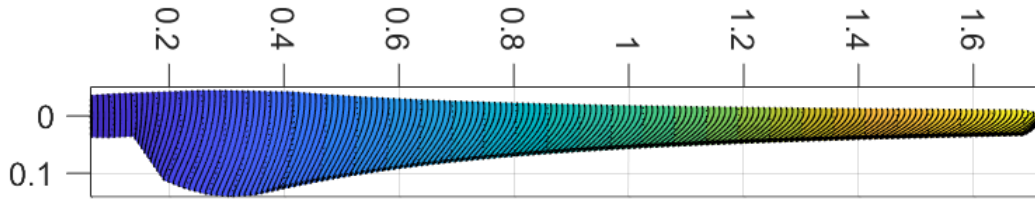


Figure 3.9: Matlab generated blade section distribution

The airfoil sections and guide curves were imported into SolidWorks and a loft was created using the components. This created a surface model that could be measured and used in SolidWorks assemblies. From this model, a blade was 3D printed in sections and assembled to have a physical model to inspect. It was found that the geometry at the hub and tip were not ideal, therefore a smoothing process was done for some of the geometry at the hub connection and tip. This decreases some of the sharp changes in geometry and decreases the obvious stress concentration areas, strengthening the blade. The resulting SolidWorks model can be seen in Figure 3.10.

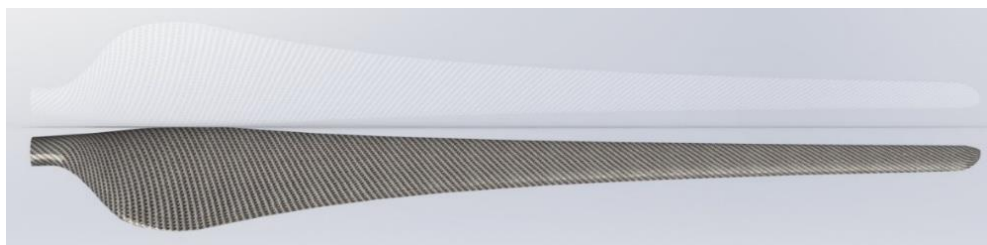


Figure 3.10: SolidWorks blade model after geometry modifications

These changes did not modify any of the blade sections generated using the twist and chord generating code, therefore no difference in airfoil performance was assumed. Table 3.1 includes a list of blade properties generated to represent the blade geometry, with the root transition region and very tip excluded due to the uncommon geometry. These blades are assumed to be rigid, therefore no pre-bend was included in the design.

Table 3.1: Blade geometric properties table

<i>Radial Station</i>	<i>Distance along pitch axis from blade root [m]</i>	<i>Chord [m]</i>	<i>Aerodynamic twist [deg]</i>	<i>Aerodynamic center [% chord]</i>	<i>Relative thickness [%]</i>	<i>Airfoil ID [-]</i>
1	0	0.05490	27.13	50	100	Cyl
2	0.01907	0.05490	27.13	50	100	Cyl
3	0.27839	0.19800	13.42	25	10	SD7032
4	0.33364	0.17409	11.00	25	10	SD7032
5	0.38890	0.15515	9.10	25	10	SD7032
6	0.44415	0.13981	7.58	25	10	SD7032
7	0.49940	0.12716	6.33	25	10	SD7032
8	0.55466	0.11657	5.29	25	10	SD7032
9	0.60991	0.10758	4.41	25	10	SD7032
10	0.66516	0.09986	3.65	25	10	SD7032
11	0.72041	0.09316	3.00	25	10	SD7032
12	0.77567	0.08729	2.43	25	10	SD7032
13	0.83092	0.08211	1.93	25	10	SD7032
14	0.88617	0.07751	1.48	25	10	SD7032
15	0.94143	0.07339	1.08	25	10	SD7032
16	0.99668	0.06969	0.72	25	10	SD7032
17	1.05193	0.06633	0.40	25	10	SD7032
18	1.10718	0.06329	0.10	25	10	SD7032
19	1.16244	0.06051	-0.17	25	10	SD7032
20	1.21769	0.05796	-0.41	25	10	SD7032
21	1.27294	0.05562	-0.64	25	10	SD7032
22	1.32820	0.05346	-0.85	25	10	SD7032
23	1.38345	0.05146	-1.04	25	10	SD7032
24	1.43870	0.04960	-1.22	25	10	SD7032
25	1.49395	0.04788	-1.39	25	10	SD7032
26	1.54921	0.04626	-1.54	25	10	SD7032
27	1.60446	0.04476	-1.69	25	10	SD7032
28	1.65130	0.00498	-1.77	25	10	SD7032

To connect the blade to the hub assembly, a blade flange was designed. With the pitch assembly discussed in section 3.1.2, it was important to design a hole pattern that aligned with the 0 degree angle of attack (AOA) plane of the blade, so the blades could be repeatedly indexed. Therefore, a flange was designed with an evenly spaced 4-bolt pattern that aligned with the 0 and 90 degree AOA axes of the blade. In between each of the bolt holes was a dowel hole to be used for alignment during the flange assembly to the blade as well as for the blade assembly to the rotor. Figure 3.11 shows a rendering of the flange design, in which the horizontal flange with the hole patterns is shown, as well as the vertical adhesion face with holes radially around the circumference to improve the adhesion of the blade skin to the interior face of the flange, as well as to decrease the weight of the flange. These were machined out of aluminum by the Advanced Manufacturing Center (AMC) at UMaine.



Figure 3.11: Blade Flange

3.2.2. Blade Mold Design

After the design of the blade surface model, molds were modeled for the composite manufacturing of the turbine blades. One of the goals for this set of blades was to achieve a smooth leading edge geometry, which is very important for the performance of the blades. Past manufacturing methods were considered, but each had their downsides. As outlined by Martin [6], one method of manufacturing is using pre-preg carbon fiber fabric with a two sided bladder mold and bladder, and curing at an elevated temperature in an oven. While this option yields blades with a very uniform surface finish and allows for the whole blade to be manufactured at one time, we were limited by the available oven dimensions. Unfortunately because

we were optimizing the scaling to capture all of the usable wind area, the blade molds would have been too large to fit in any of the available ovens, and the blade geometry would have proved very difficult in creating a suitable bladder insert. The second method is the traditional butterfly blade manufacturing method, which involves infusing two halves of the blade individually, and adhering them together along the leading and trailing edges. This is a simple composite infusion, but the assembly process leads to rough connections along the seams, especially on the leading edge, which is not ideal for the turbine performance.

Taking those methods into consideration, a hybrid-butterfly manufacturing process was designed. This involved infusing the blade in two parts, but instead of the seam lying on the leading edge, it is moved to the center of the pressure side of the airfoil. This was to be accomplished by infusing the whole suction side and half of the pressure side as one part using a mold assembly that is clamped together to create the concave geometry. The rest of the suction side was to be infused separately using an additional mold. A cross-sectional sketch of the molds in infusion configuration can be seen in Figure 3.12 below.

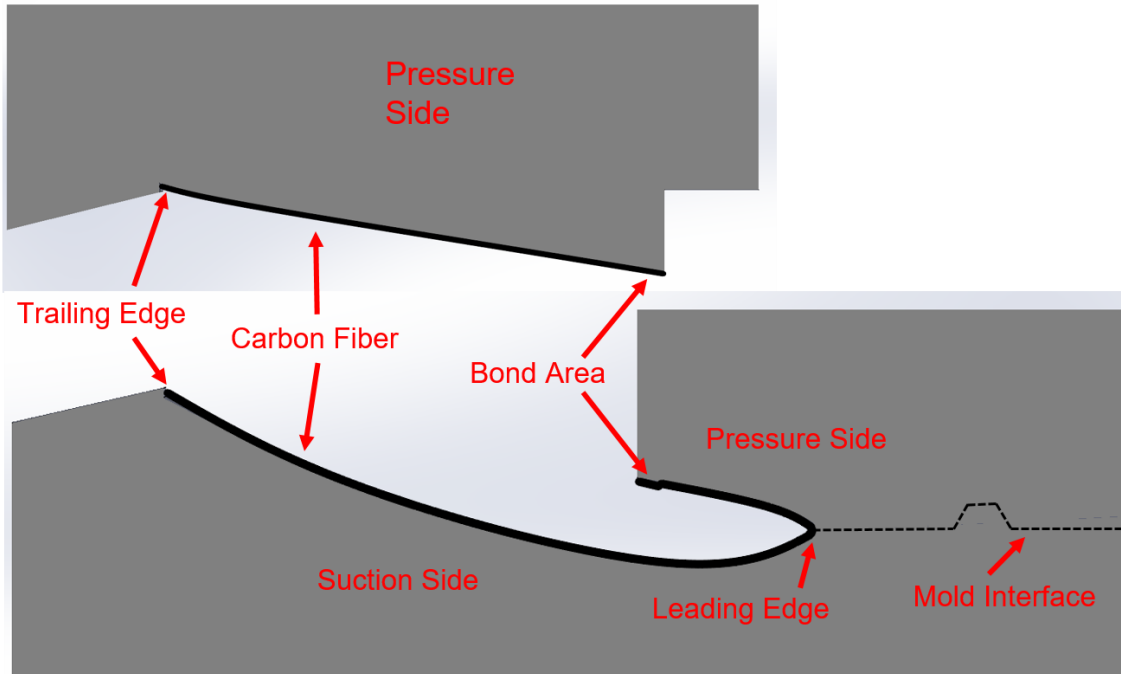


Figure 3.12: Cross-sectional view of blade molds

These blade molds were created using the surface model of the blade and extracting the geometry from a blank. These mold models were then sliced to account for clamping during the infusion process as well as to create geometry in the infused part that would make the skins easy to trim and assemble. A beveled groove and ridge were designed into the two part mold assembly with a reference face on one end, to ensure a tight fit between the two molds during an infusion. An alignment groove was also designed into the end of the largest mold, allowing for the alignment and assembly of the blade flange during the skin assembly process. This is shown below in Figure 3.13.

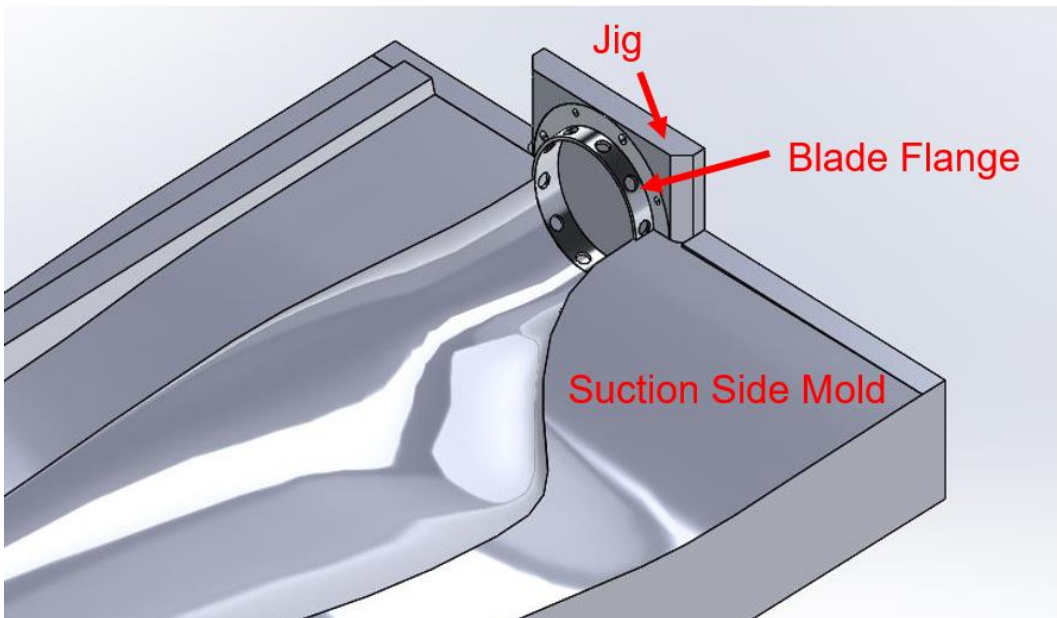


Figure 3.13: Blade flange assembly jig

The material which was chosen for the blade molds was a high-density Polyurethane (HDPE) foam. This material is very easy to machine, resistant to high temperatures and most chemicals, and holds a machined geometry well. 65 inch long blanks were taken to Lyman-Morse Boatbuilding Inc. (Figure 3.14) where they were machined using the solid models generated in SolidWorks.



Figure 3.14: Mold Machining at Lyman-Morse Boatbuilding Inc.

After the machining was completed, the full set of blade molds, pictured in Figure 3.15 were brought back to the ASCC and set up in the Composites Manufacturing Laboratory (CML) to be cleaned and prepped.



Figure 3.15: Full set of Blade Molds

As a validation of machining accuracy, the Frasier and Raab Orthopedics (FARO) scanning arm at the AMC was used to check the tolerancing of the mold surface to the SolidWorks model of the molds. This was found to be within an acceptable tolerance range of ± 0.001 inches.

3.2.3. Blade Manufacturing Process

The manufacturing process utilized in the fabrication of the blade skins was VIP. This process uses the negative pressure of a vacuum pump to pull air from a part to be infused, while pulling resin into the part from a resin inlet. The process is outlined in a detailed procedure found in Appendix C. Both blade skin parts were infused at once by running two resin lines from one feed bucket as seen in Figure 3.16, and pulling from a vacuum pump connected through a resin trap pot into both parts. The order of procedure was to wax and buff the molds to create a relief surface, then the carbon fiber was laid in place, followed by a peel ply for release of the part from the disposable layers above. This was covered by a mesh flow media to help with resin flowing from one side through a channel of spiral wrap tubing, to the other side where the vacuum was connected into another channel of spiral wrap tubing. After the infusion started, it took approximately 45 minutes for the resin to start to harden, and cured enough to be taken from the mold after another 12 hours.

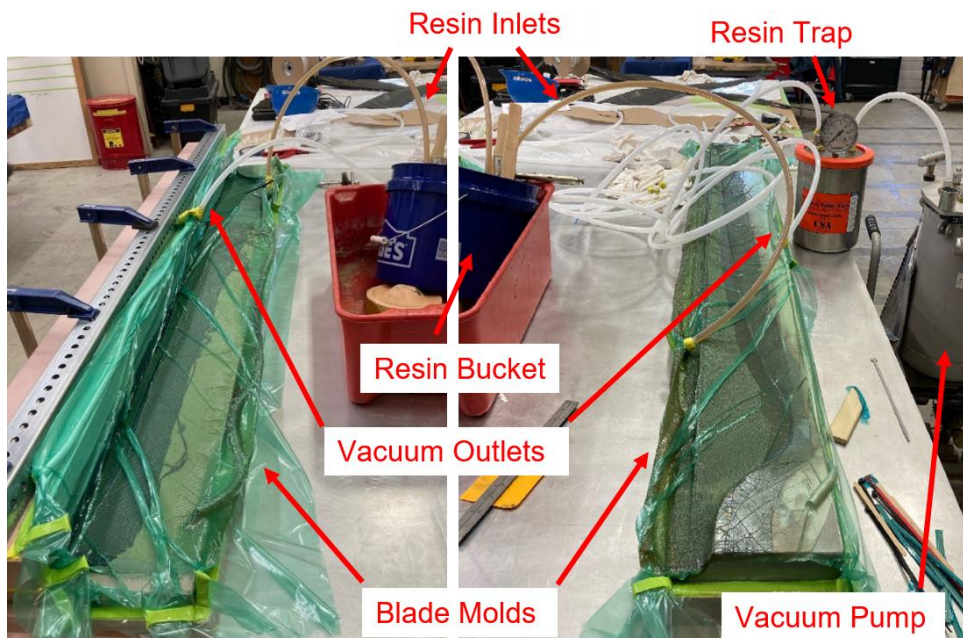


Figure 3.16: Blade Infusion Set-up

After the parts were infused and removed from the mold, they were trimmed, cleaned, and sanded. The blade assembly process was done in the largest mold and consisted of adhering two 2 pound foam spars that matched the interior geometry of the blades using a two part 2 pound expanding foam, seen in Figure 3.17 (a). The foam spars were cut to the general geometric shape needed and sanded to further match the profile. They provided structural support by joining the upper and lower blade skins, therefore increasing the effective moment of inertia. After the blade spars were adhered in place, the other half of the pressure side skin was adhered to the blade spars, and to the two connection seams of the large section of the blade. At the connection seam running along the center of pressure face, a step down was infused into the part, creating a lap joint where Methacrylate adhesive was laid as a bead and the two parts were pressed together by distributed loads. For the trailing edge, adhesive was laid in a bead along the lower blade skin surface and the two faces were pressed together using a distributed load, yielding a complete blade geometry as shown in Figure 3.17 (b). The blade was then adhered to the blade flange using the jig and alignment grooves discussed previously. The blade flange was cleaned and sanded before the adhesive was added to the inner surface. Once in place, an outward pressure was applied by an expanding tube plug to press the blade skin out against the flange, Figure 3.17 (c).

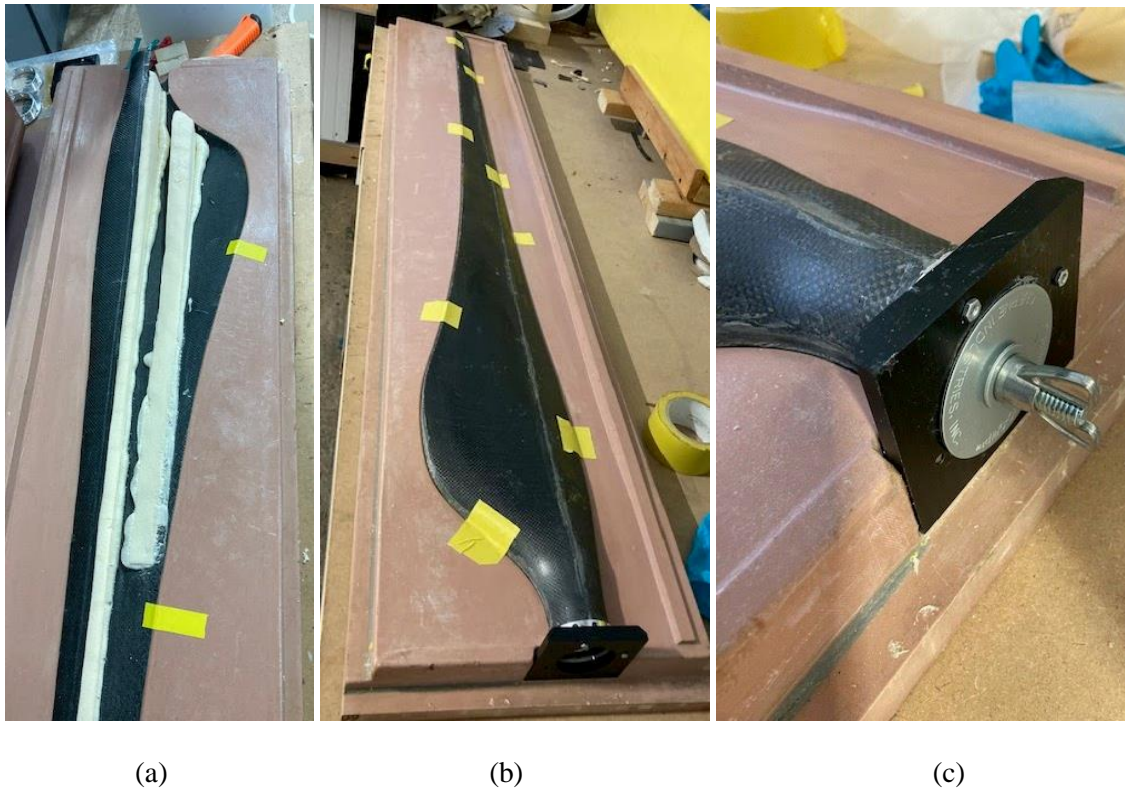


Figure 3.17: Blade Assembly (a) Adhesion of spars (b) Adhesion of skin (c) Adhesion of flange

After the assembly process, a heat gun was used to heat the blade skins to 80 degrees C, which helped complete the curing process of the part. This process was repeated until a set of four blades were made. An example of the finished geometry can be seen in Figure 3.18.



Figure 3.18: Finished Blade

3.3. Tower Design

The tower used was designed for a previous basin model test and consisted of a 50.8 mm diameter thin walled aluminum tube attached to a base flange for mounting to the basin structure, and a tower top flange for connecting to the load cell and RNA assembly. The original goal for the experiment was to mount the tower by the base flange, therefore a Hammer Test was conducted to find the tower damping coefficient. The time history was collected by measuring the moments at the tower top, Figure 3.19, and points were selected from the upper peaks to calculate the tower damping coefficient as well as the 1st bending frequency. The damping coefficient was found to be 0.24% and the 1st mode frequency was 4.15 Hz. These values matched the targets scaled from the IEA 15 MW tower, therefore it was deemed an acceptable tower to use for this basin test.

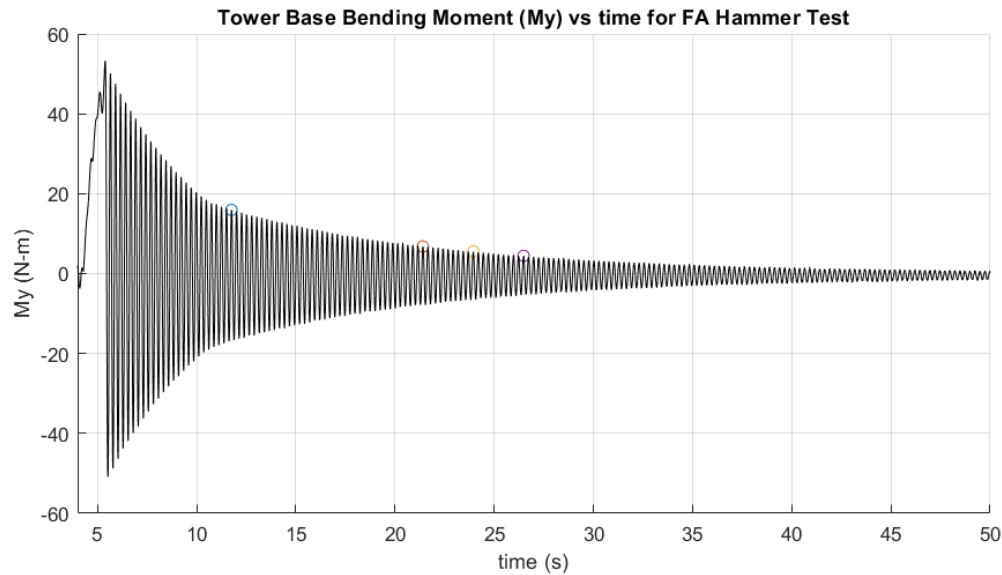


Figure 3.19: Tower Hammer Test Free Decay Graph

During initial testing, it was found that an excitation in the frequency range of 1P was being amplified through the tower, therefore the tower was tethered at three points right below the tower top load cell, as shown in Figures 3.1 and 4.6. This allowed for the performance of the turbine to be captured without the effect of a large magnitude vibration due to the tower bending.

3.4. Full Assembly

After all of the components were manufactured, they were assembled and the instrumentation was wired together. Pitch control operational checks were conducted to validate the operation of the active blade pitch. The turbine was then ready for basin testing. Figure 3.20 shows the turbine in the fully assembled state without completed wire tail.



Figure 3.20: Fully assembled turbine

CHAPTER 4: MODEL CHARACTERIZATION AND PERFORMANCE RESULTS

4.1. Physical Characterization

The important next step after building the components of the turbine was to characterize their structural and dynamic properties. This was accomplished through methods of mass measurement, center of gravity balancing, swing testing to find inertial values, as well as loading to characterize the deflection of members. These were measured as outlined below, and are shown in Table 2.2 in section 2.2 as well as fully captured in the FOCAL Campaign 1 Validation Definition Document [18]. The importance of the full turbine characterization was to make sure it was representative of the full-scale IEA 15 MW turbine, and measure the exact properties for modelers to build simulation models of the as-built design to validate the performance seen in the basin testing using an aero-elastic design code for horizontal axis wind turbines (OpenFAST). This section will also cover the basin testing procedure used to create C_p and C_t surface plots for use in performance control of the turbine in an actively changing wind environment. For the purposes of this thesis, the focus related to the control response was to validate the correct response of the mechanical system, as the in-depth control response will be covered in further detail in research to be published by another member of the FOCAL team.

4.2. Blade Characterization

The blades were the most important components of the turbine to fully characterize, as they determined the dynamic response of the turbine to the wind environment, as well as the loading that would be experienced by the pitch and rpm control systems during operation. During the process of characterizing the blades, small adjustments were made to the masses by injecting needed amounts of expanding foam into the blades to balance out the mass, moment of inertia, and stiffness of the blades as best as possible.

4.2.1. Blade Dynamic Testing

Testing was conducted on the blades to validate characteristics related to the dynamic performance of the turbine blades. Mass was measured by using a sensitive scale that could detect up to a one one-hundredth of mass difference. The distance of the CG was found by balancing the blades on a small rod and marking

the point where the blade was completely balanced. After these tests were done and adjustments were made to the mass and CG, the blades were then tested for their inertial properties.

The blade inertia testing was done by conducting a swing test of the blade as shown in Figure 4.1. The inertia of the frame that was used was found by performing a swing test with a dummy weight hung from a rod at a known distance from the center of the rotating shaft center. The test frame used was an old nacelle with a drive shaft supported by two radial support bearings. A rotary encoder was attached to the end of the driveshaft where the motor used to be, it was used to track the rotation of the driveshaft as a voltage vs. time output. After the calibration test runs were complete, and the inertia of the fixture was found, and a blade was attached to the mounting fixture with the 0 degree AOA axis along the swing path.

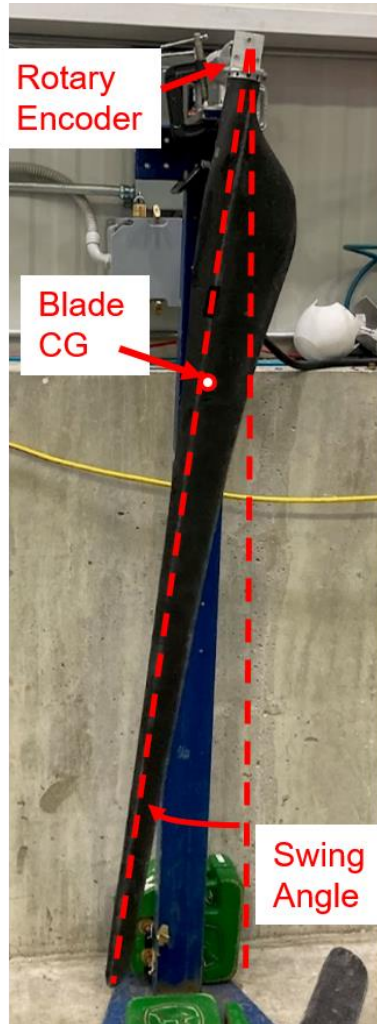


Figure 4.1: Blade Inertia Testing Setup

A Data Acquisition System (DAQ) controlled by a Labview program was used to collect the encoder data. The swing amplitude was monitored in the Waveform Chart and the data collection was stopped once the swing amplitude was damped out. The Labview data was imported into Matlab where a script was implemented to find the points located at the peaks of swing data starting at the second peak and the following couple dozen peaks, Figure 4.2. From these peaks, the damped and natural frequencies were found. The moment of inertia was found about the CG of the blades and was translated to about the root connections point, and about the hub center. The code used to run these calculations can be found in Appendix E.

The inertial testing process was repeated with the blade mounted with the 90 degree AOA axis in the direction of swing, and the blade inertial values were calculated for that case. Table 4.1 shows the measured blade properties for all of the blades tested where I_{xx} represents the blade inertia with the 0 degree AOA axis in the direction of swing about the center of the drive shaft. And in turn, I_{yy} represents the blade inertia with 90 degree AOA axis in the direction of swing about the center of the drive shaft. These values were average as can be seen compared to the full scale target values in Table 2.2, where the as-build blade inertia is much higher than scaled. This is due to the constraints of the blade construction process, where even using extremely light weight materials, there was no mass budget after construction to ballast the blade after assembly, causing the CG to be closer to the tip of the as-built blade than targeted, therefore increasing the moment of inertia values.

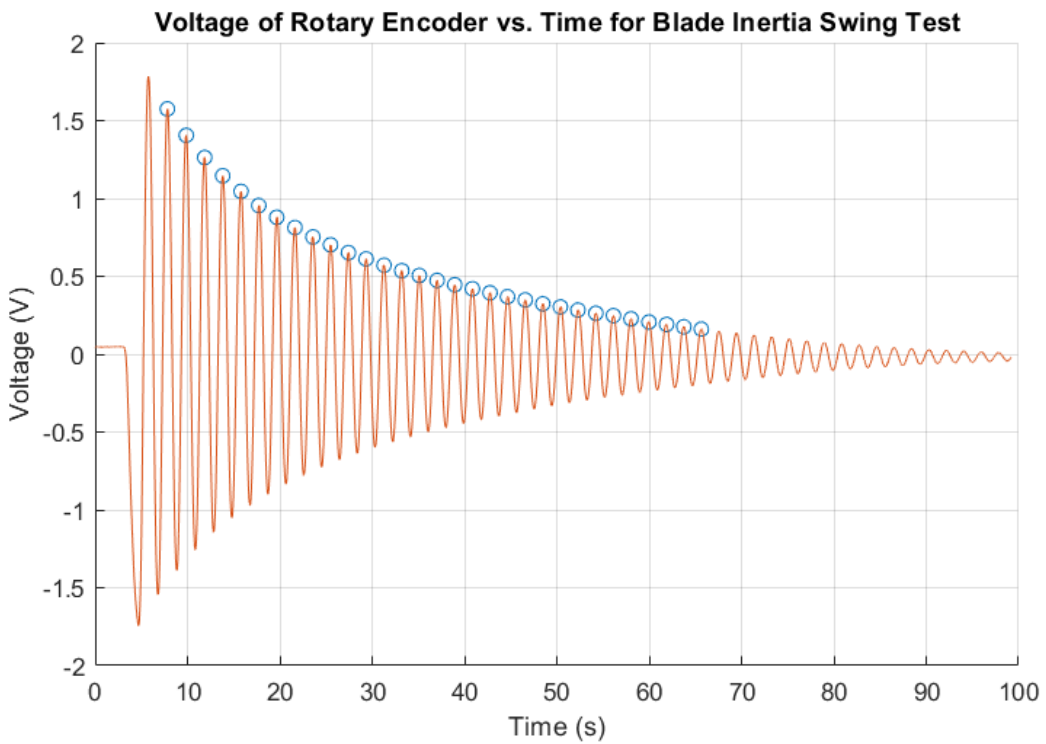


Figure 4.2: Blade Inertia Testing Encoder Voltage vs. Time test plot

Table 4.1: Individual blade properties

Blade	Mass (kg)	CGz (m)	Ixx (kg*m^2)	Iyy (kg*m^2)
1	0.23658	0.537	0.1161	0.1210
3	0.23466	0.540	0.1161	0.1203
4	0.23553	0.540	0.1160	0.1242
Spare (7)	0.23683	0.533	0.1160	0.1196
Average of blade in-use	0.23559	0.539	0.1161	0.1218

4.2.2. Blade Structural Testing

Blade structural testing was conducted to find the actual deflection response of the manufactured blades in the edge-wise configuration (as pictured in Figure 4.3) and in the flap wise direction to inform the operating limits of the turbine. These tests were conducted by loading the blade with known masses suspended from a string at 70% blade length, and measuring the tip deflection at each case.

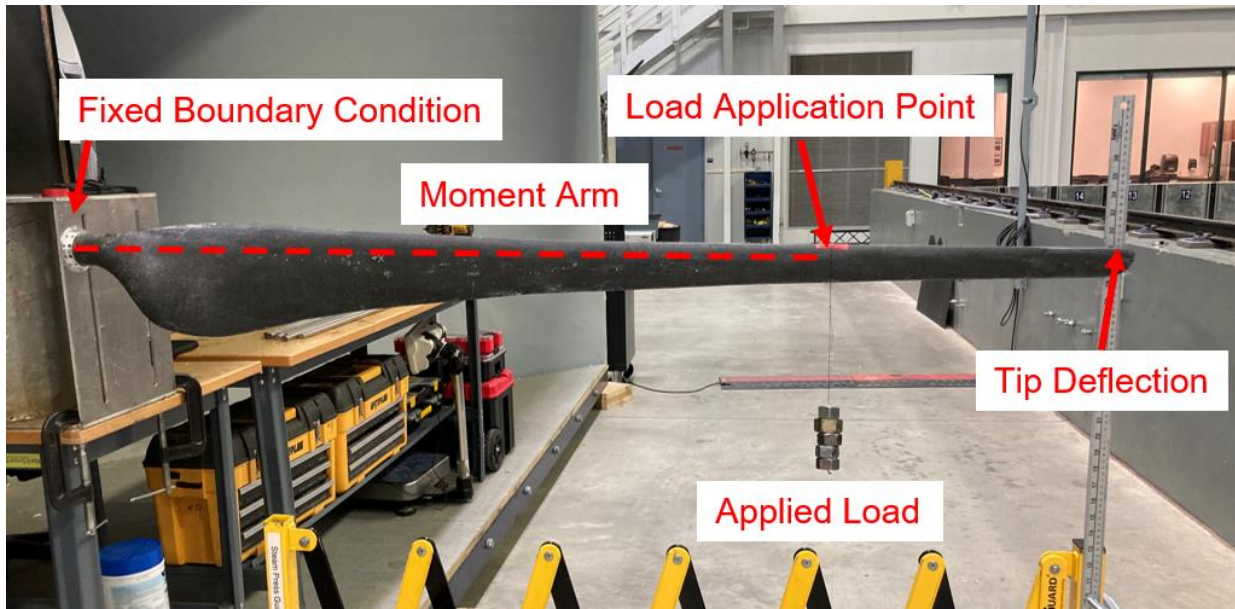


Figure 4.3: Blade deflection testing (edgewise configuration shown)

The tip deflections are plotted for each of the blades in the flap-wise direction in Figure 4.4 (a) and in the edge-wise direction in Figure 4.4 (b). The stiffness data was utilized by modelers to create more realistic elastic blade models. For the IEA 15 MW turbine blades, a 4 meter full-scale (0.057 meters model-scale) pre-bend was designed into the blades to account for the deflection during operation. Comparing that value to the flap-wise FOCAL blade deflection data, the deflection seen is comparable to the deflection that the full-scale blades were designed to be able to accommodate. For example, the rated model-scale loading condition was estimated to be around 3 Newtons per blade, and when the blades where loaded at 0.7 blade length with a point load of that magnitude, an average blade deflection of 0.048 meters was found. Therefore, the stiffness of the full-scale blade was found to be comparable to that of the IEA 15 MW blade. The blades were not designed with this target in mind due to the other design parameter targets, but could be used as design parameter for future blade designs since it has been shown to be feasible. Furthermore, coupon tests were performed on the composite lamina to find an estimate of actual material properties. This procedure is outlined in Appendix D, results showed significantly lower tensile strength and modulus than predicted by the manufacturer. This is predicted to be due to the use of only one layer of carbon fiber, causing larger areas filled with low-strength resin.

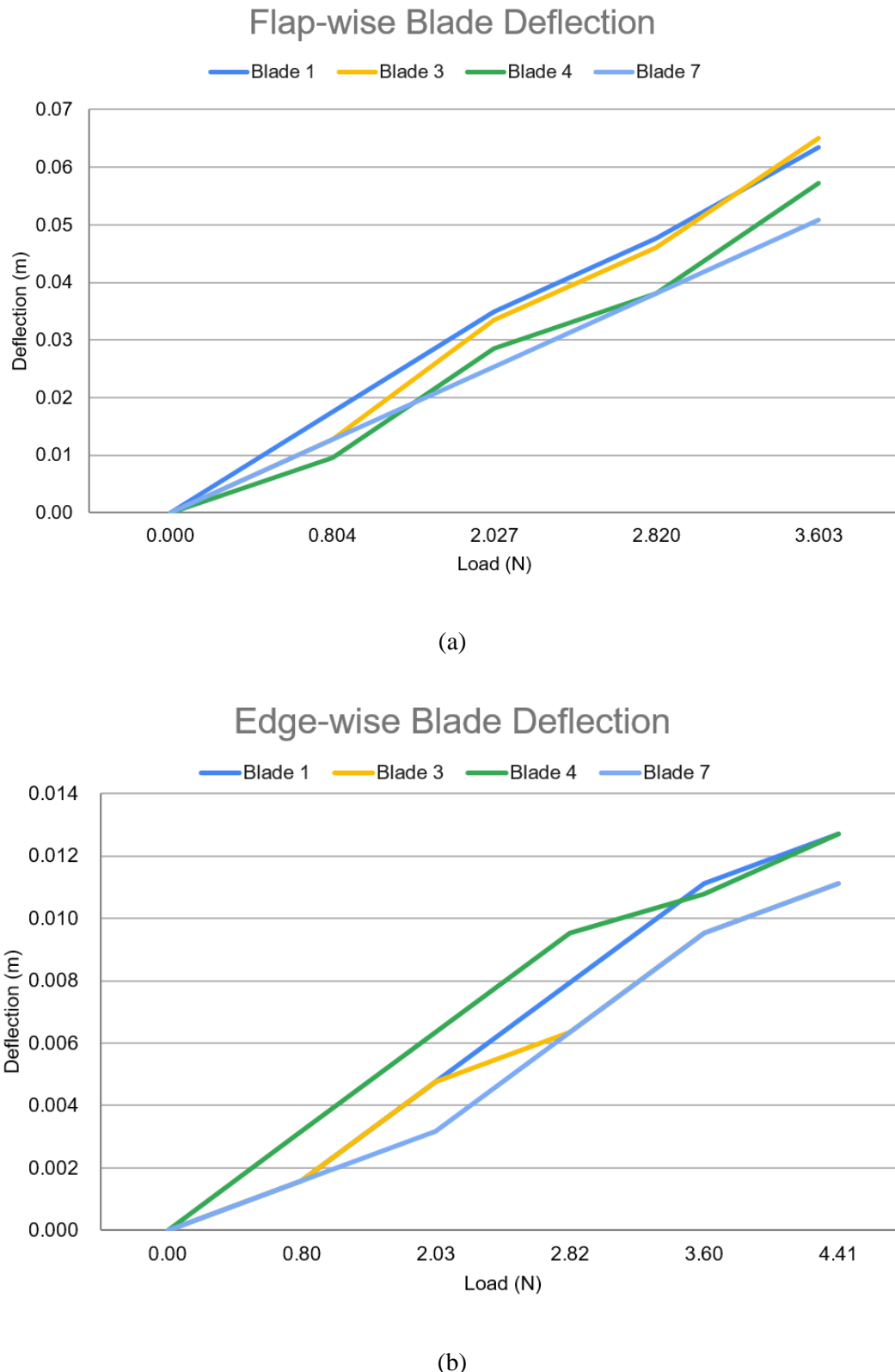


Figure 4.4: Blade Deflection chart for Flap wise (a) and Edge wise (b) tests

4.2.3. Blade Surface Scanning

To understand the actual geometry of the manufactured blades, the AMC FARO arm was employed to create a surface point cloud of the blade in reference to indexes on the blade flange. This process is outlined in detail in Appendix F. From this point cloud data, the blade was binned into 0.1 inch sections along the blade length, and cross sectional geometry sections were generated, which were compared to the cross sectional shape of the SolidWorks model blade at the same station along the blade. From these sections, a midline was estimated, and from which twist and chord length could be estimated. The data was also evaluated for lateral offset at each section. At the time of the writing of this thesis, the process for determining those values is still being developed and is part of the goals of future research on this project. An additional goal for these section in the future is to be able to run them in Xfoil to obtain a more realistic performance with features like a thicker trailing edge and seam bumps. As a sample, the blade station at 70% chord is shown in Figure 4.5 below for both scan and SolidWorks data along with their estimated chord lines.

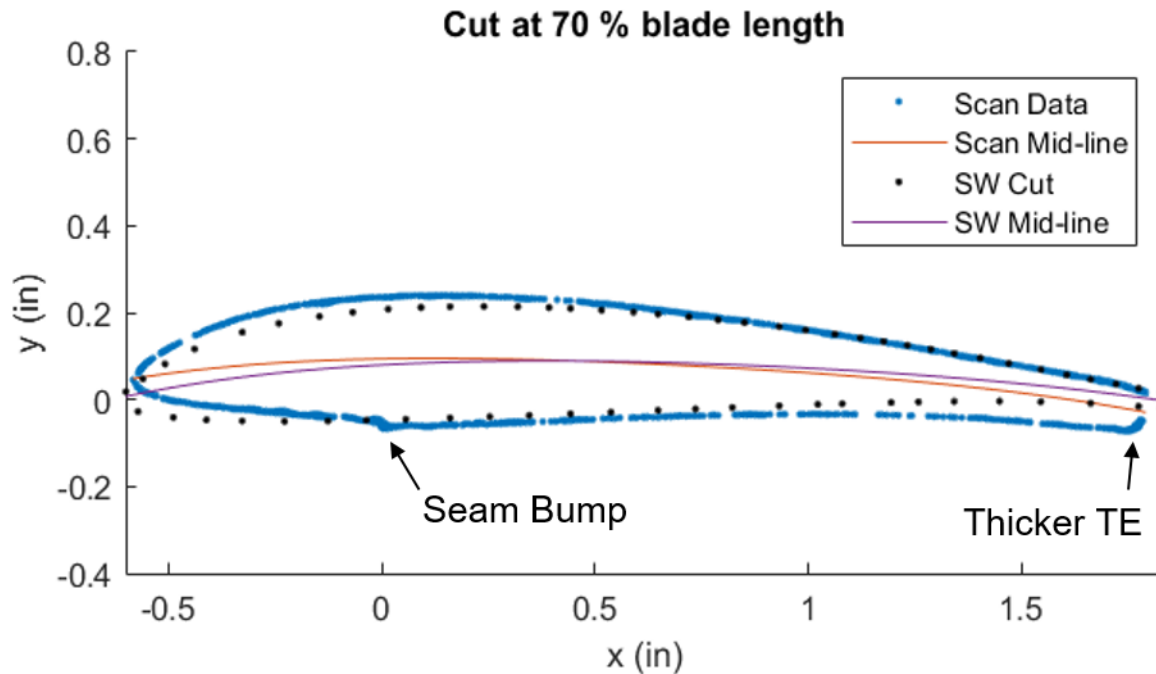


Figure 4.5: Scan and SolidWorks data for the 70% span station with estimated mid-lines

4.3. Data Acquisition and Controls

All wires running from the instrumentation on the turbine were run down the outside of the tower, as seen in Figure 4.6, and along the bridge of the basin where they terminated at the control center located on-shore. The major components of the on-shore control center were the cRio, power supply, and motor controller, as the pitch controls were located on the hub of the turbine.

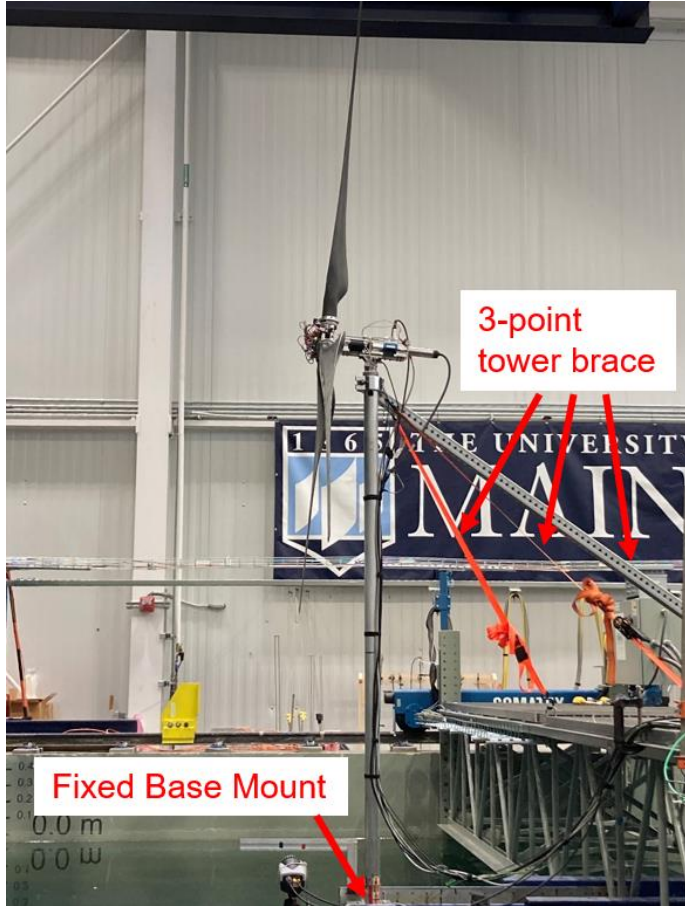


Figure 4.6: Turbine configuration during basin testing

A data acquisition system was built with a Labview interface as pictured in Figure 4.7 utilizing ROSCO. This interface was a joint venture between NREL, the ASCC, Det Norske Veritas (Norway) and Germanischer Lloyd (Germany) (DNV-GL), and Evergreen Innovations. This dashboard allowed the team to monitor the real-time responses of the turbine as well as to see the set points that were being read into the controls. This interface also controlled the data points that were output into the test data file to be read using a Matlab script.

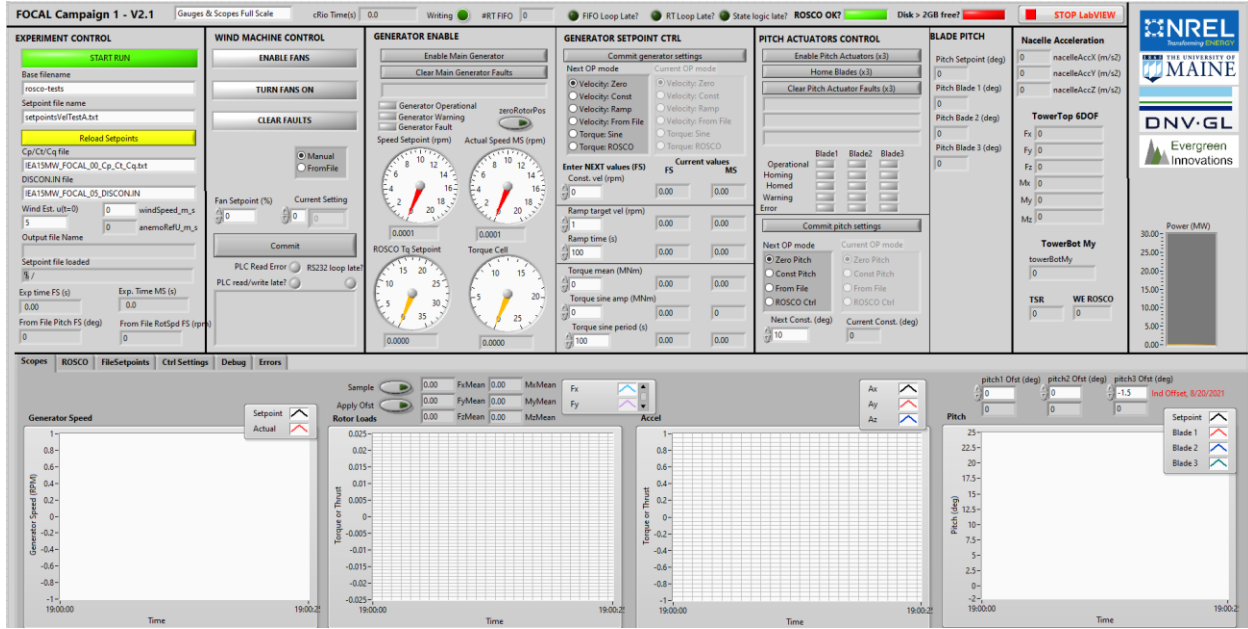


Figure 4.7: Labview dashboard for basin testing

4.4. Wind Turbine Performance

Turbine performance was tested at a steady wind state to collect performance data over a range of AOAs and TSRs. The goal of the characterization testing was to create C_p and C_t surface maps over that range of AOA and TSR to be referenced in active turbine controls using ROSCO. The turbine response was then validated over multiple dynamic wind cases, which were not part of the scope of this thesis research, but a sample of the test data is included here to demonstrate the mechanical and turbine instrumentation operation accomplished through this model.

4.4.1. Uniform Wind Environment Testing

Testing was conducted at a set wind speed and the rotor was stepped through rpm set points. These tests were repeated for multiple AOA values to cover the full range of operation of the turbine. In order to control the turbine for each test case, set point files were generated to feed into the Labview controls. The set points were generated using a Matlab script with the output as a matrix that the controller can recognize. One example of a set point file used is mapped and shown in Figure 4.8.

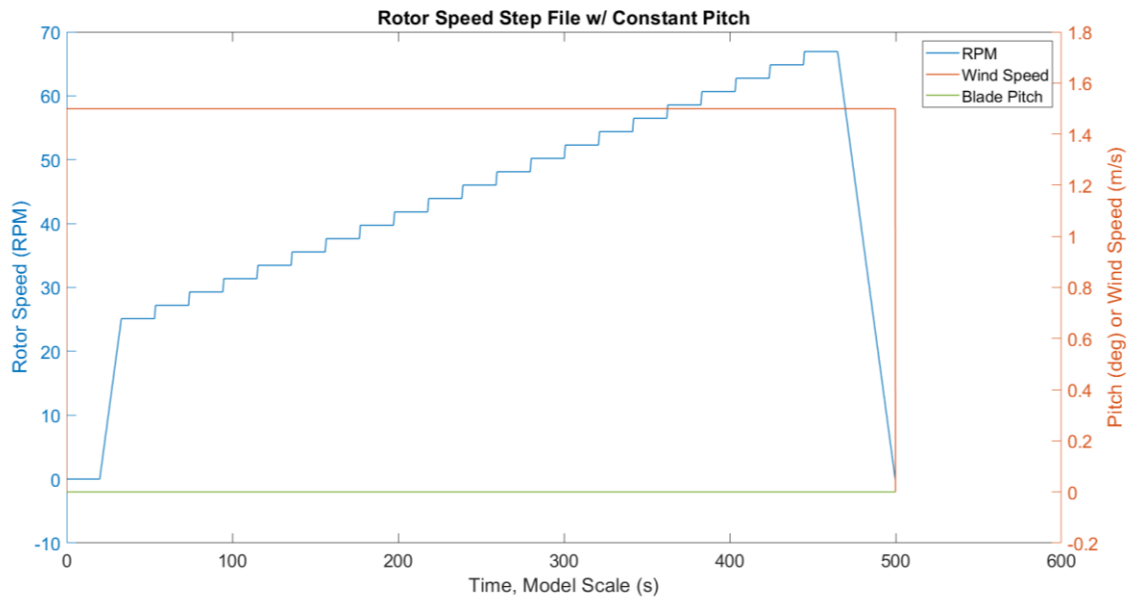


Figure 4.8: Rotor Speed Step File at 0 degree AOA and Uniform Wind Environment

The turbine ran through the set point file, and the DAQ system collected the environmental values and turbine response over the time period. The Labview program then generated a dataset with the responses and a Matlab script was used to generate meaningful plots. Figure 4.9 below shows the turbine response to the set point file, with some variation measured in the actual wind speed due to the normal basin environmental factors.

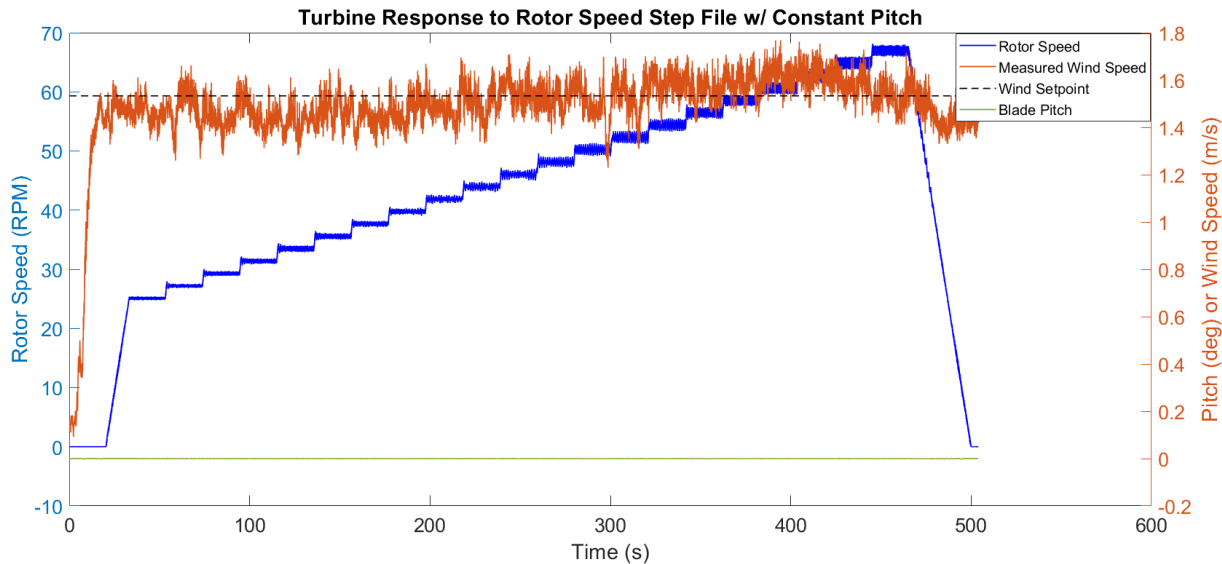
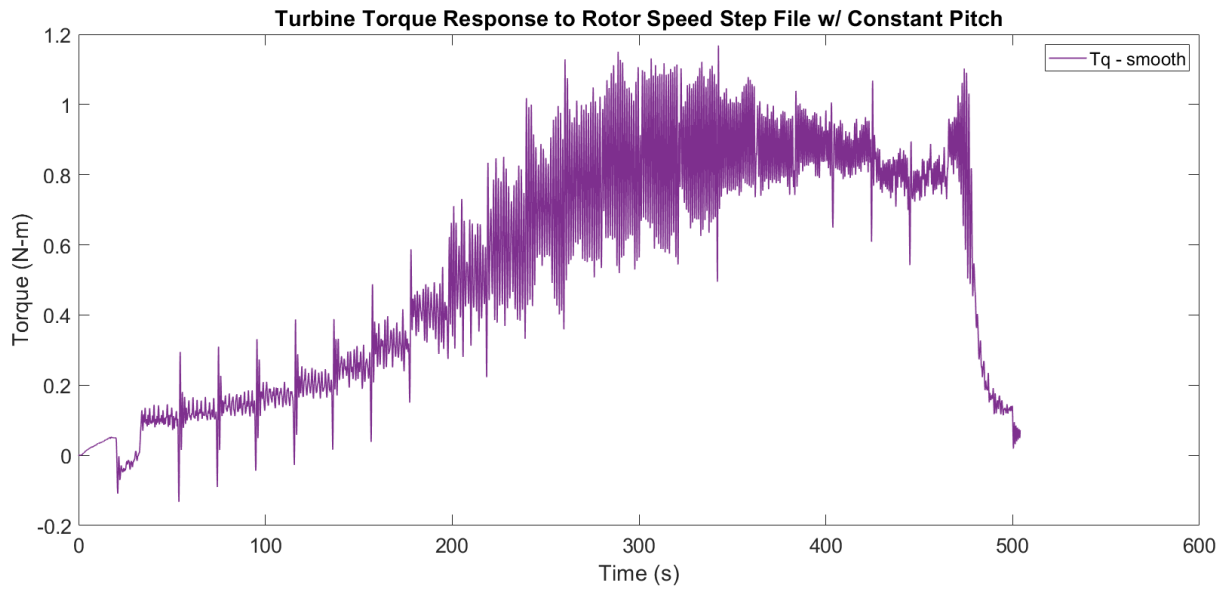
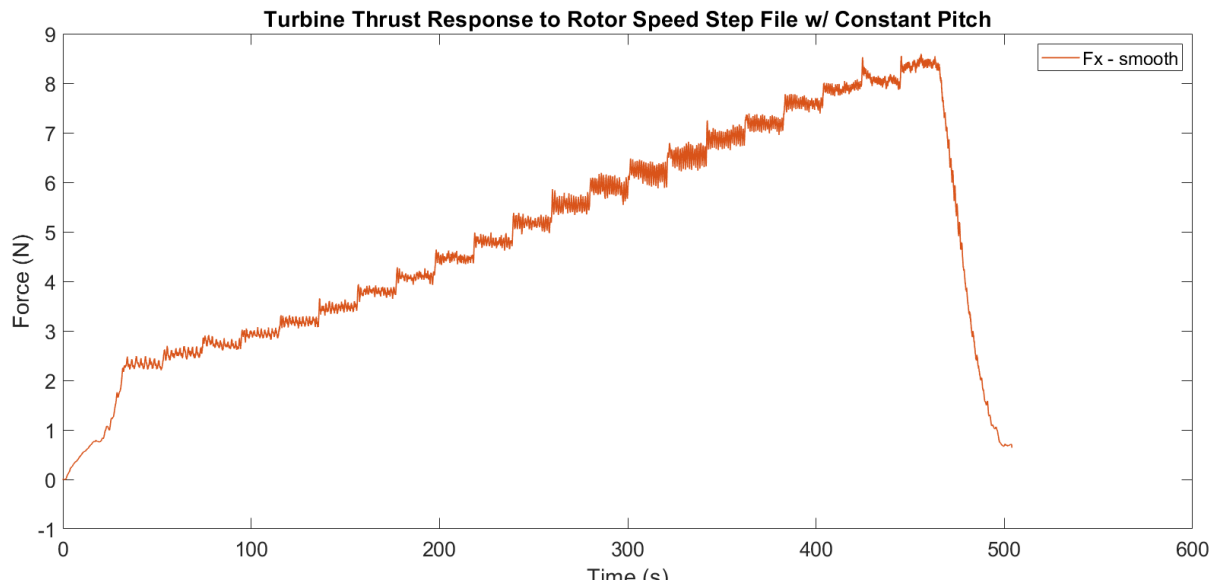


Figure 4.9: Response to rotor speed step file at 0 degree AOA

Two of the most important plots for the performance analysis of the turbine are the torque and thrust responses of the turbine. These are needed to calculate the Cp and the Ct. Time histories of torque and thrust can be seen below in Figure 4.10 (a) and (b). One point of notice in the torque response was the increase in noise between 200 and 350 seconds of testing. This response is what is seen in the transition zone of a turbine being rotated by a source other than the wind. In the transition zone, the flow is beginning to connect and generate lift on the airfoil. Because the pitch of the blades and wind speed are being held at a constant set point, in order to reach the rated operation zone where the turbine would be generating power (torque), the rotor rotational speed does not reach rated until around 63 rpm, therefore in order to reach that point, the turbine is forced through the zone of aerodynamic stall where lift is decreased and drag is increased. In a turbine driven by the wind, the blade pitch is controlled to minimize the amount of time that the blades are experiencing this unstable response, but for the sake of mapping the Cp and Ct responses for the full range of blade pitch and rpm, measuring this instability was crucial. This response was seen less in the thrust variation due to the decreased effect of the drag component of the blade on the thrust outputs.



(a)



(b)

Figure 4.10: Torque (a) and Thrust (b) response to rotor speed step file at 0 degree AOA

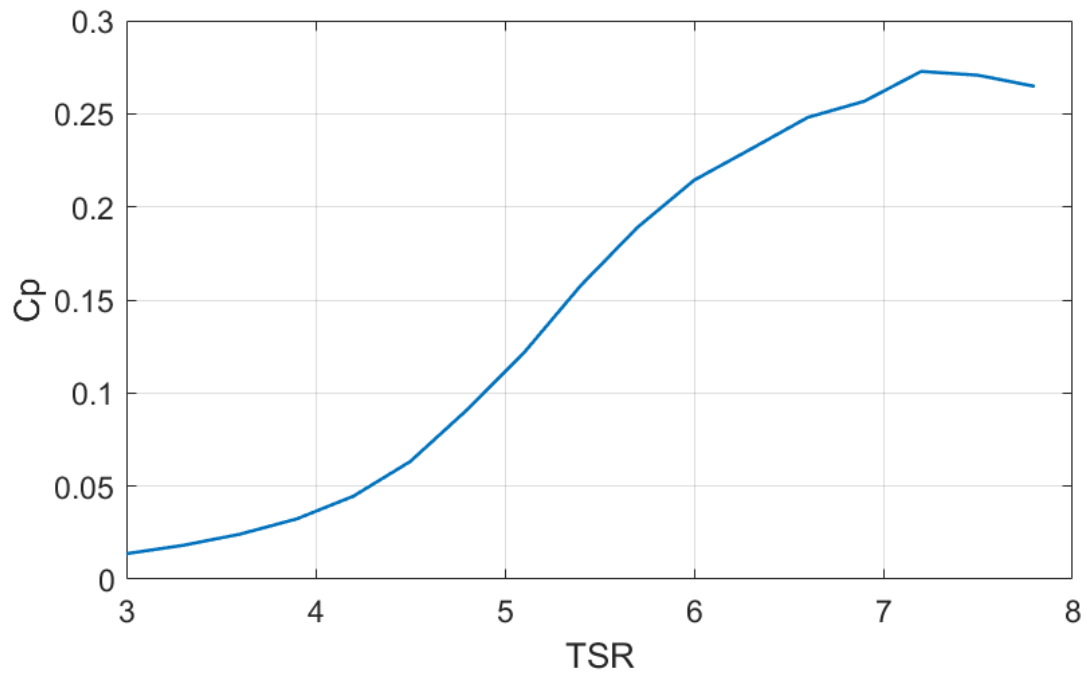
Once these response files were created, the steps were discretized and the average rpm, torque, and thrust values were calculated for each set point. These values were then used along with the average wind flow velocity to calculate the C_p , C_t , and TSR for each set point. As described in Equation 2.3, TSR calculates the ratio of the rotor tip speed and the inflow velocity at hub height. In order to calculate C_p , power (P) first needs to be found at each set point, this is done by multiplying the torque by the rotor rotational speed. After these values were calculated, C_p was found using the equation:

$$C_p = \frac{P}{\frac{1}{2} \rho U^3 A} \quad (4.1)$$

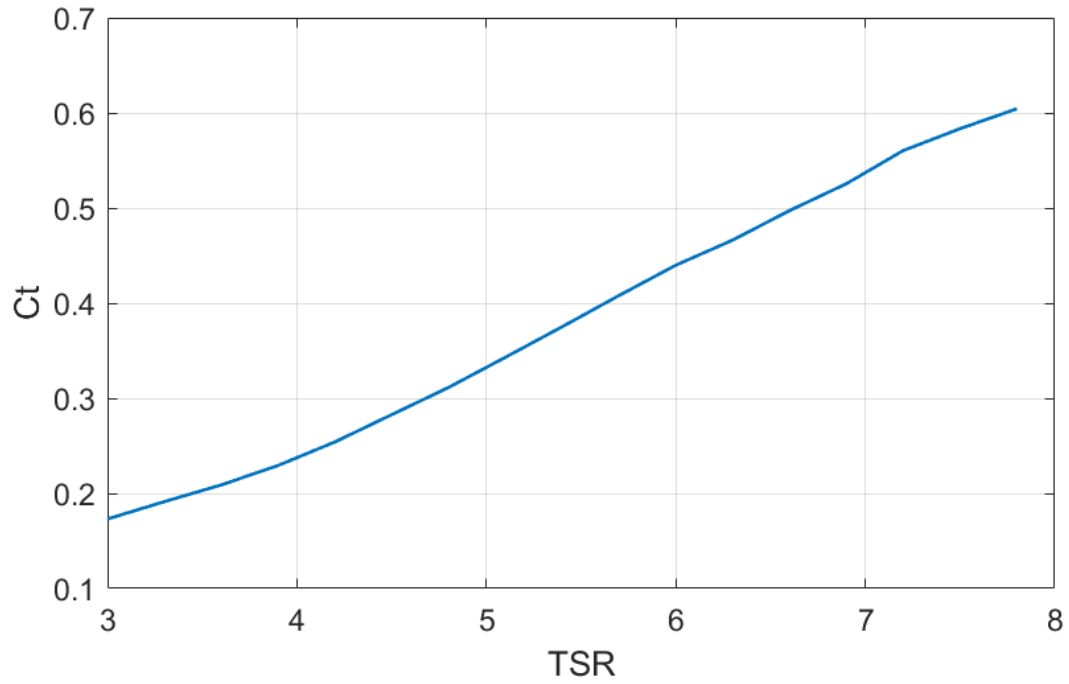
Where ρ is the air density, U is the wind inflow speed, and A is the swept area of the rotor. The calculations for C_t were found using the equation:

$$C_t = \frac{T}{\frac{1}{2} \rho U^2 A} \quad (4.2)$$

Where T is the measured thrust. These calculated values were plotted versus the TSR value at each set point, and the resulting plots can be seen in Figure 4.11 (a) and (b).



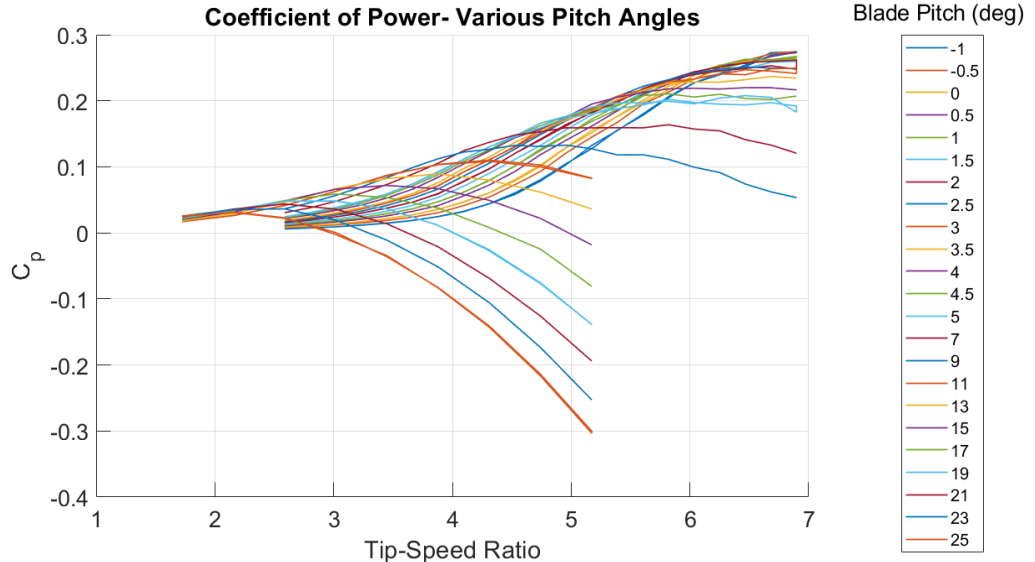
(a)



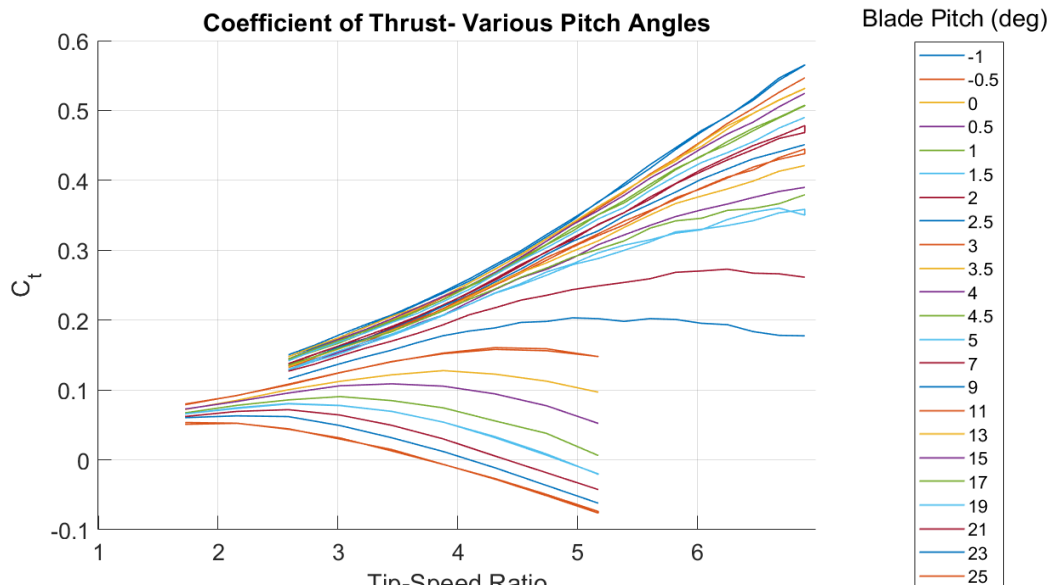
(b)

Figure 4.11: C_p (a) and C_t (b) curves at 0 degree AOA

The process described above was repeated for blade pitch angles between -1 degrees and 25 degrees. This created a surface plot of C_p vs. Blade Pitch vs. TSR and C_t vs. Blade Pitch vs. TSR as depicted in the waterfall plots in Figure 4.12 (a) and (b). These plots sufficiently covered the range of operation for the turbine and acted as a look-up chart for a performance target.



(a)



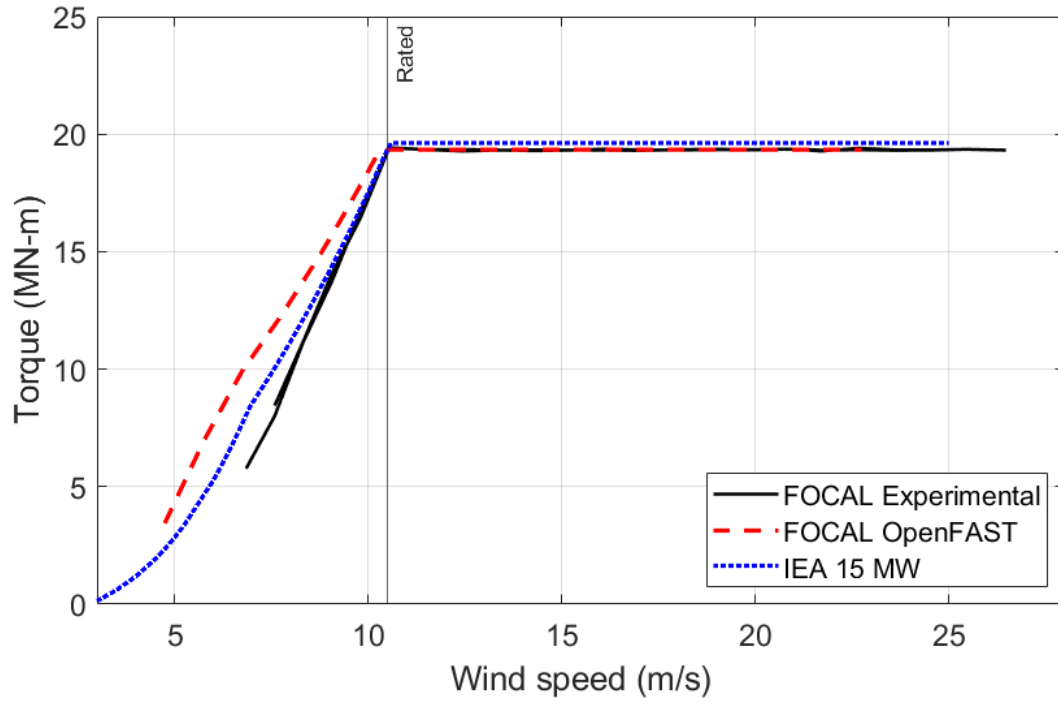
(b)

Figure 4.12: C_p (a) and C_t (b) surface plots over range of TSR and Blade Pitch

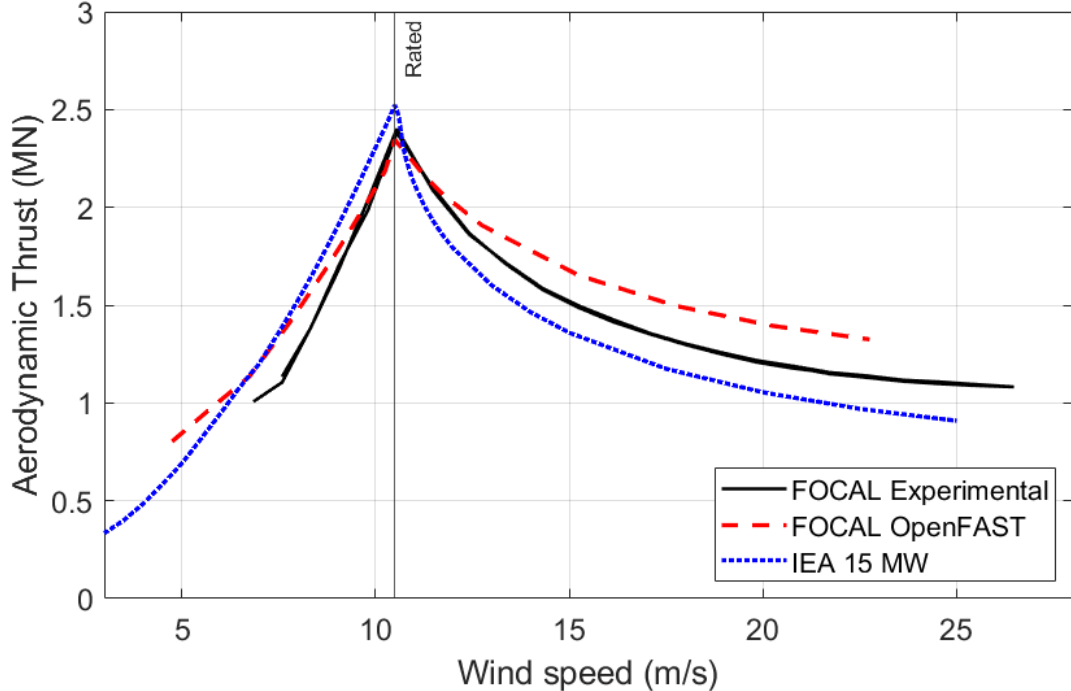
4.4.2. Turbine Response Validation

In addition to characterizing the performance of the turbine, the purpose of creating Cp and Ct surface maps over a range of pitch angles and TSR is to use those as an input to the ROSCO controller. This allows the turbine to operate independent of predetermined rpm and blade pitch set points, and to use the changing wind speed of the environment and the relation through TSR to the resulting torque and thrust responses to determine the optimal change in operational setting to achieve optimal performance. The controller monitors and makes fine adjustments to rpm under rated conditions, and to the blade pitch in above rated conditions to tune in the performance response throughout the test. Through using the Cp and Ct data to actively control the turbine, this allowed for an experiment to be run with the turbine over a range of wind speeds starting in below rated, through transition, and into the rated and above rated conditions. From this experiment, the torque and thrust values were measured, giving an expected performance in a real operational environment.

In order to validate the performance seen of the as-build basin tested turbine, an OpenFAST model was developed using the as-built properties at full scale, outlined in the as-build design document [18]. This model was used to run the same cases as described for the basin tested as-built model using the ROSCO controller feedback. And therefore created a set of torque and thrust performance predictions for a range of wind speed values, as well as the rpm and blade pitch settings used to accomplish those results. Figure 4.13 (a) and (b) shows a comparison of the IEA 15 MW torque and aerodynamic thrust to the FOCAL Experimental turbine and the FOCAL OpenFAST simulation turbine, and Figure 4.14 (a) and (b) show the corresponding controller response blade pitch and rpm settings for each case.

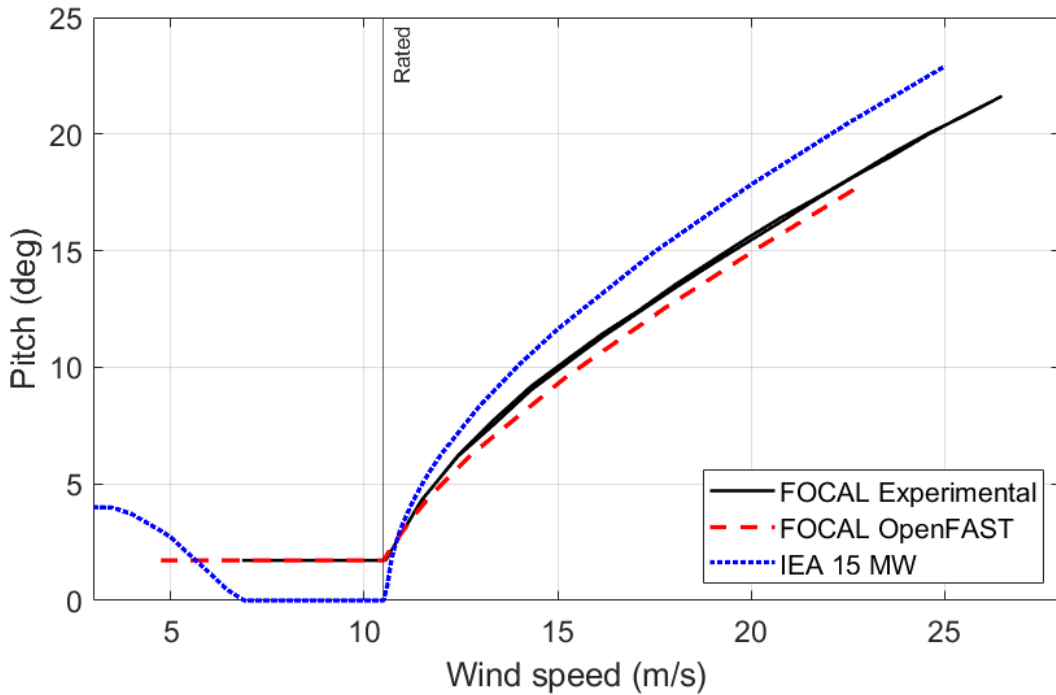


(a)

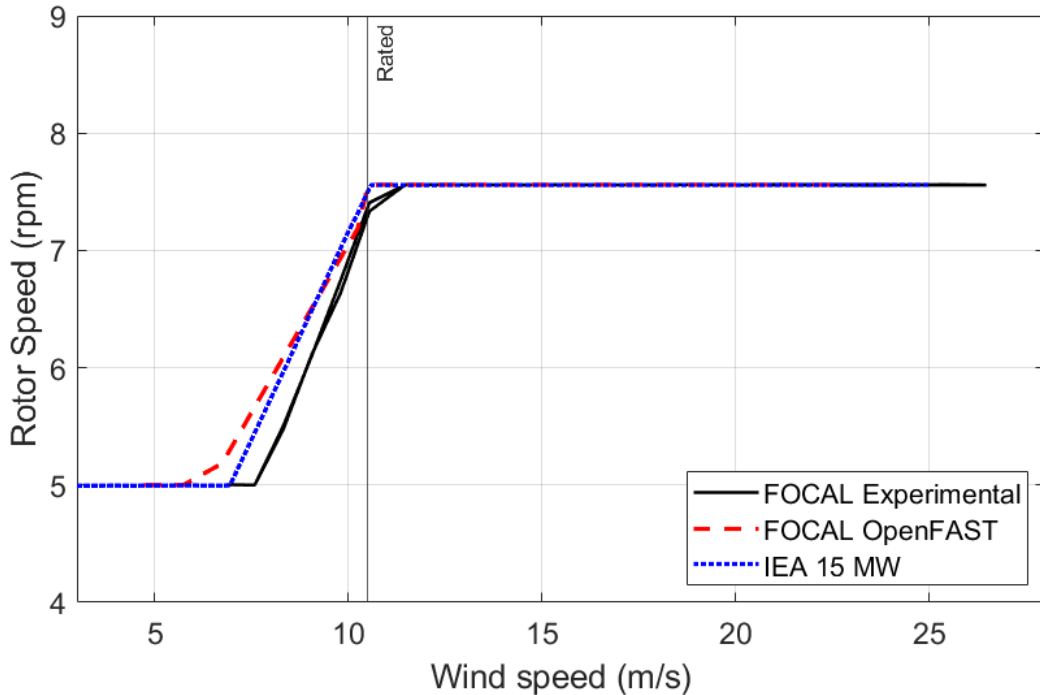


(b)

Figure 4.13: Full-scale experimental and theoretical Torque (a) and Thrust (b) performance curves of as-built scale model compared to IEA 15 MW performance



(a)



(b)

Figure 4.14: Full-scale experimental and theoretical Blade Pitch (a) and RPM (b) response curves of as-built scale model compared to IEA 15 MW response

The shown rated wind speed condition is the IEA 15 MW full scale wind speed value of 10.5 m/s. In order to show the comparison at rated, the FOCAL Experimental and FOCAL OpenFAST data wind speed was shifted back down by 20% to reflect the true rated condition. The FOCAL experimental results appear as a double blade line because the tests were run as wind speeds increased then decreased through the range shown. The thrust results for the IEA 15 MW turbine as presented in the reference document [3] represent the Rotor Thrust as opposed to the aerodynamic thrust. This means that the effect of the rotor mass was being translated through the shaft during operation, further increasing the values. In order to properly scale the aerodynamics of the rotor, that portion of the thrust force was excluded to determine the FOCAL targets by subtracting the blade and connector mass. The calculation for aerodynamic thrust is as shown below.

$$Thrust_{Aero} = Thrust_{Rotor} - [(3 * m_{blade} + m_{connector}) * g * \sin(6 \deg)] \quad (4.3)$$

Where m_{blade} is the individual IEA 15 MW turbine blade mass of 65.25 tons, and $m_{connector}$ is the blade connection mass of 58 tons, and g is the acceleration due to gravity. For example, at rated the IEA 15 MW turbine has a rotor thrust of 2.78 MN and a corresponding aerodynamic thrust of 2.52 MN. The aerodynamic thrust target values were further reduced to account for the difference in fresh vs. salt water design. Figure 4.13 (b) shows the aerodynamic thrust response for the IEA 15 MW turbine, which when adjusted for fresh water conditions, results in a rated trust target of 2.45 MN. The rated aerodynamic thrust value for the as-built FOCAL turbine was found to be 2.42 MN, which only differed by 1.2%, which was deemed to be close enough for performance-match target. As seen in Figure 4.13 (a) the IEA 15 MW turbine reaches a rated torque at 19.6 MN-m, which when adjusted to the fresh water target is 19.1 MN-m. The as-built FOCAL turbine reaches rated at 19.3 MN-m, which differed from the target by only 0.87%, deemed an acceptable error. Therefore, taking into account the performance match and fresh water adjustments, it can be concluded that the as-built FOCAL model accomplished the goal of being a performance-matched scale model of the IEA 15 MW reference turbine. The IEA 15 MW turbine response above rated also followed a difference pitch control pattern due to the differences in rotor design, meaning that the blades were feathered more to accomplish the same torque response.

The OpenFAST model does not account for the real world variations in blade geometry due to manufacturing and utilizes mathematical models that can only capture limited environmental variations seen in actual operation. But most importantly, the OpenFAST model only reads in airfoil performance data for each blade section at the rated Reynold's number, therefore, as seen in the torque and thrust plots, the performance curves for the OpenFAST model differ from the experimental results for much of the below rated and above rated condition ranges. But as can be noted from the figures, around rated, the predicted and actual operational performance is very similar. Because the controller only adjusts rpm below rated, the differences in performance in that range are due to the difference in control of rotor speed between the simulation and experimental model, but in the above rated zone, rpm is held constant and the differences result from the blade pitch response. In the above rated condition, a higher blade pitch angle can be used to accomplish the same torque value due to the Reynold's number effects resulting in a lower actual needed thrust force than predicted by the simulation.

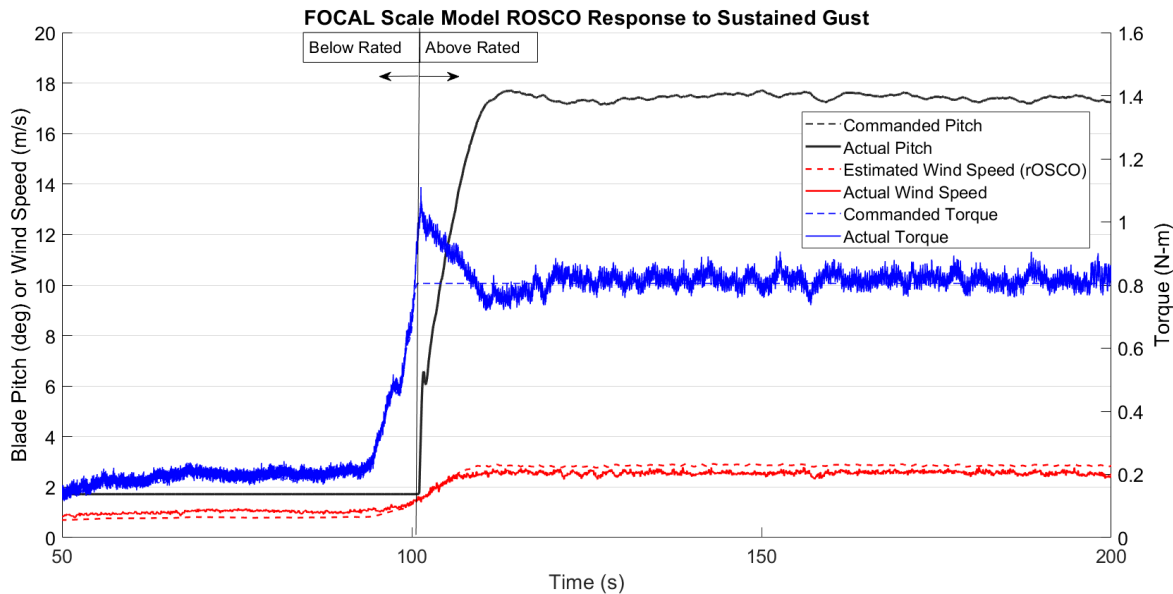


Figure 4.15: Turbine response to sustained gust

After the validation of the performance match, much more work was done by other members of the FOCAL team to evaluate the turbine response using ROSCO. For the sake of completeness, this thesis includes a sample of one such test run as seen in the TORQUE publication [19] but does not claim

ownership of the results created from that research. Figure 4.15 shows the turbine response to a wind gust that carries the turbine from below rated to an above rated set point. As shown in blue, the controller sets the torque target to the rated condition and adjusts the blade pitch from 2 degrees before the gust to just above 17 degrees at the sustained higher wind speed, as can be seen with the black line. The turbine pitch controls were much more sensitive and quick responding than pitch controls that would be on an actual full-scale turbine, therefore the pitch response rate was limited in ROSCO to minimize the amount of overshoot in pitch. Because the measured blade pitch shown as a solid black line in the figure below, and the ROSCO commanded pitch, shown as a dashed black line, are directly on top of each other, that shows that the pitch assemblies are operating as designed with no binding during active pitching to be seen. The variation seen in the actual torque is mostly due to wind speed variability, and is adjusted for by the constant slight changes to blade pitch, resulting in an overall torque average in the above rated zone that is very close to the commanded torque.

CHAPTER 5: CONCLUSIONS

The purpose of the research outlined in this thesis was to scale, design, manufacture, assemble, characterize, and test a performance-matched 1/70th scale model of the IEA 15 MW turbine. This campaign was unique, as it is the first known test of a performance matched modal turbine tested in a wind environment with active blade pitch controls as specified by a full scale turbine controller using the characterized Cp and Ct maps found for the specific turbine. The test result also acts as a validation dataset for modelers when testing model simulation codes in OpenFAST to predict the response of the system in any wind environment. The characterization work outlined in this thesis also supports that the turbine would provide the correct forces and frequencies to run a realistic wind/wave basin test when affixed to a scaled floating hull platform. Therefore the goals of the research were largely met through the realization of the FOCAL 1/70th scale model for basin testing.

5.1. Overview of Design and Results

The final design of the model was suitable for the testing conducted in the test program. The scale model turbine design was ultimately successful in producing an accurately scaled thrust output at the turbine's rated operational TSR. The scale model's active blade pitch systems were also effective at providing a reliable response of blade pitch change in manual testing as well as under feedback control in a wind environment without binding. This resulted in a reliable controller implementation where rotor torque was controlled with only minor resulting noise, which was mainly due to the wind field. The turbine nacelle and hub were also adequate at providing the structure needed to house the needed instrumentation. The blades performed as well as predicted, with minor issues due to flexibility. Throughout the testing of the turbine, areas of improvement were identified for future turbine designs.

One area of potential design improvement would be in the orientation, layering, and reinforcing of the manufactured blade skins. The method used had proved adequate for model testing in past research of scale model turbines with smaller rotor diameters and airfoils that had a larger thickness to chord ratio, but issues were found with deflection when building a blade that was as long and as thin as the FOCAL

blades. For future blade designs, flexibility could be a target for scaling as it was shown that the “rigid” target was not very feasible for this type of blade design, but the flexibility was within the correct ballpark of the full-scale blades. This could be done by using material testing data like that shown in Appendix D, and running a finite element analysis of a blade design, or to experimentally test different spar designs to accomplish a target flexibility. As these blade get longer and thinner, pre-bend could also be designed into the blades to provide further deflection protection. A second consideration would be in further weight reduction in the nacelle and hub by use of more specialized light weight components. Due to the small scaling ratio from full scale to model scale, the mass targets proved to be very challenging to meet even while building most components out of thin aluminum, carbon fiber, and foam. Another additional challenge to be addressed in future research would be into further vibration analysis due to turbine rotation to reduce the noise during operation. Testing could be done to determine if the source is aerodynamic and due to blade geometry variation by modeling the blades from 3D scan data and running the as-built blade in OpenFAST. Alternatively, data collected from a wake survey could be analyzed to determine if the blades are stalling at different times or in different areas of the wind field. The nacelle could also be evaluated to determine if there is any binding of bearing during operation causing cyclical forcing.

5.2. Future Work

Future research is planned for the scale turbine model in campaign 4 of the FOCAL program. This will involve mounting the turbine to a scale floating hull model equipped with tuned mass dampers (TMDs), and testing the full assembly as shown in Figure 5.1 in a combination of Froude scaled wave environments with corresponding performance-matched wind cases. The campaign will test the response of both blade pitch and TMD controls together using ROSCO while the floating system is subject to multiple test cases. This data will be used to further validate computer models of the fully-coupled servo-aero-hydro-elastic systems used to test a wide range of operational cases.



Figure 5.1: Turbine/Hull assembly for combination wind and wave testing

As mentioned in section 4.2.3, further work is planned in capturing the actual geometry of each blade using 3D scan data. These properties can be used by modelers to adjust their geometric and aerodynamic models of the blades to further tune the torque and thrust response of the computer simulated models. A Matlab tool is in development to convert the 3D point cloud from the scanner to usable section data. Also relating to blades, the current design could be improved upon by further developing the manufacturing process outlined in section 3.2.3 as it proved to yield a good leading edge geometry. Additional research could be done into light-weight methods of reinforcing the blade skin to provide further support to the blade structure, and therefore decreasing the flexibility of the finished blade. This would allow for operation in a wider range of above rated conditions and allow the C_p and C_t maps to be expanded further.

5.3. Contributions

In conclusion, the 1/70th scale wind turbine was found to meet the required targets for operation for the performance-matched scale model of the IEA 15 MW reference wind turbine. The turbine matched the rated thrust and torque targets and proved to show a comparable response under torque control using ROSCO over a full range of operating conditions. A list of accomplishments from this research are as follows:

- Design of accurate and robust blade pitch control mechanisms
- Design of new blade manufacturing method that yielded well-performing turbine blades
- Building of a performance-matching 1/70th scale model of the IEA 15 MW Turbine
- Validation of active blade pitch controls under full torque control using ROSCO

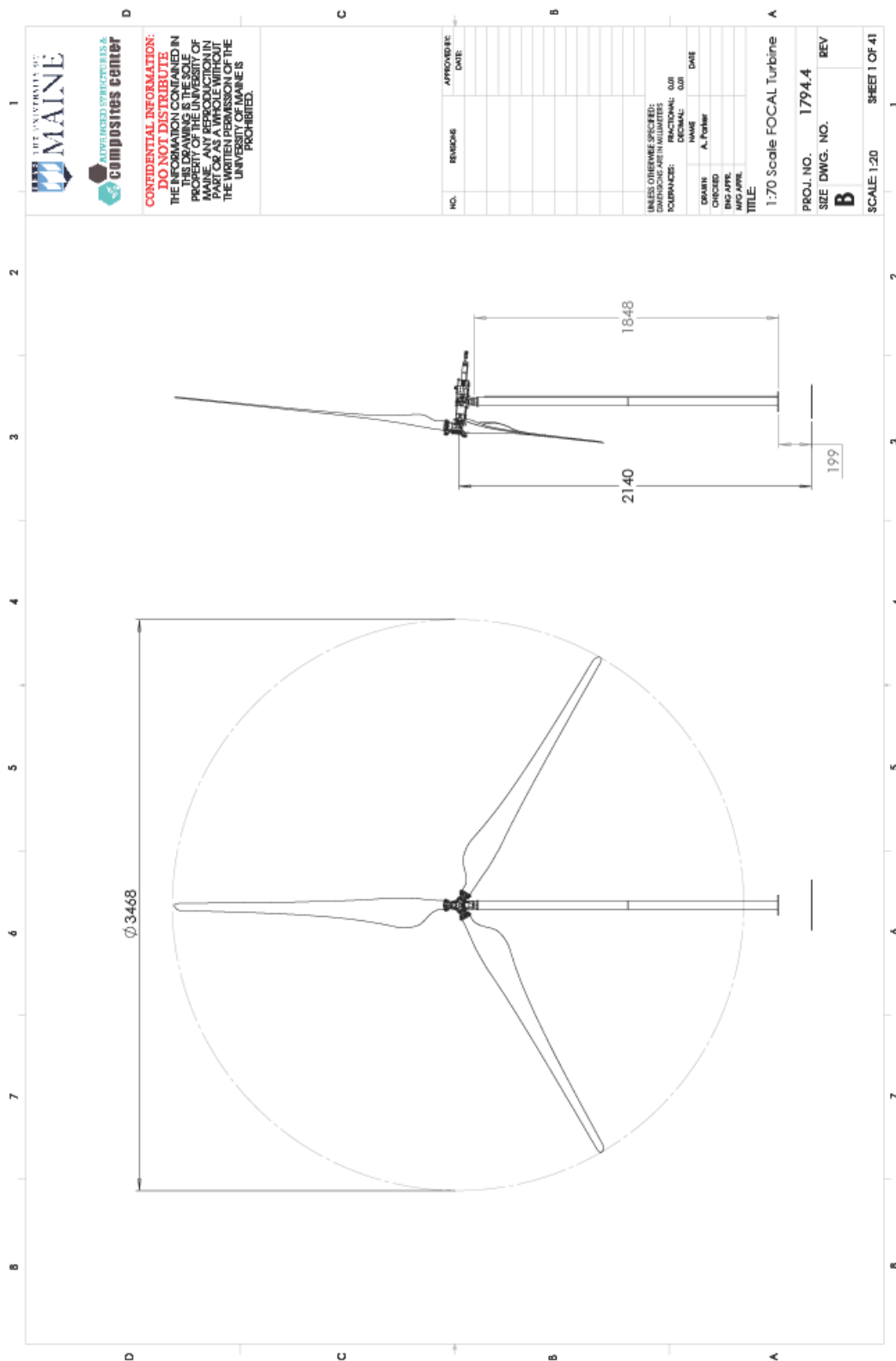
This research will hopefully support further development of simulation modeling of turbines utilizing open source full scale controllers, and act as a validation of design for the IEA 15 MW reference turbine. Ultimately, this research will support the further development and commercialization of offshore floating wind energy in the United States and aid in the future growth of green energy production.

BIBLIOGRAPHY

- [1] Schwartz, M., et. al. 2010 Assessment of offshore wind energy resources for the United States, National Renewable Energy Lab. (No. NREL/TP-500-45889)
- [2] Allen, C., et. al. 2020 Definition of the UMaine VolturnUS-S reference platform developed for the IEA Wind 15-megawatt offshore reference wind turbine, National Renewable Energy Lab. (No. NREL/TP-5000-76773)
- [3] Gaertner, E., et. al. 2020 Definition of the IEA 15-Megawatt Offshore Reference Turbine, National Renewable Energy Lab. (No. NREL/TP-5000-75698)
- [4] Heronemus, W. E. 1972 Pollution-Free Energy From Offshore Winds, Eighth Annual Conference and Exposition Marine Technology Society, Washington D.C.
- [5] Musial, et. al. 2004 Feasibility of floating platform systems for wind turbines. In 42nd AIAA aerospace sciences meeting and exhibit (p. 1007)
- [6] Martin, H.R. 2011 Development of a scale model wind turbine for testing of offshore floating wind turbine systems.
- [7] Martin, H.R., et. al., 2014. Methodology for wind/wave basin testing of floating offshore wind turbines. Journal of Offshore Mechanics and Arctic Engineering, 136(2).
- [8] Bottasso, C.L., et. al. 2014 Wind tunnel testing of scaled wind turbine models: Beyond aerodynamics. Journal of wind engineering and industrial aerodynamics (Vol. 127, p.11-28)
- [9] Sandner, F., et. al. 2015 Model building and scaled testing of 5MW and 10MW semi-submersible floating wind turbines. In Proceedings of 12th Deep Sea Offshore Wind R&D Conference, EERA DeepWind'2015
- [10] Yu, W., et. al, 2018 Qualification of innovative floating substructures for 10MW wind turbines and water depths greater than 50 m. Technical report, LIFES50+ project.
- [11] Bayati, I., et. al. 2016 On the functional design of the DTU10 MW wind turbine scale model of LIFES50+ project. In Journal of Physics: Conference Series (Vol. 753, No. 5, p. 052018). IOP Publishing.
- [12] Bayati, I., et. al. 2016\ Wind tunnel validation of AeroDyn within LIFES50+ project: imposed Surge and Pitch tests. In Journal of Physics: Conference Series (Vol. 753, No. 9, p. 092001). IOP Publishing.
- [13] Bayati, I., et. al. 2016 On the aero-elastic design of the DTU 10MW wind turbine blade for the LIFES50+ wind tunnel scale model. In Journal of Physics: Conference Series (Vol. 753, No. 2, p. 022028). IOP Publishing.
- [14] Abbas, N., et. al. 2021 A Reference Open-Source Controller for Fixed and Floating Offshore Wind Turbines, Wind Energ. Sci. Discuss. (Preprint wes-2021-19)
- [15] NREL: ROSCO Toolbox. Version 2.3.0, https://github.com/NREL/ROSCO_toolbox/tree/focal, 2021.
- [16] Kimball, R., et. al. 2014 Wind/wave basin verification of a performance-matched scale-model wind turbine on a floating offshore wind turbine platform. In International Conference on Offshore Mechanics and Arctic Engineering (Vol. 45547, p. V09BT09A025). ASME.

- [17] Goupee, A.J., et. al., 2015. A Calibrated Blade-Element/Momentum Theory Aerodynamic Model of the MARIN Stock Wind Turbine. The Twenty-fifth International Ocean and Polar Engineering Conference.
- [18] Roberts, A., et. al. 2021 FOCAL Campaign 1 Validation Definition Document. National Renewable Energy Lab. (No. NREL To be published)
- [19] Kimball, R., et. al. 2022 Results from the FOCAL experiment campaign 1: turbine control co-design, In Proceedings of 9th The Science of Making Torque from Wind Conference, TORQUE, Delft Netherlands (Accepted for publication)
- [20] NREL: IEA 15-240-RWT. <https://github.com/IEAWindTask37/IEA-15-240-RWT>, 2021.

APPENDIX A: SHOP DRAWINGS OF THE FOCAL TURBINE ASSEMBLY



ITEM NO.	PART NUMBER	QTY.
1	FN_FOCAL Nacelle	1
2	R_Rotor Assembly	1
3	TW_Tower assembly	1
4	Water line	1

D

C

B

A

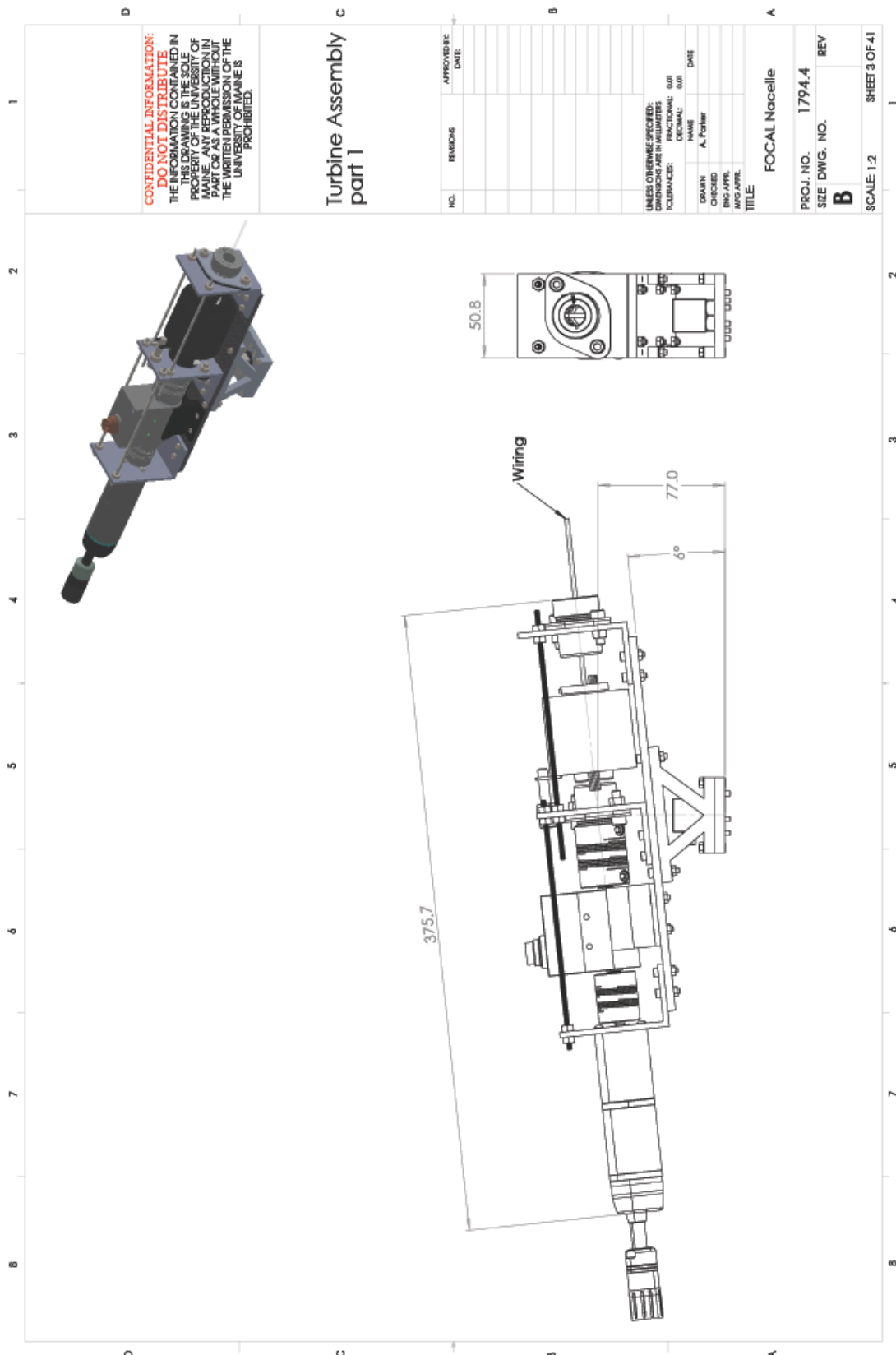
**CONFIDENTIAL INFORMATION:
DO NOT DISTRIBUTE**
THE INFORMATION CONTAINED IN THIS DRAWING IS THE SOLE PROPERTY OF THE UNIVERSITY OF MAINE. ANY REPRODUCTION IN PART OR AS A WHOLE WITHOUT THE WRITTEN PERMISSION OF THE UNIVERSITY OF MAINE IS PROHIBITED.

NO.	REVISION	APPROVED BY:

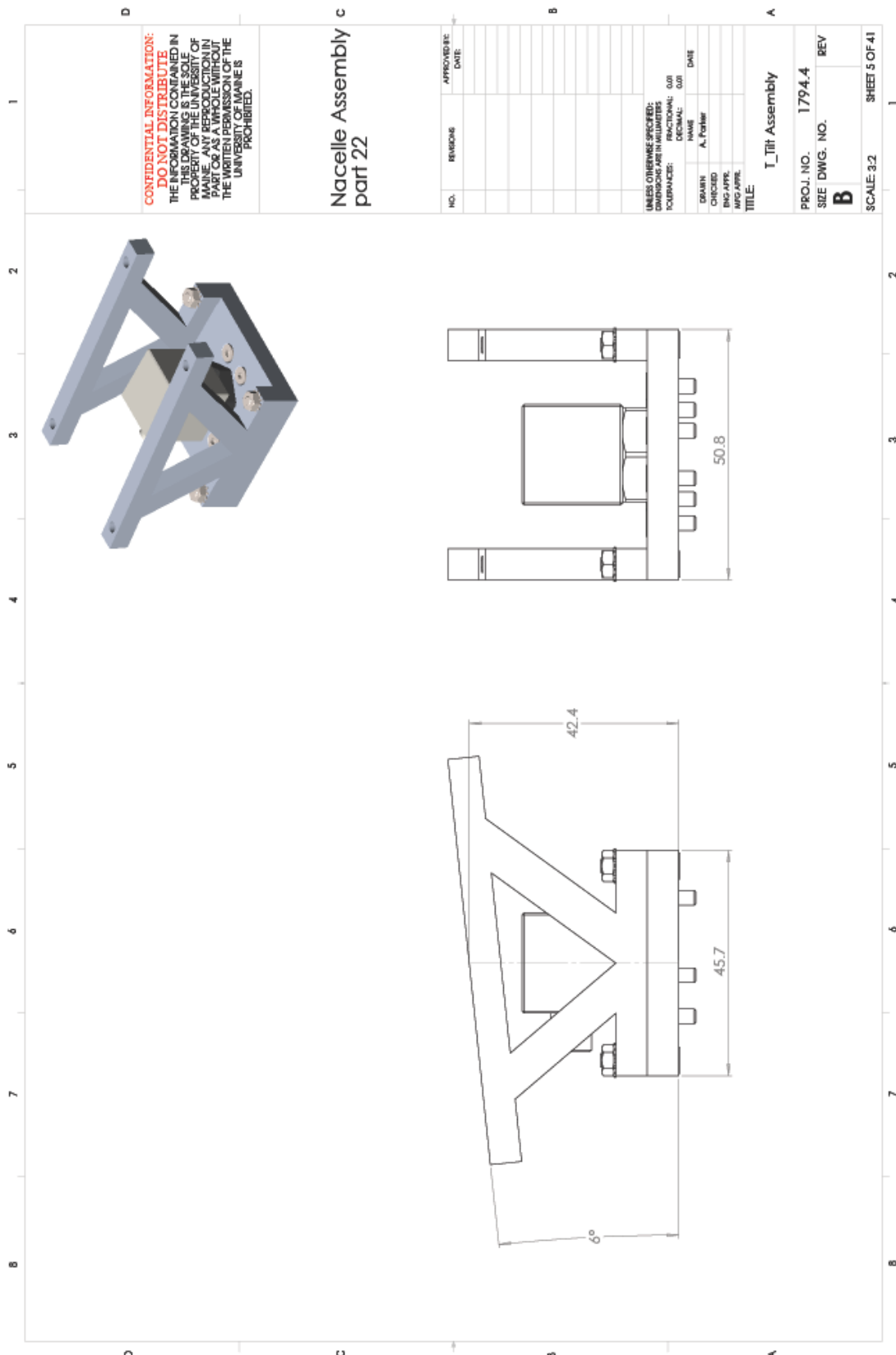
UNLESS OTHERWISE SPECIFIED:
DIMENSIONS ARE IN MILLIMETERS
TOLERANCES: FRACTIONAL: .001
DECIMAL: .001
NAME: DATE
DRAWN BY: A. Palmer
CHECKED BY: ENE APP.
MFG APP.
TITLE: 1:70 Scale FOCAL Turbine

PROJ. NO.	1794.4
SHEET DWG. NO.	B
REV	

SCALE: 1:16 SHEET 2 OF 4



ITEM NO.	PART NUMBER	QTY.	
1	FNL_Nacelle_Motor_ARSG030B-020C-3V1B5-HI0GSN-FUN	1	
2	FN3_Slip ring_Moog-AC6438-12	1	
3	FN4_Base plate_McMaster-B194K42	1	
4	McMaster1434K15	2	
5	B18.3.4M - 3 x 0.5 x 6 SBHCS --N	4	
6	socket head cap screw_#am	4	
7	B18.3.1M - 3 x 0.5 x 12 Hex SHCS - 1/2-12NHX	12	
8	B18.3.1M - 6 x 1.0 x 30 Hex SHCS - 30NHX	1	
9	B18.3.1M - 3 x 0.5 x 16 Hex SHCS - 16NHX	4	
10	B18.2.4.1M - Hex nut, Style 1, M5 x 0.8 --D-N	4	
11	B18.2.4.1M - Hex nut, Style 1, M3 x 0.5 --D-N	20	
12	B18.2.4.1M - Hex nut, Style 1, M6 x 1 --D-N	1	
13	B18.3.5M - 3 x 0.5 x 12 Socket FCHS - 1/2N	4	
14	B18.21.2M-External Tooth Lock Washers_AM3	4	
15	B18.2.4.2M - Hex nut, Style 2, M4 x 0.7 --D-N	16	
16	FN7_Saddle for Torque sensor	1	
17	FN9_Aluminum Mounts	1	
18	FN9_Aluminum Mounts	1	
19	FN9_Aluminum Mounts	1	
20	FN10_Snap ring spacer	2	
21	McMaster 95412A305	4	
22	T_Tilt Assembly Rev 2	1	
23	Nacelle Wiring	1	
24	McMaster 2463K51	1	
25	McMaster 9506T6	1	
26	McMaster 5909K12	2	
27	McMaster 5909K72	2	
28	McMaster 2463K6	1	
29	Torque Sensor_Interface_T6	1	



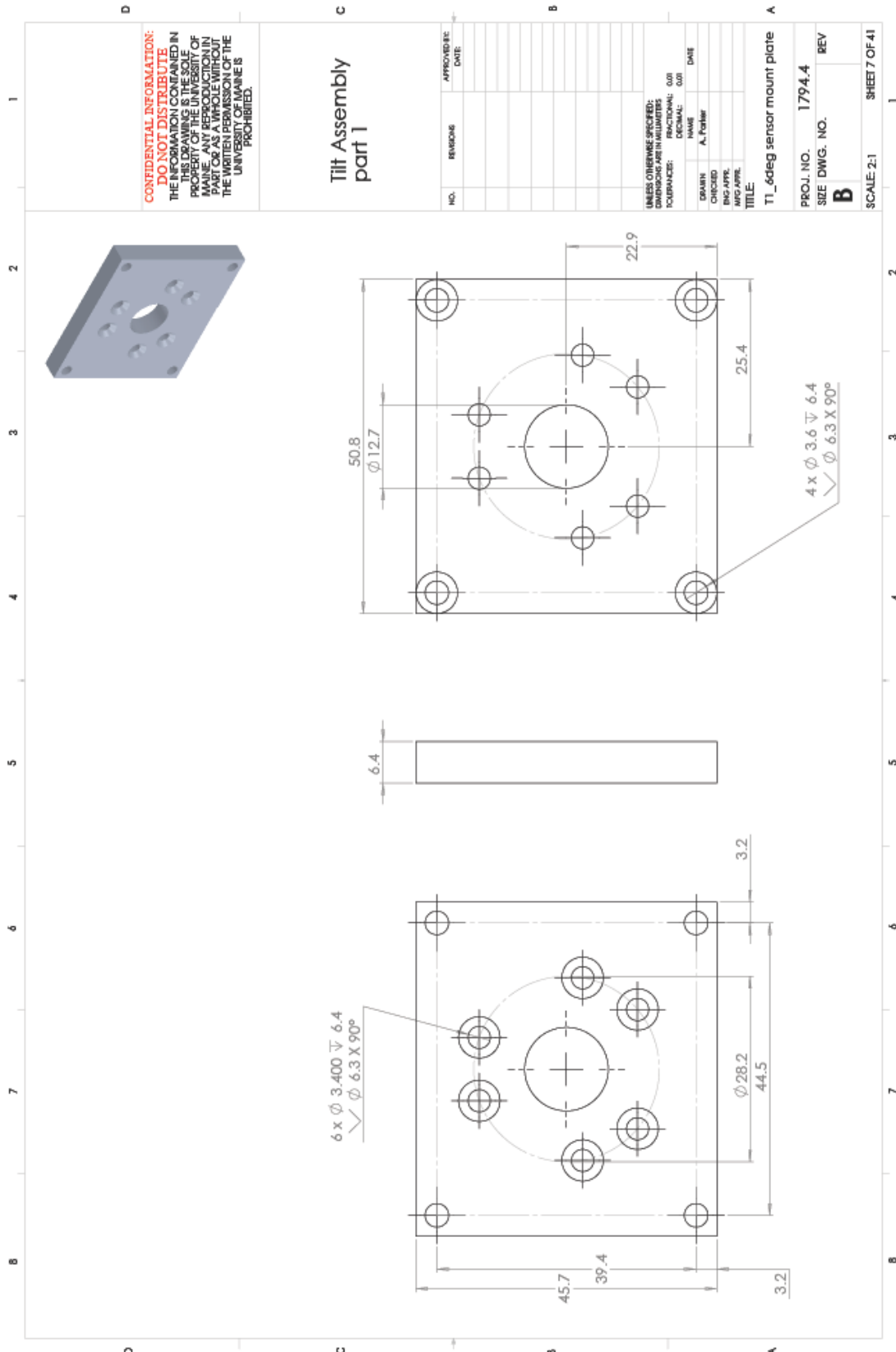
ITEM NO.	PART NUMBER	QTY.
1	T1_6deg Force sensor mount Rev 2	1
D 2	ASME B18.21.1 -0.129	4
3	B18.2.4.1M - Hex nut, Style 1, M3 x 0.5 -D-N	4
4	B18.3.5M - 3 x 0.5 x 16 Socket FCHS - 16N	4
5	B18.3.5M - 3 x 0.5 x 10 Socket FCHS - 10N	6
C 6	T2_6deg mounting wedge	2
7	PCB 080A12	1
8	PCB 081B05	1
9	PCB Accelerometer_3713F 112G	1

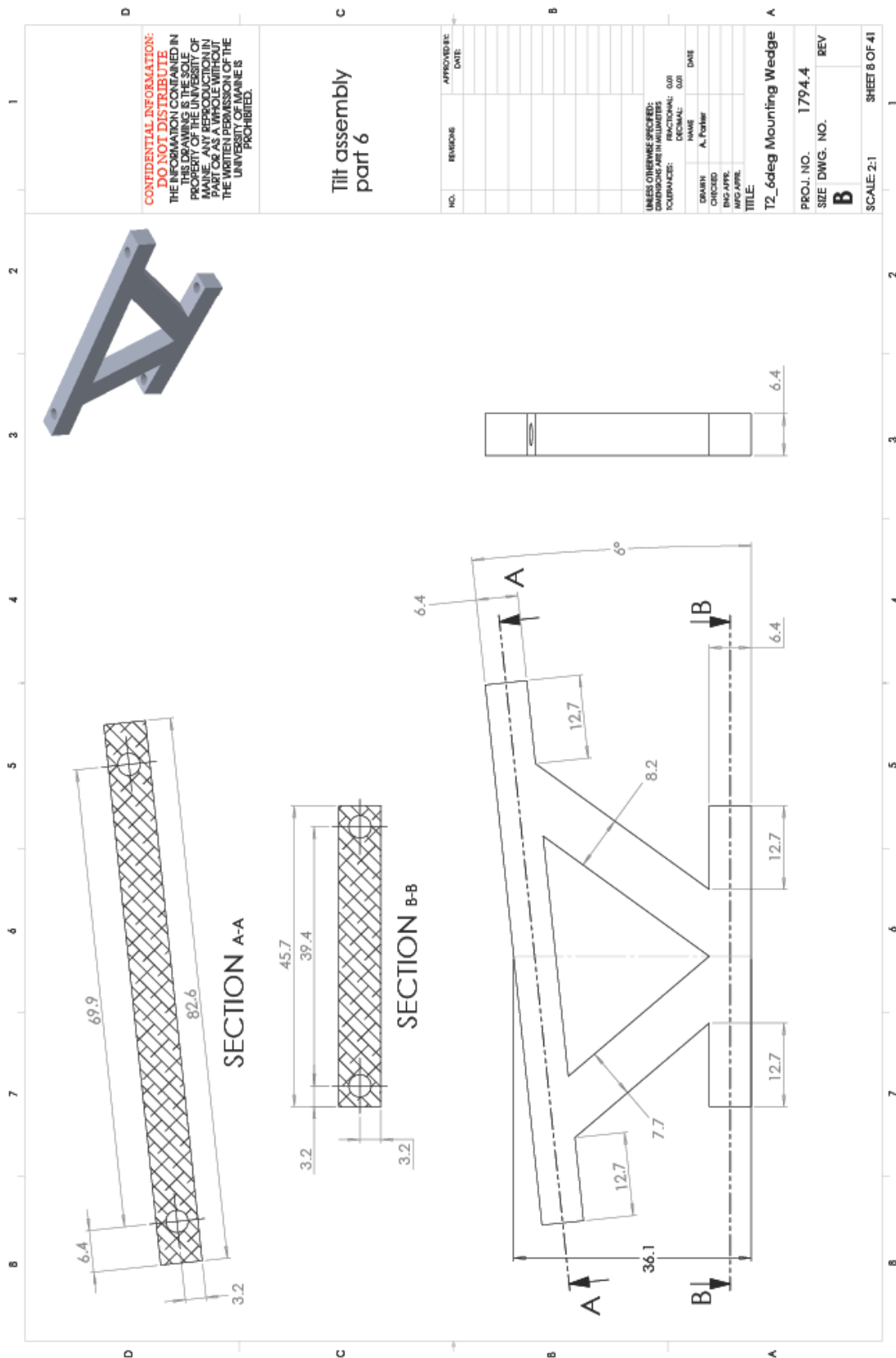
CONFIDENTIAL INFORMATION:
DO NOT DISTRIBUTE
 THE INFORMATION CONTAINED IN THIS DRAWING IS THE SOLE PROPERTY OF THE UNIVERSITY OF MANITOBA. ANY REPRODUCTION IN PART OR AS A WHOLE WITHOUT THE WRITTEN PERMISSION OF THE UNIVERSITY OF MANITOBA IS PROHIBITED.

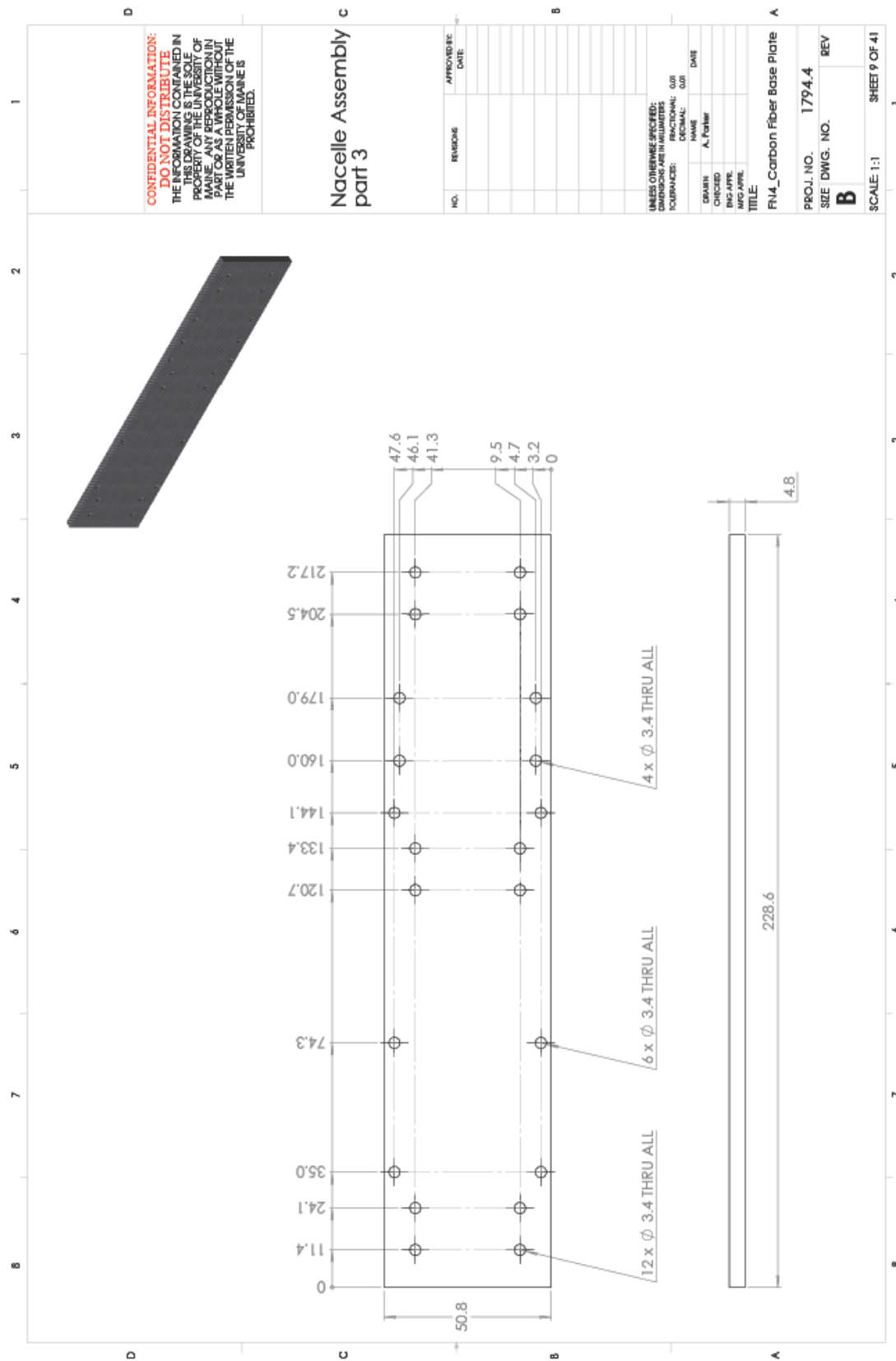
UNLESS OTHERWISE SPECIFIED:
 DIMENSIONS ARE IN MILLIMETERS
 TOLERANCES: FRACTIONAL: 0.001
 DECIMAL: 0.001
 NAME: DATE
 DRAWN BY: A. Poirier
 CHECKED BY: EKG APP.
 MFG APPROV.
 TITLE: T_Tilt Assembly

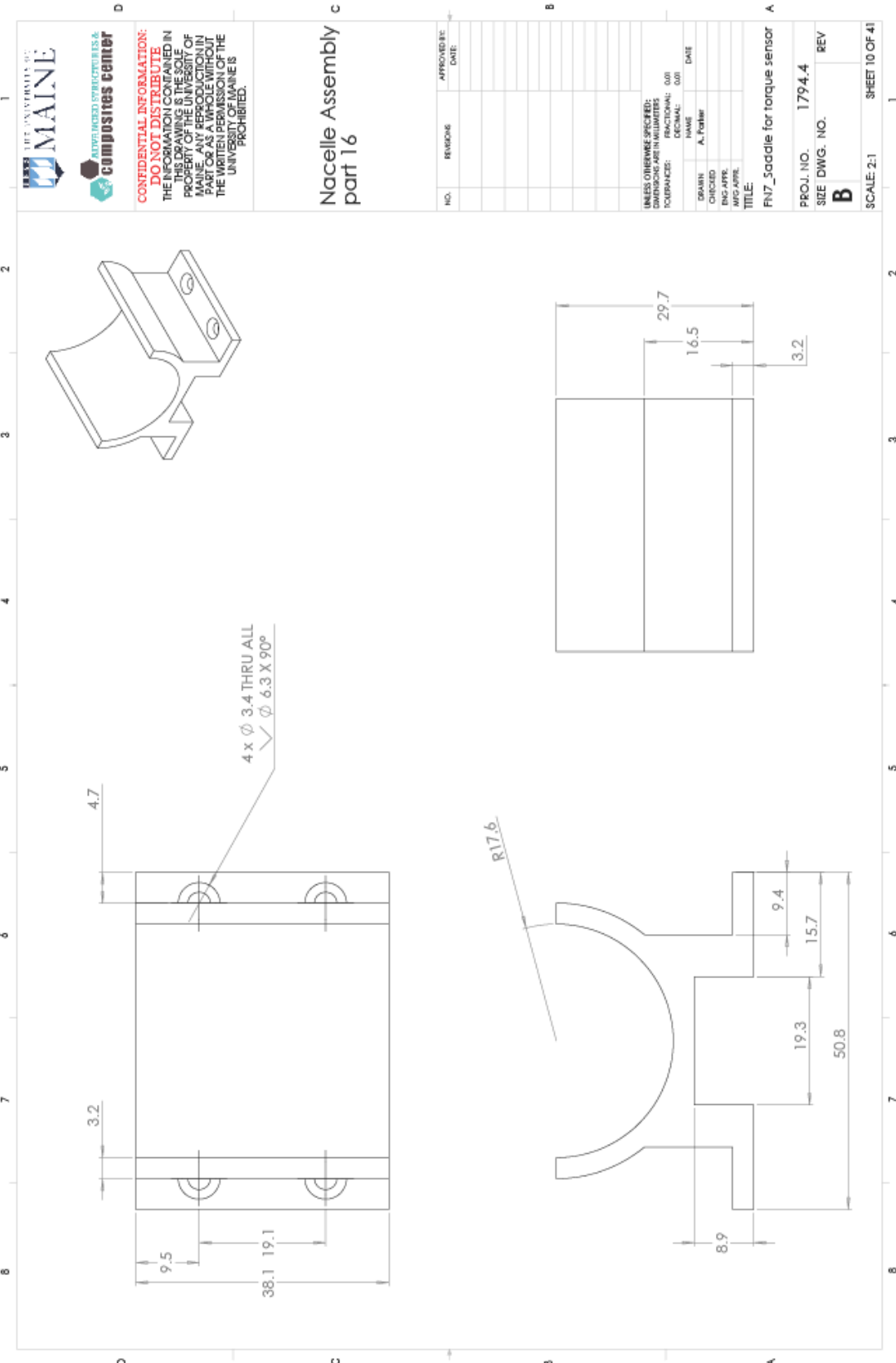
PROJ. NO. 1794.4
 SHEET DWG. NO. REV
B

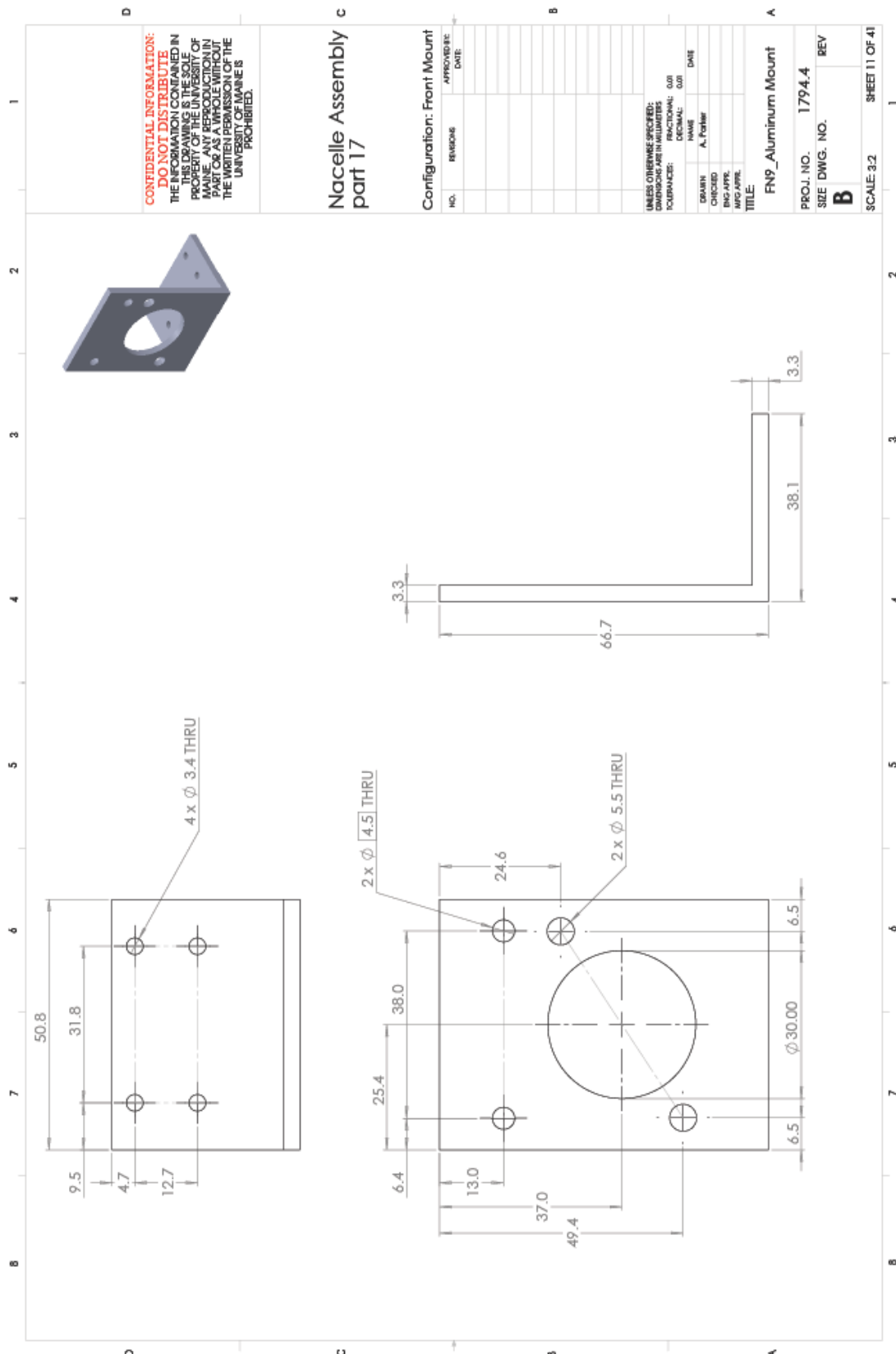
SCALE: 3:2 SHEET 6 OF 41

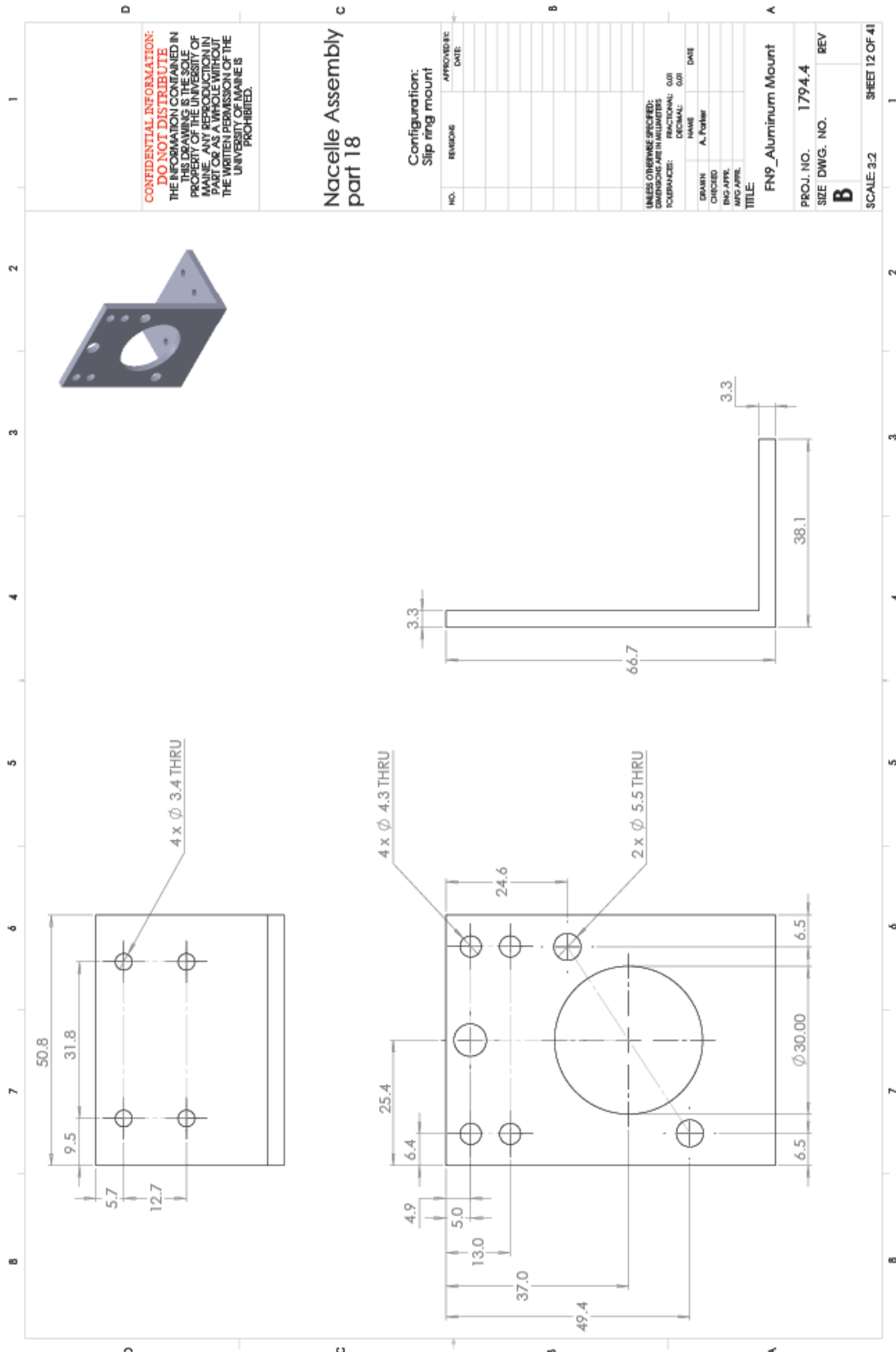


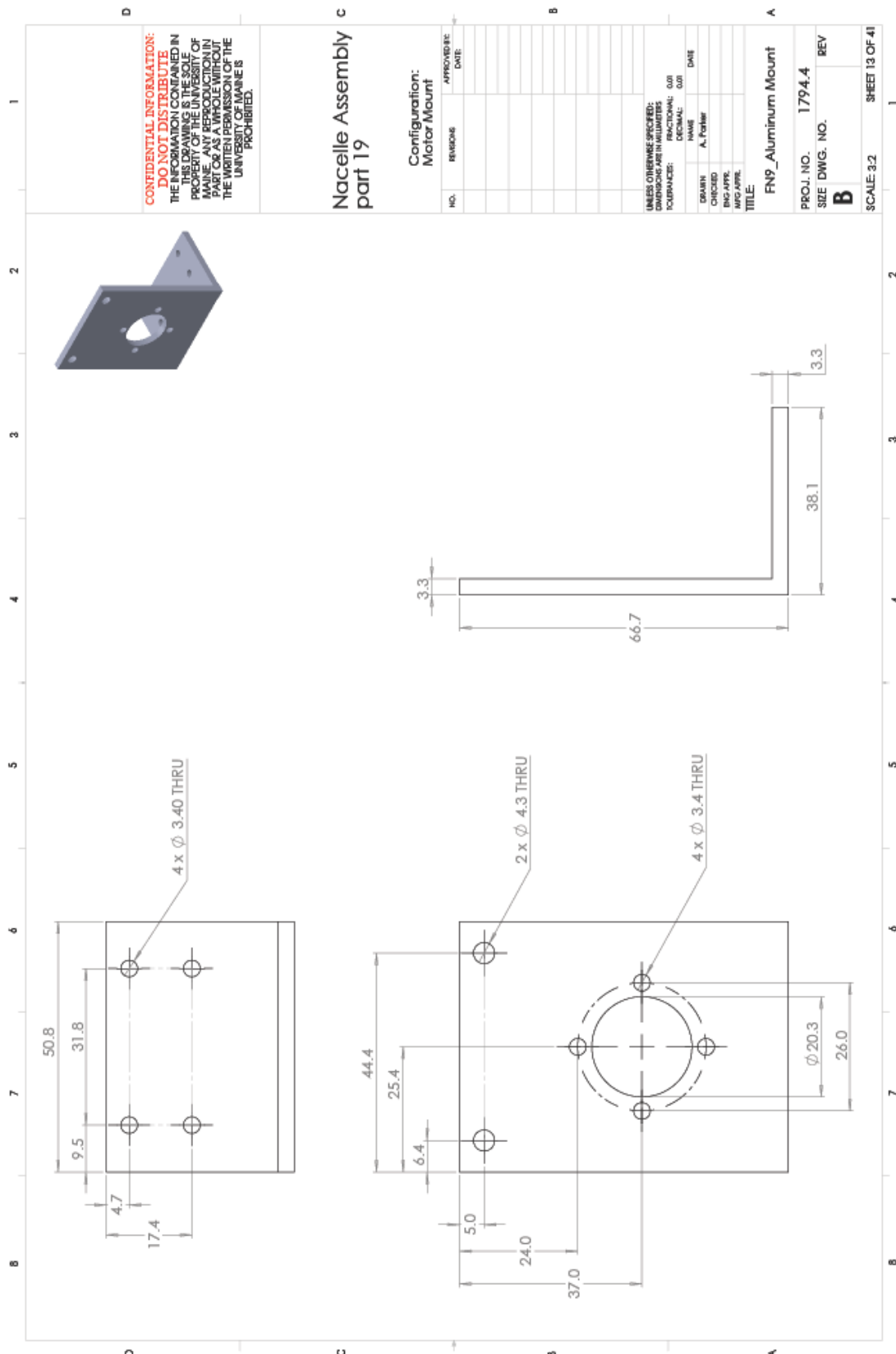


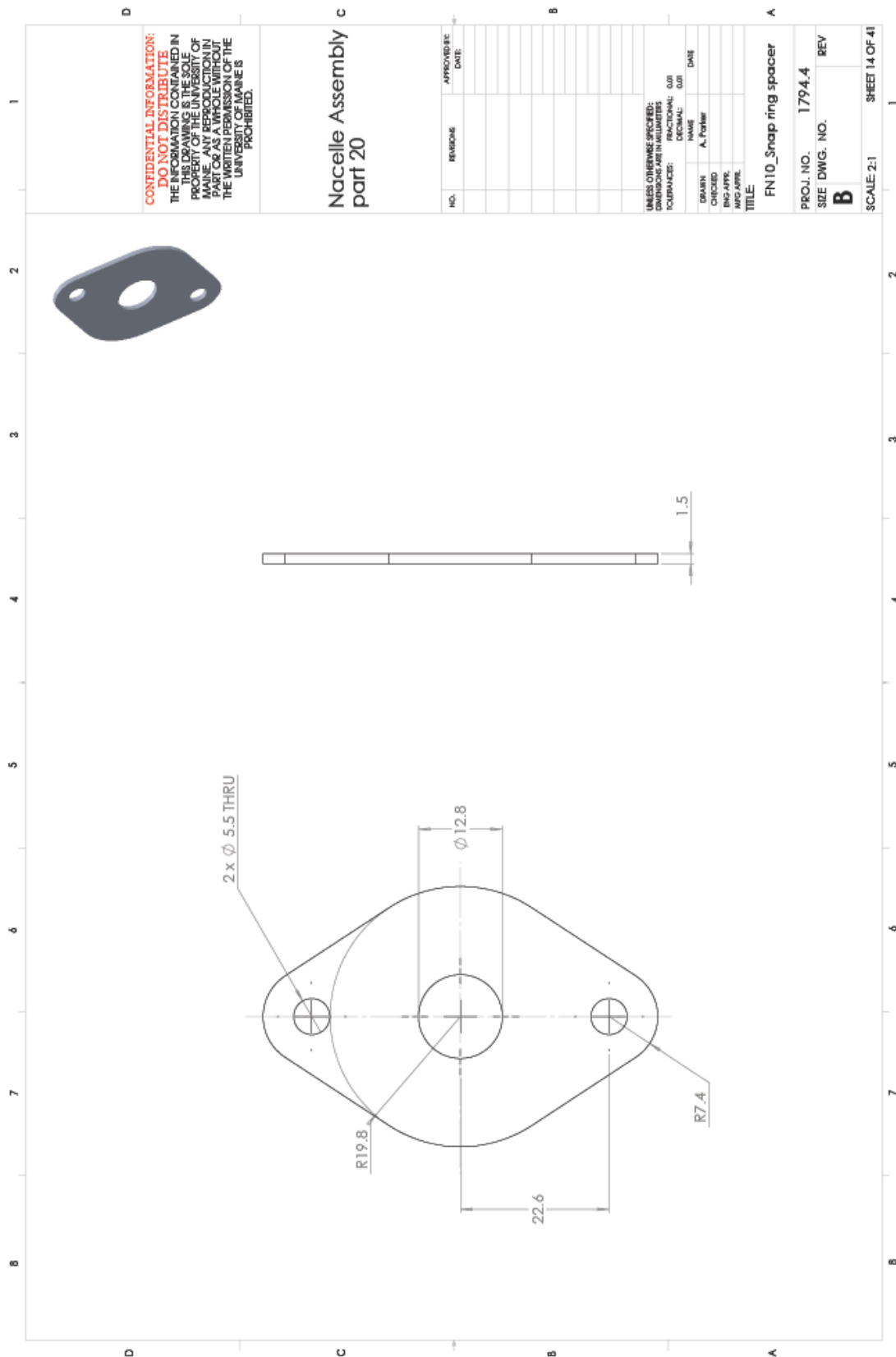


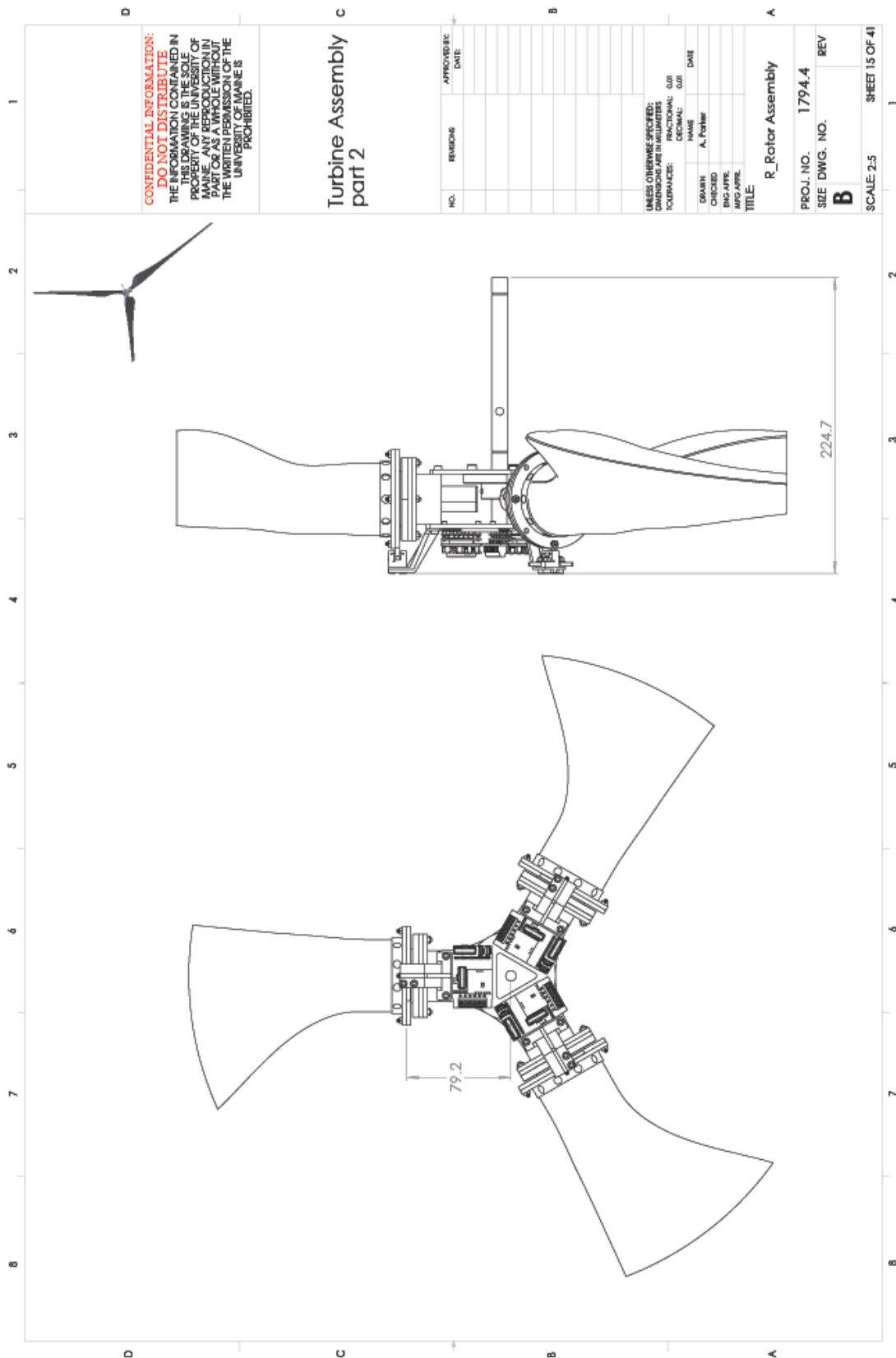




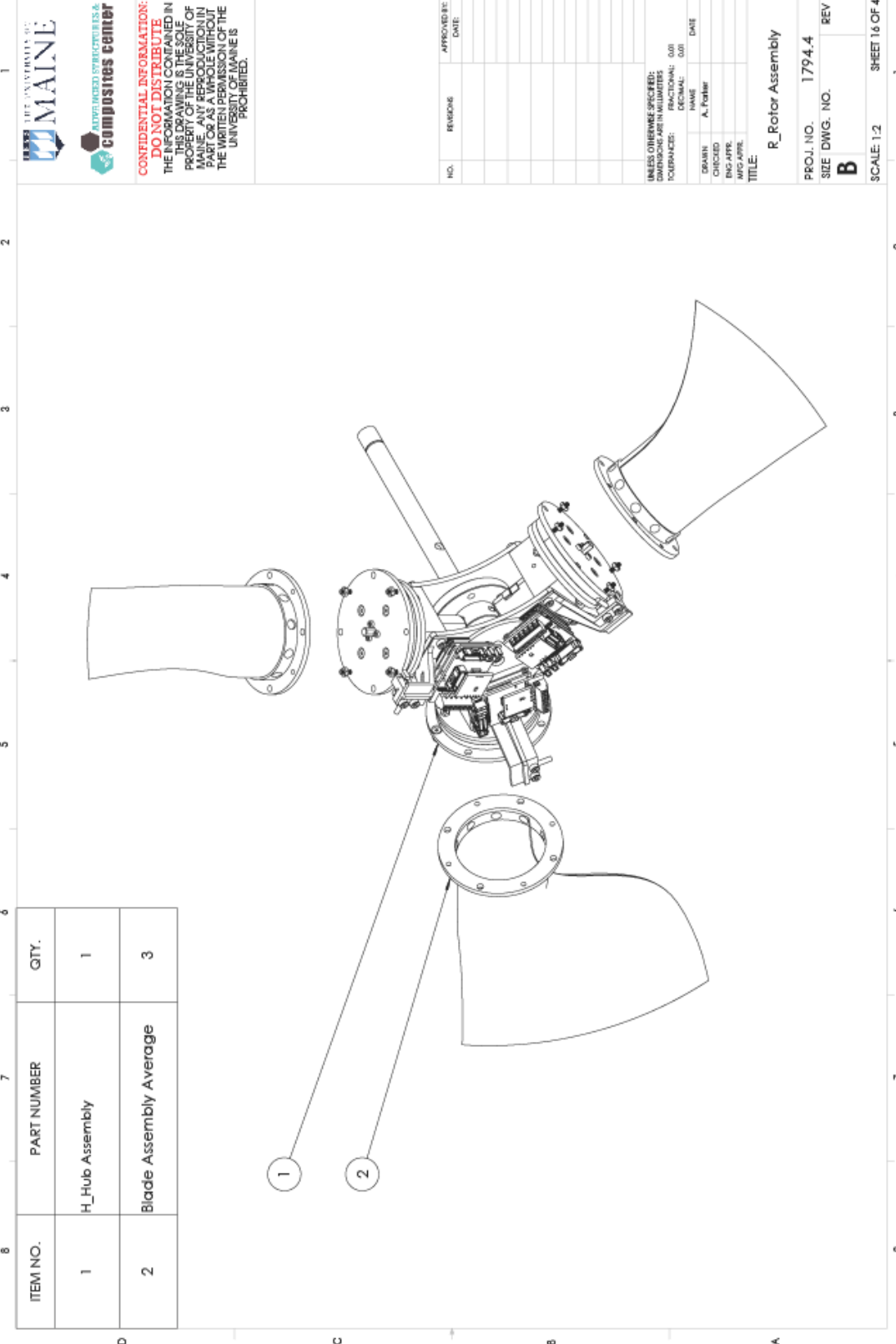


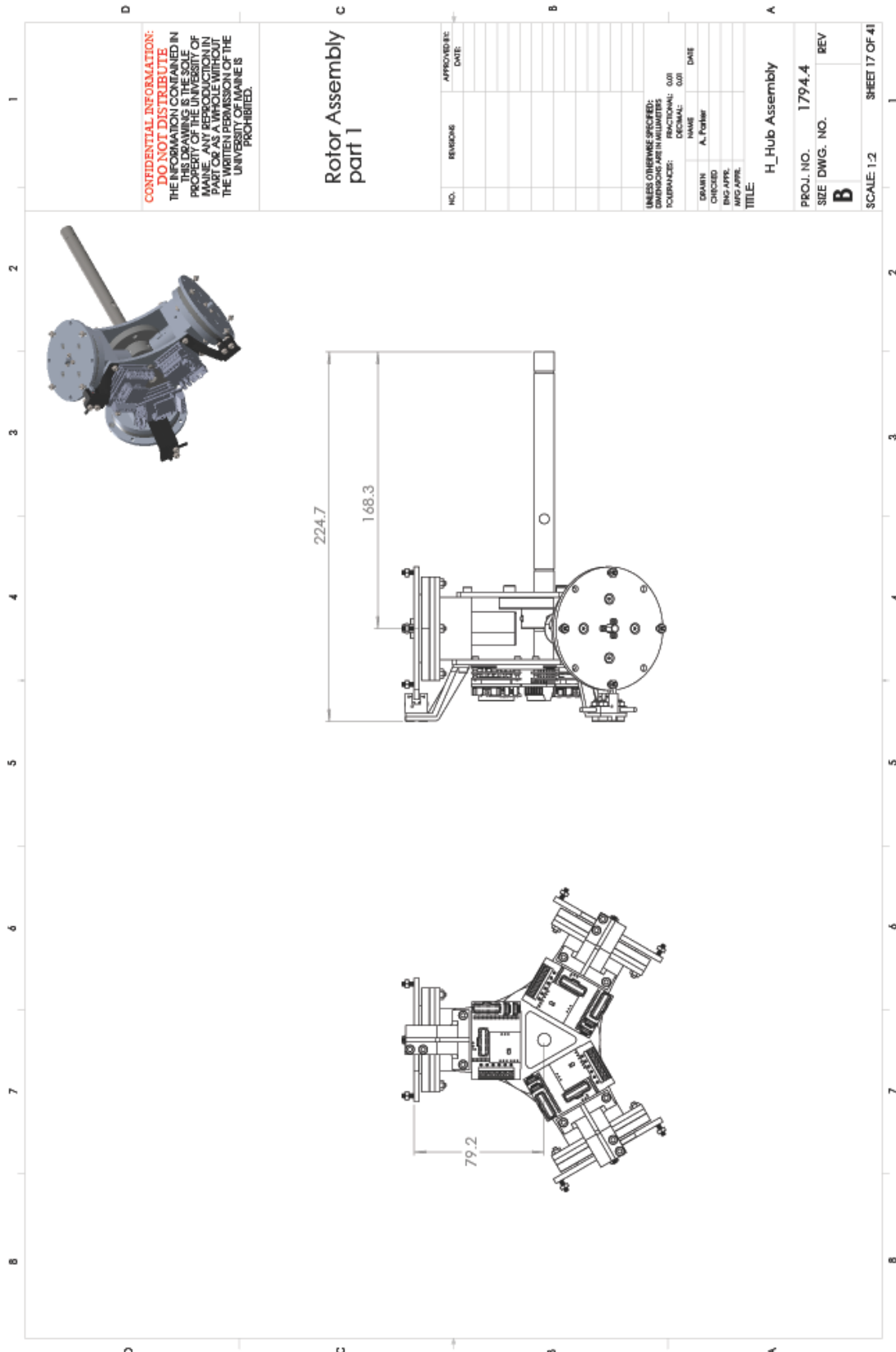


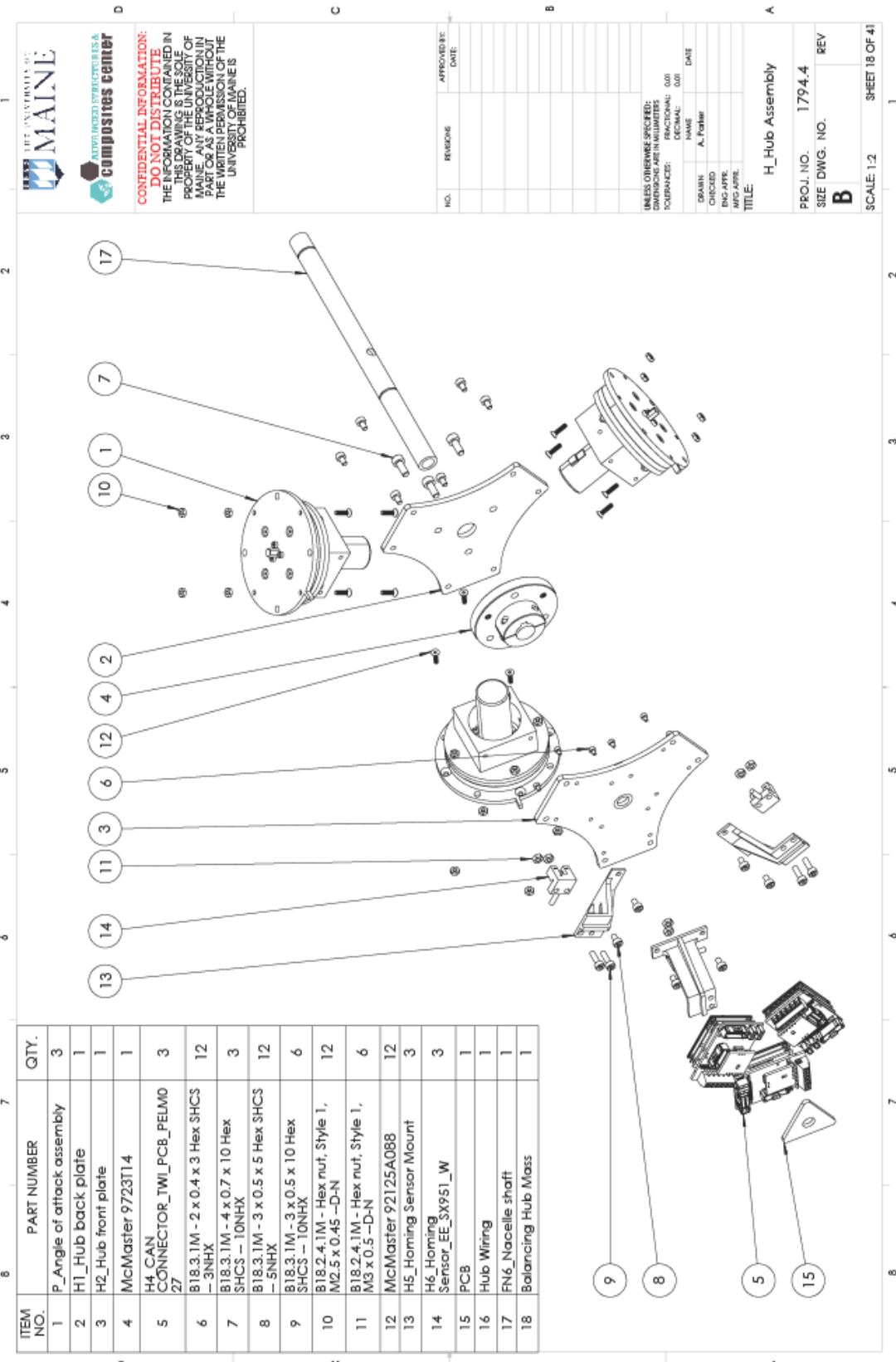


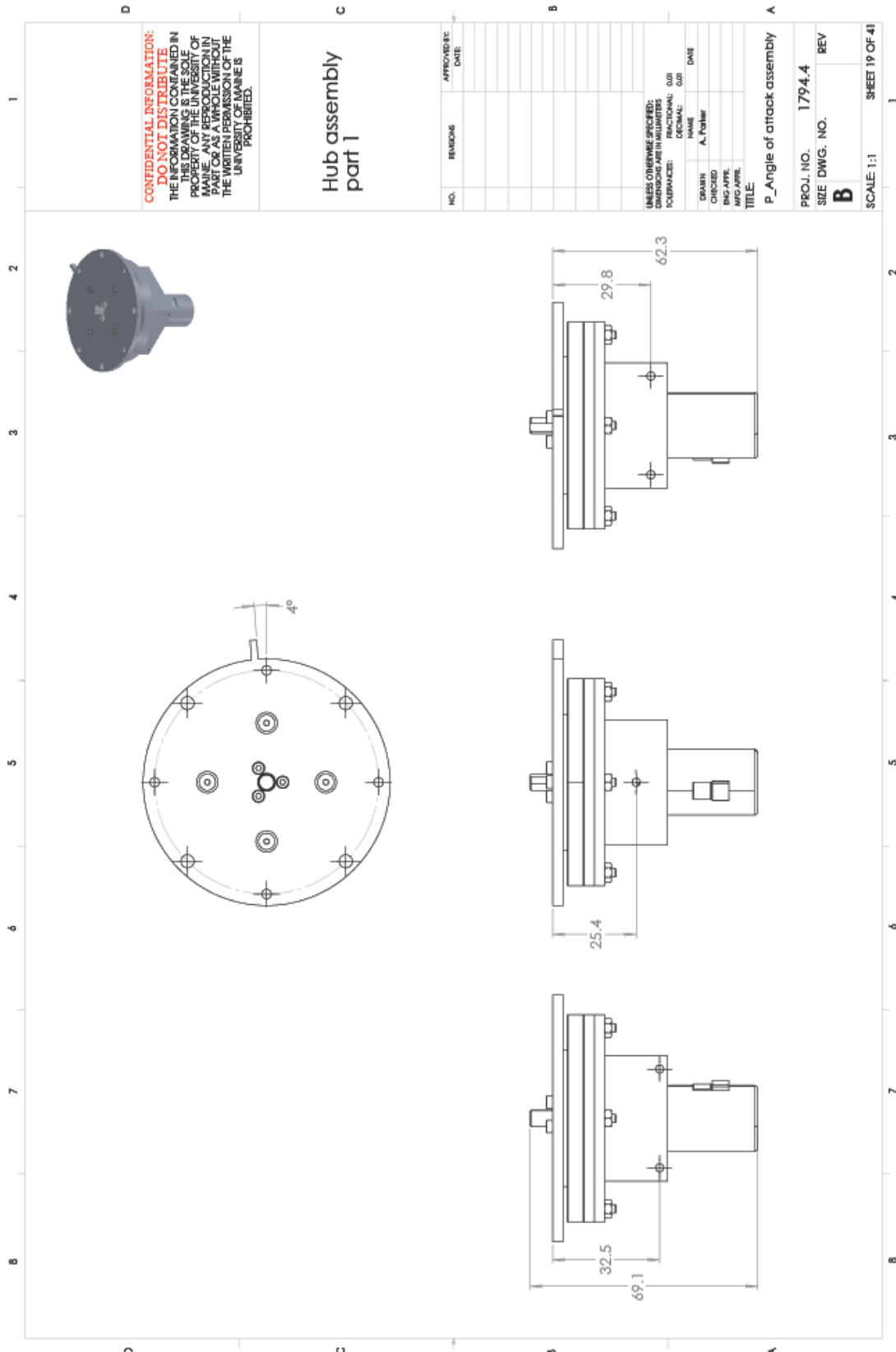


ITEM NO.	PART NUMBER	QTY.
1	H_Hub Assembly	1
2	Blade Assembly Average	3









ITEM NO.	PART NUMBER	QTY.
1	P1_Pitch Transducer_RSF-5B-XXX-US050-BC	1
D 2	P2_Bearing_CRBTF305AT	1
3	McMaster 92125A088	6
4	B18.3.1M - 2.5 x 0.45 x 12 Hex SHCS -- 12NHX	4
5	B18.3.1M - 2 x 0.4 x 12 Hex SHCS -- 12NHX	2
6	B18.3.1M - 2 x 0.4 x 3 Hex SHCS -- 3NHX	3
C 7	B18.2.4.1M - Hex nut, Style 1, M2 x M2.5 x 0.45 -D-N	4
8	B18.2.4.1M - Hex nut, Style 1, M2 x 0.4 -D-N	2
9	P3_Mounting block	1
10	P4_Bearing mount 2	1
11	P5_Bearing mount 3	1
B 12	P6_Attachment hub 2	1
13	P7_Attachment hub 3	1

1
2
3
4
5
6
7
8
9
10
11
12
13

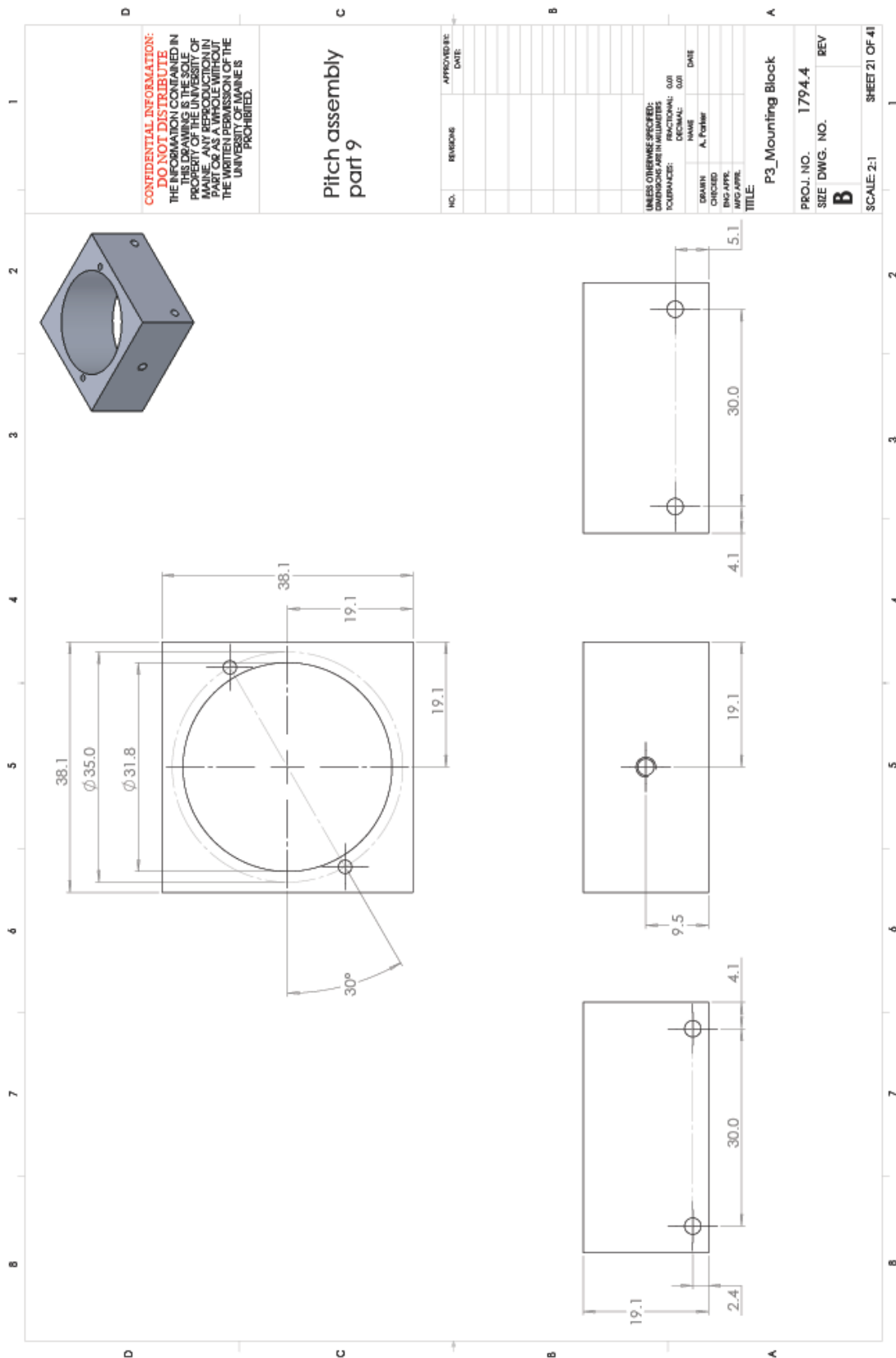
MAIN

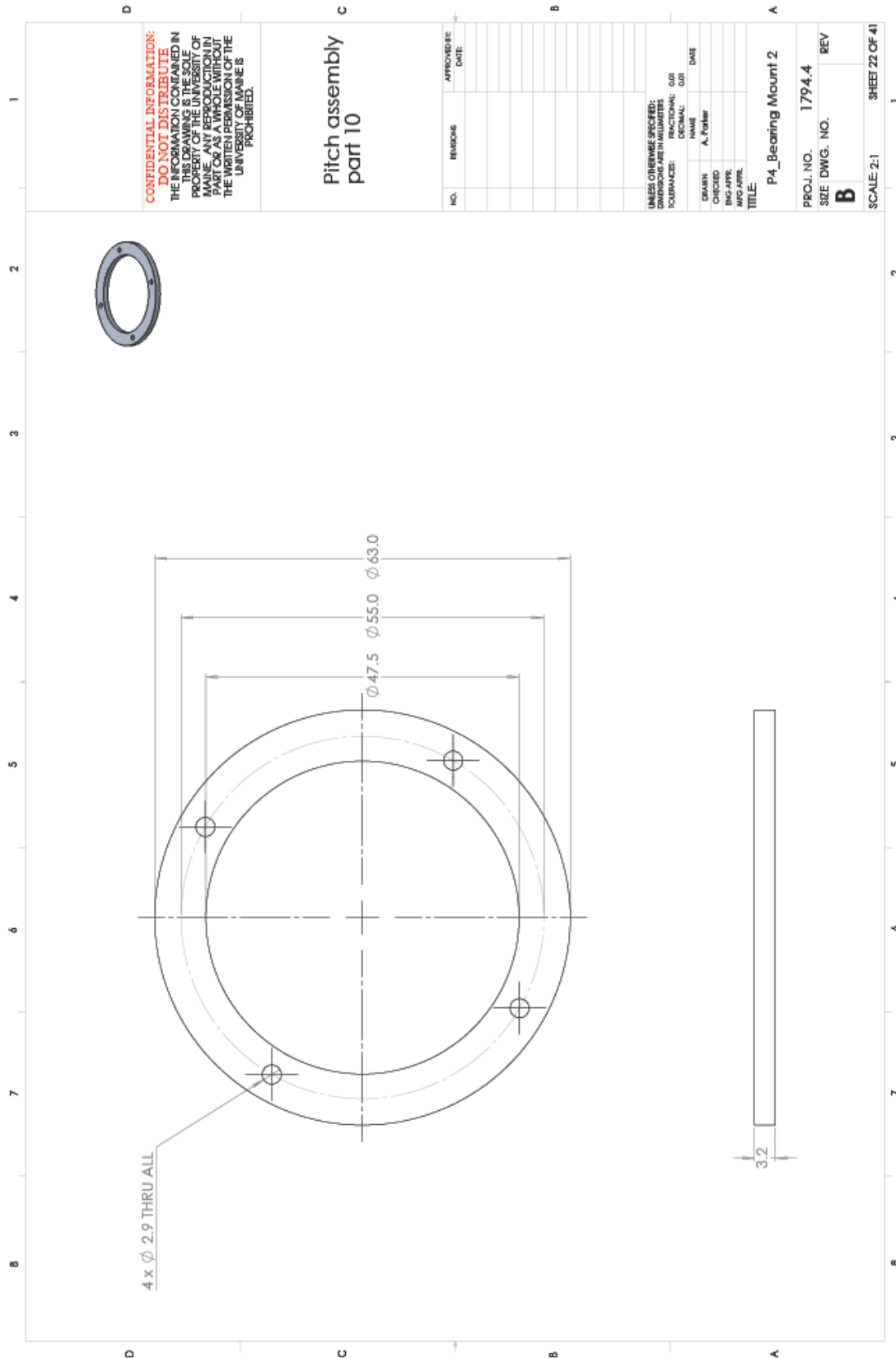
ADVANCED STRUCTURES &
COMPOSITES CENTER

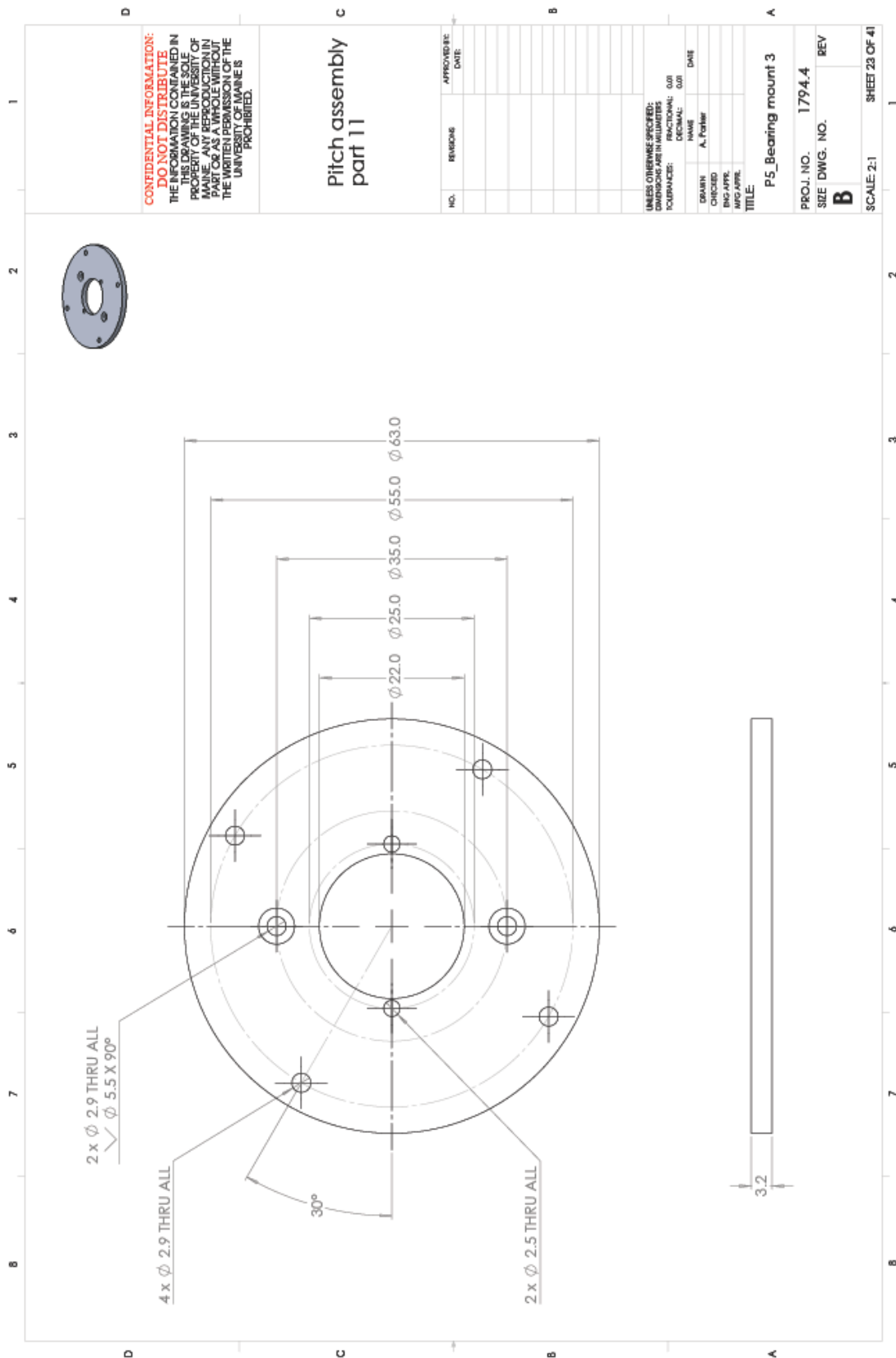
CONFIDENTIAL INFORMATION:
DO NOT DISTRIBUTE
THE INFORMATION CONTAINED IN THIS DRAWING IS THE SOLE PROPERTY OF THE UNIVERSITY OF MANITOBA. ANY REPRODUCTION IN PART OR AS A WHOLE WITHOUT THE WRITTEN PERMISSION OF THE UNIVERSITY OF MANITOBA IS PROHIBITED.

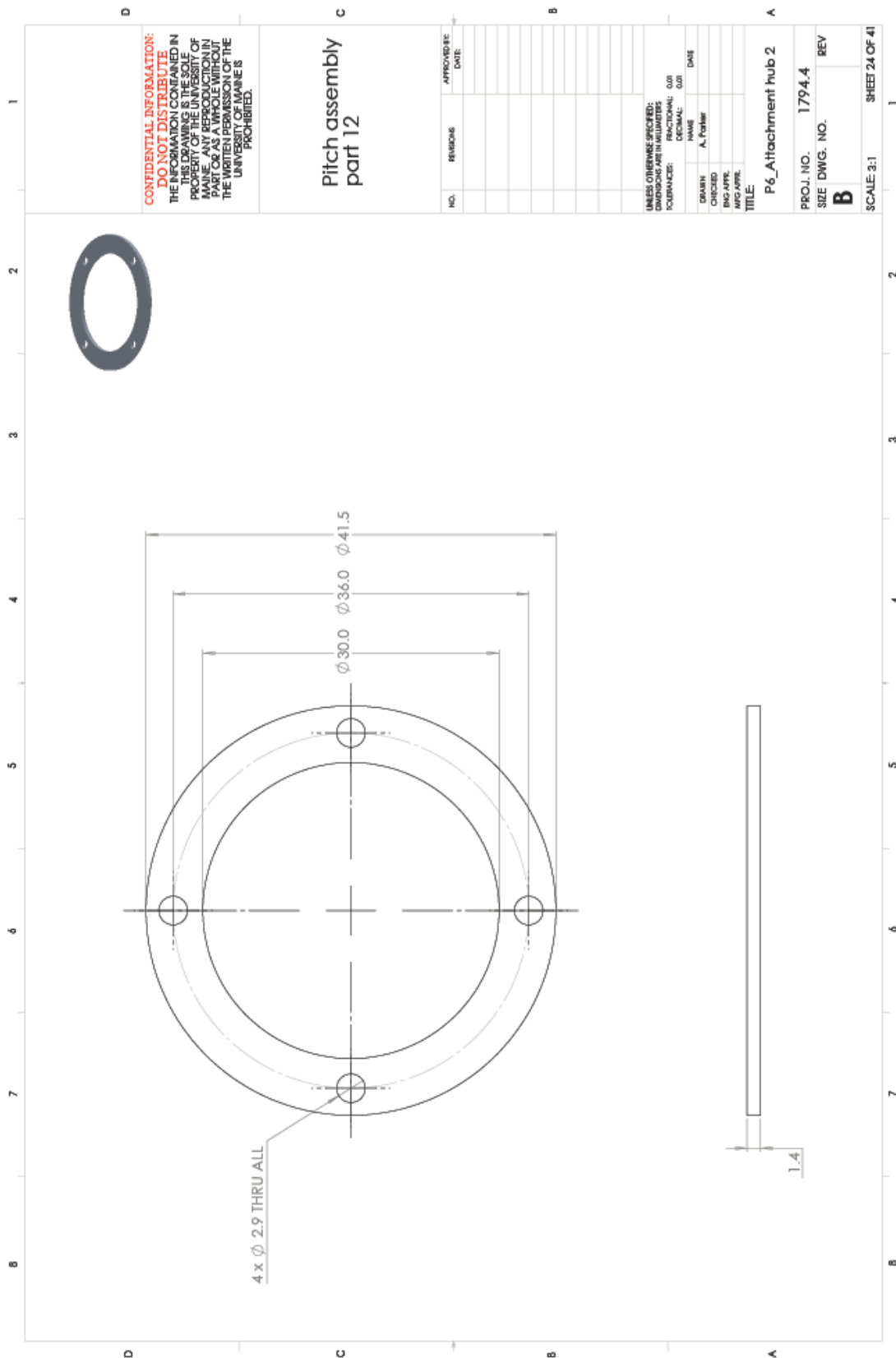
UNLESS OTHERWISE SPECIFIED:
DIMENSIONS ARE IN MILLIMETERS
TOLERANCES:
FRACTIONAL: .001
DECIMAL: .001
NAME: DATE
DRAWN BY: A. Palmer
CHECKED BY: REV
ENG APP: WIG APPROV: TITLE:
P_Angle of attack assembly

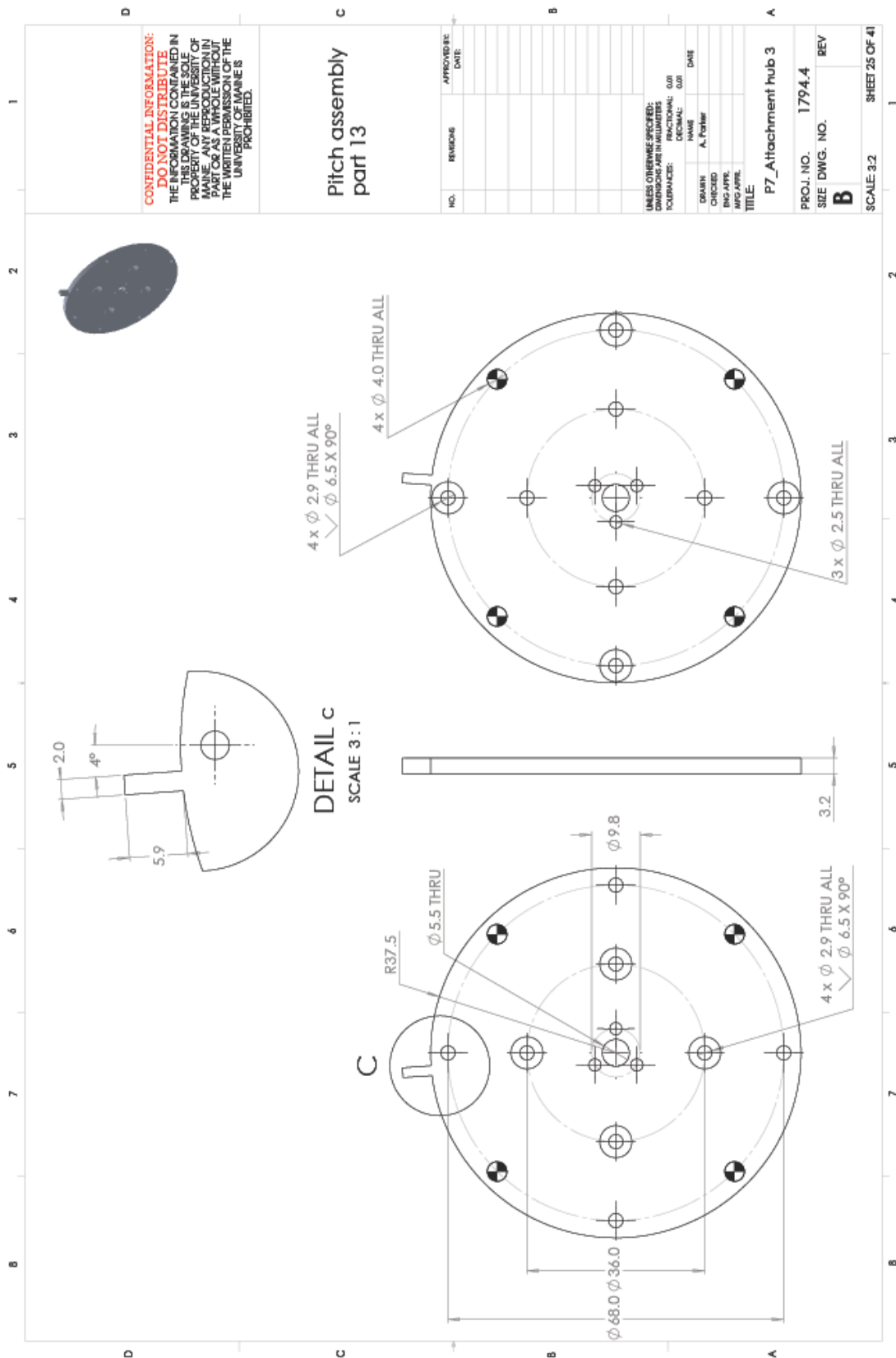
PROJ. NO. 1794.4
SHEET DWG. NO. B
REV
A
SCALE: 1:1 SHEET 20 OF 41

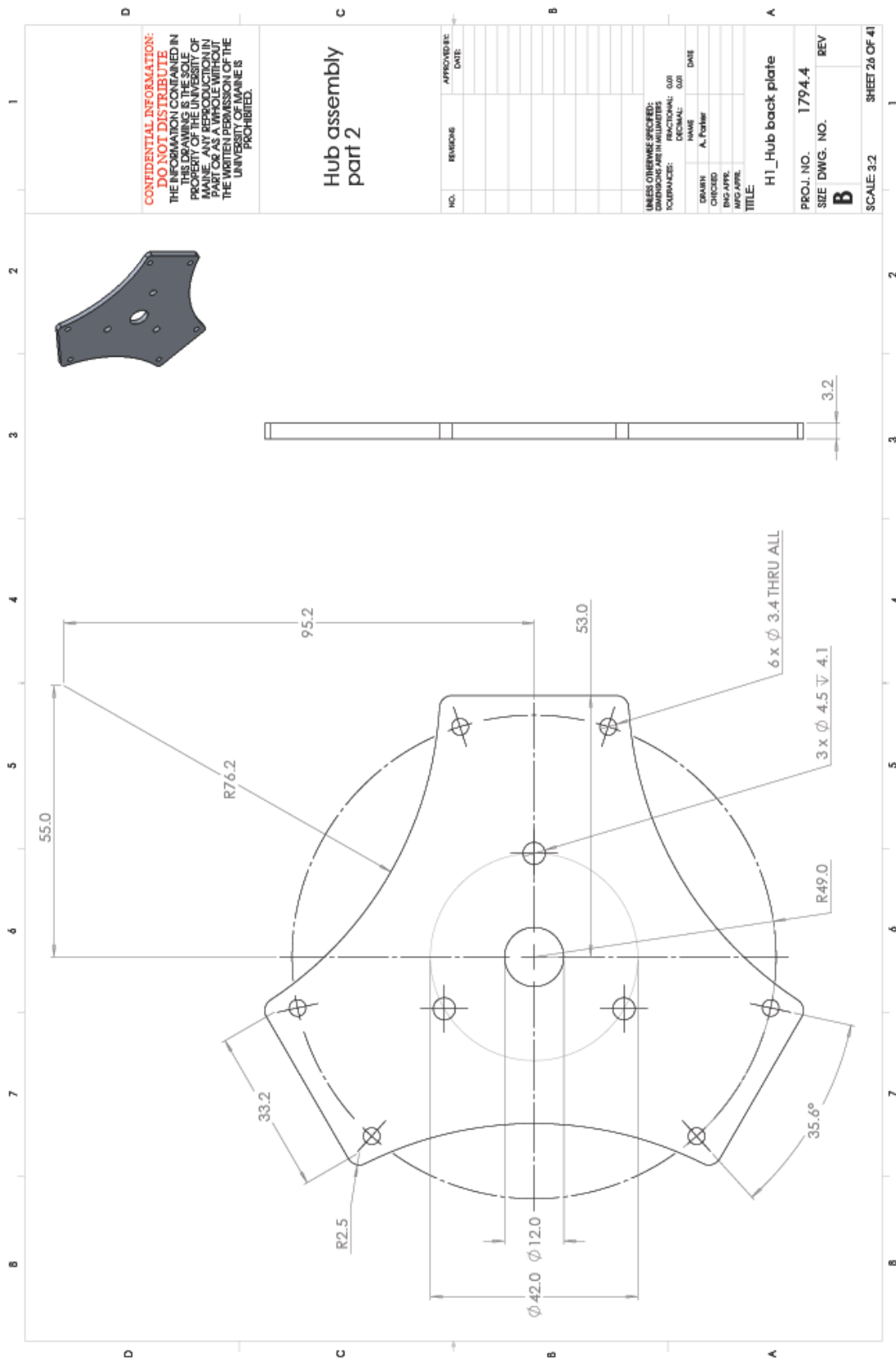


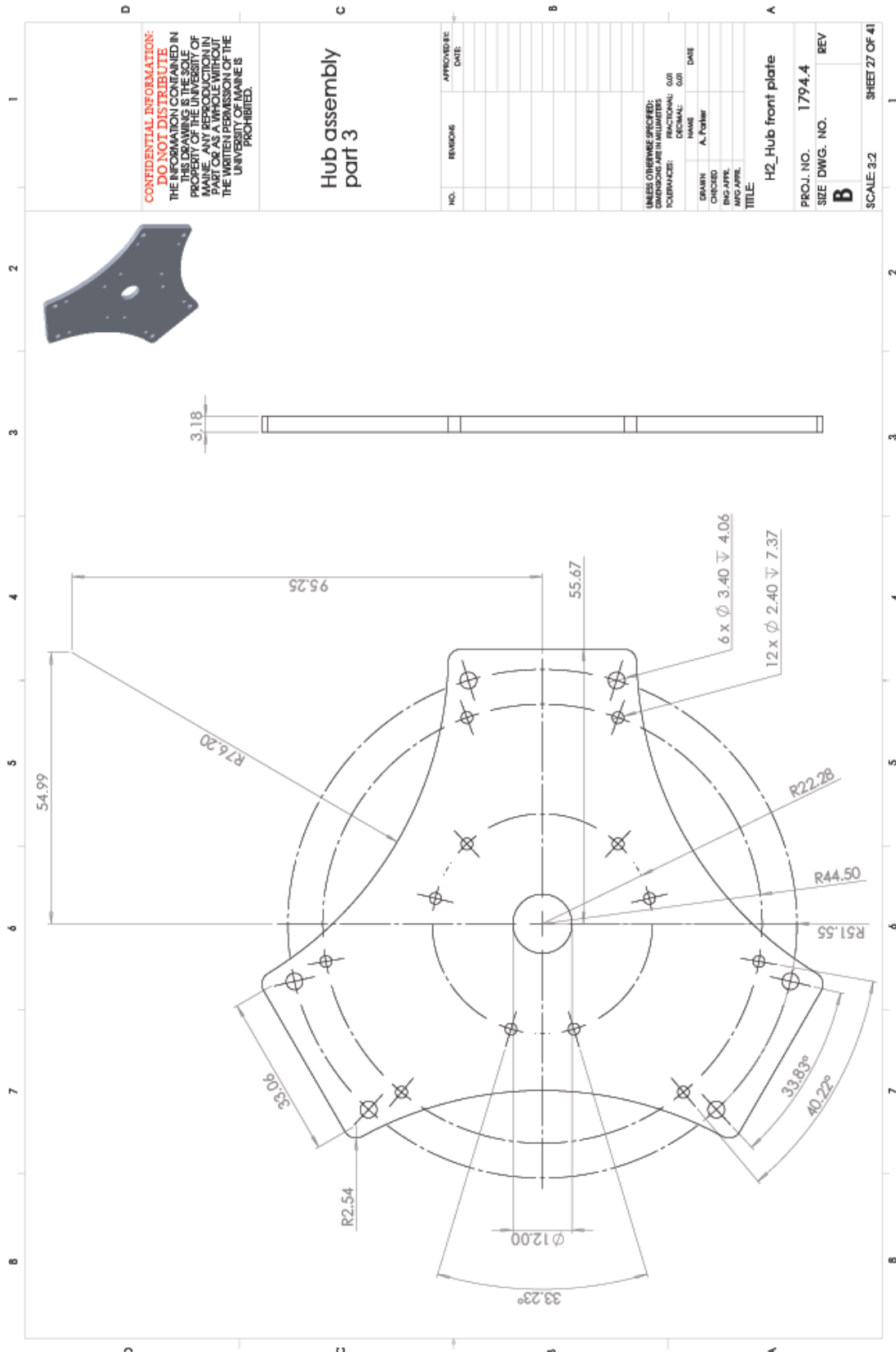


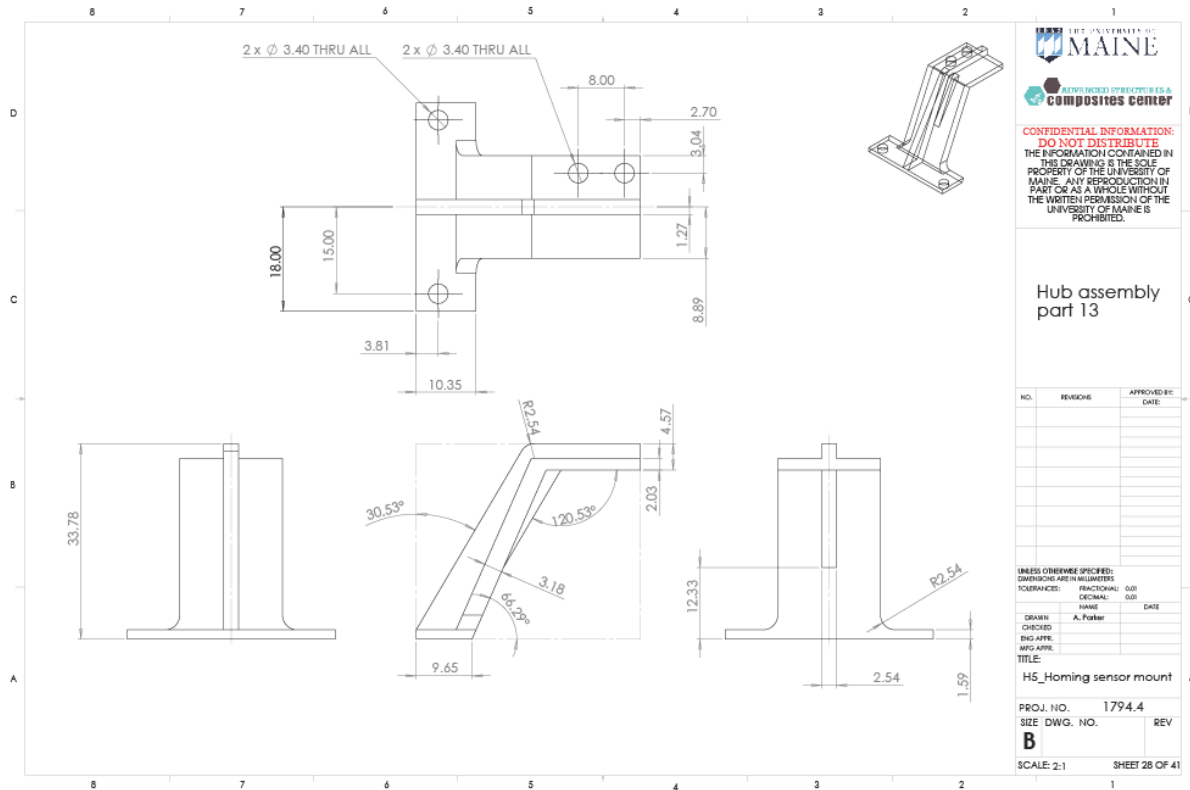


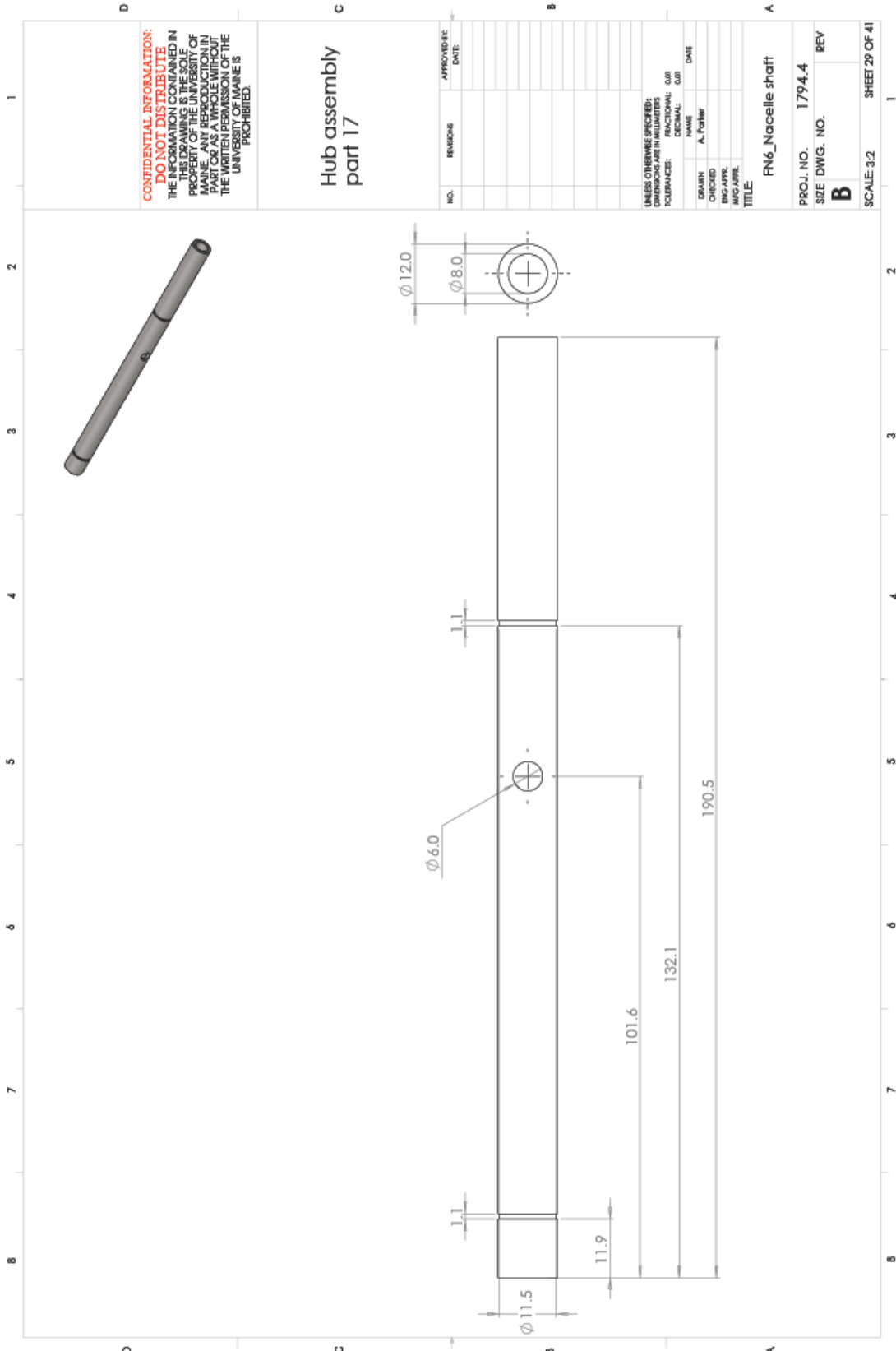


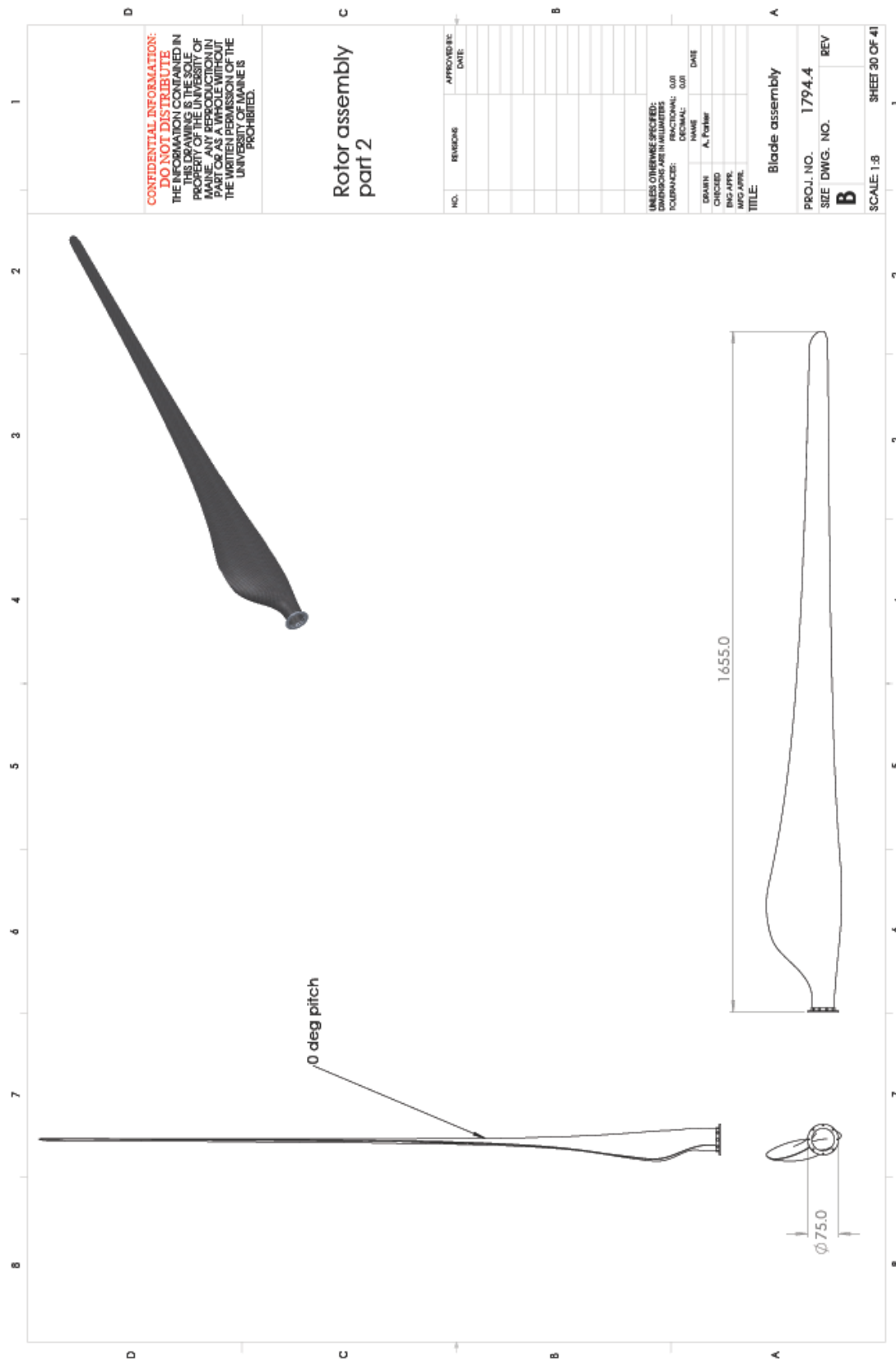












ITEM NO.	PART NUMBER	QTY.
1	P9_Blade flange	1
2	P8_FOCAL_blade_SD7032_swModified	1
3	P10_Center spar	1
4	P11_Short side spar	1

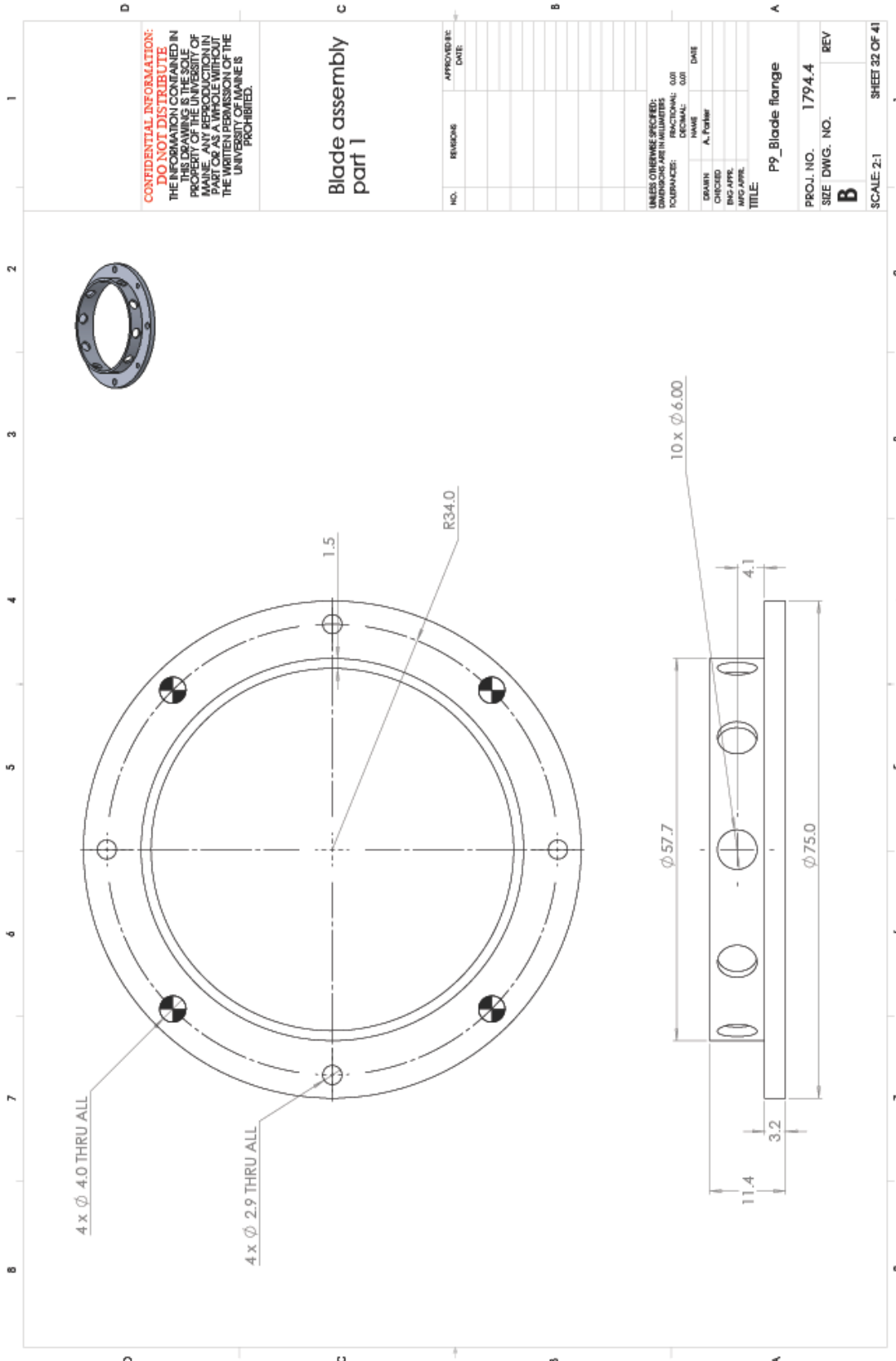
C D

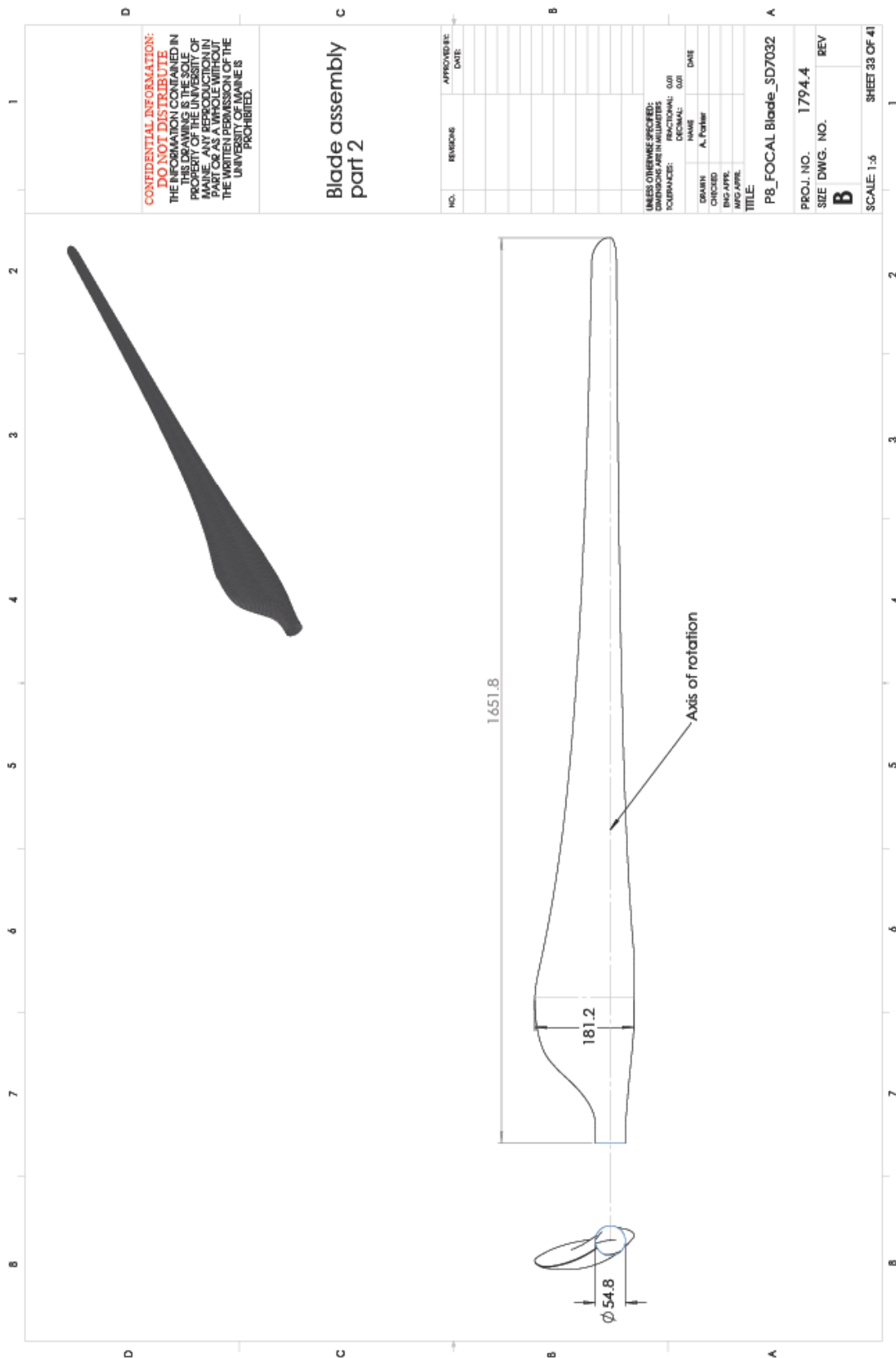
A B

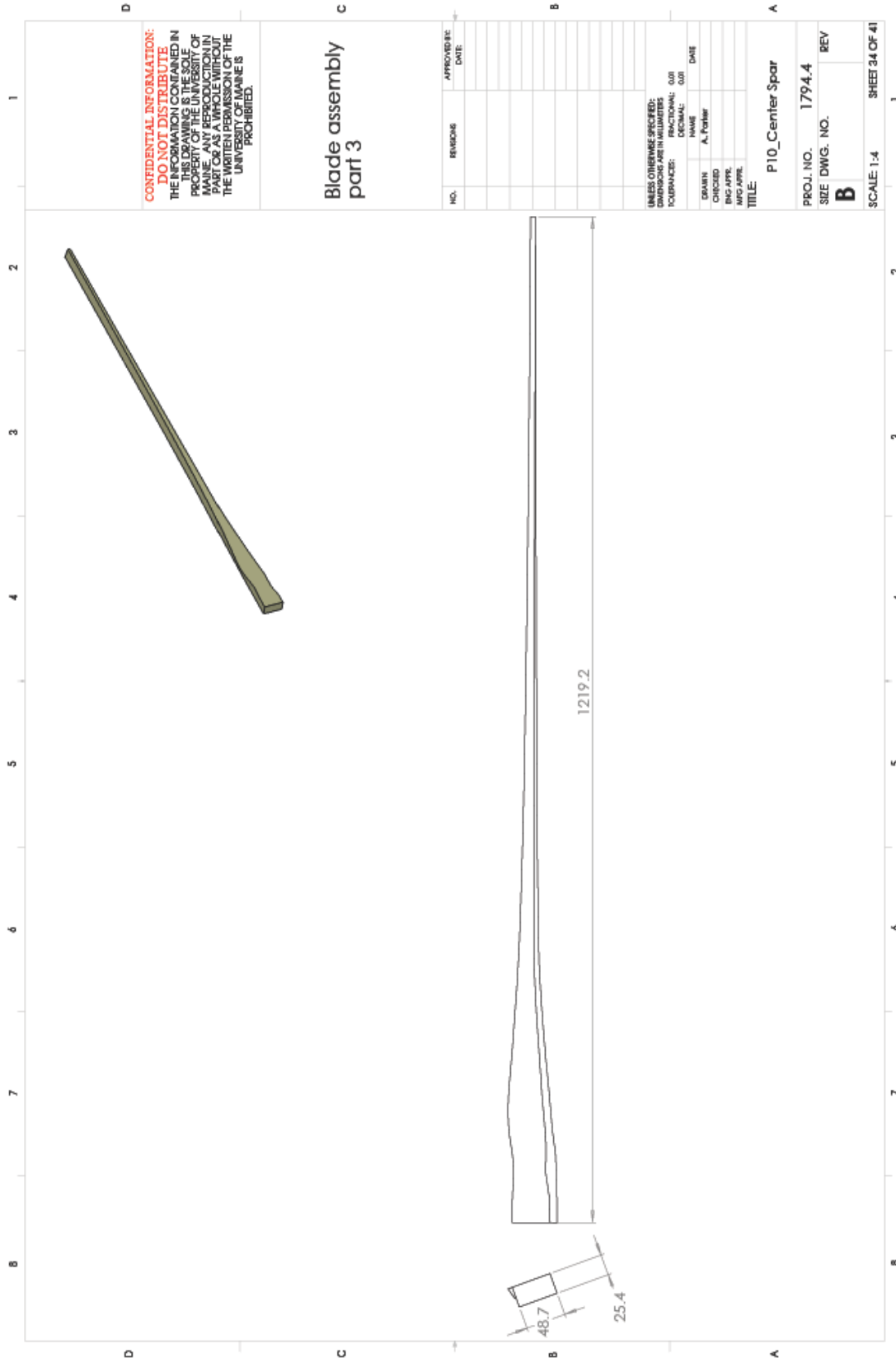
CONFIDENTIAL INFORMATION:
DO NOT DISTRIBUTE
THE INFORMATION CONTAINED IN THIS DRAWING IS THE SOLE PROPERTY OF THE UNIVERSITY OF MANITOBA. ANY REPRODUCTION IN PART OR AS A WHOLE WITHOUT THE WRITTEN PERMISSION OF THE UNIVERSITY OF MANITOBA IS PROHIBITED.

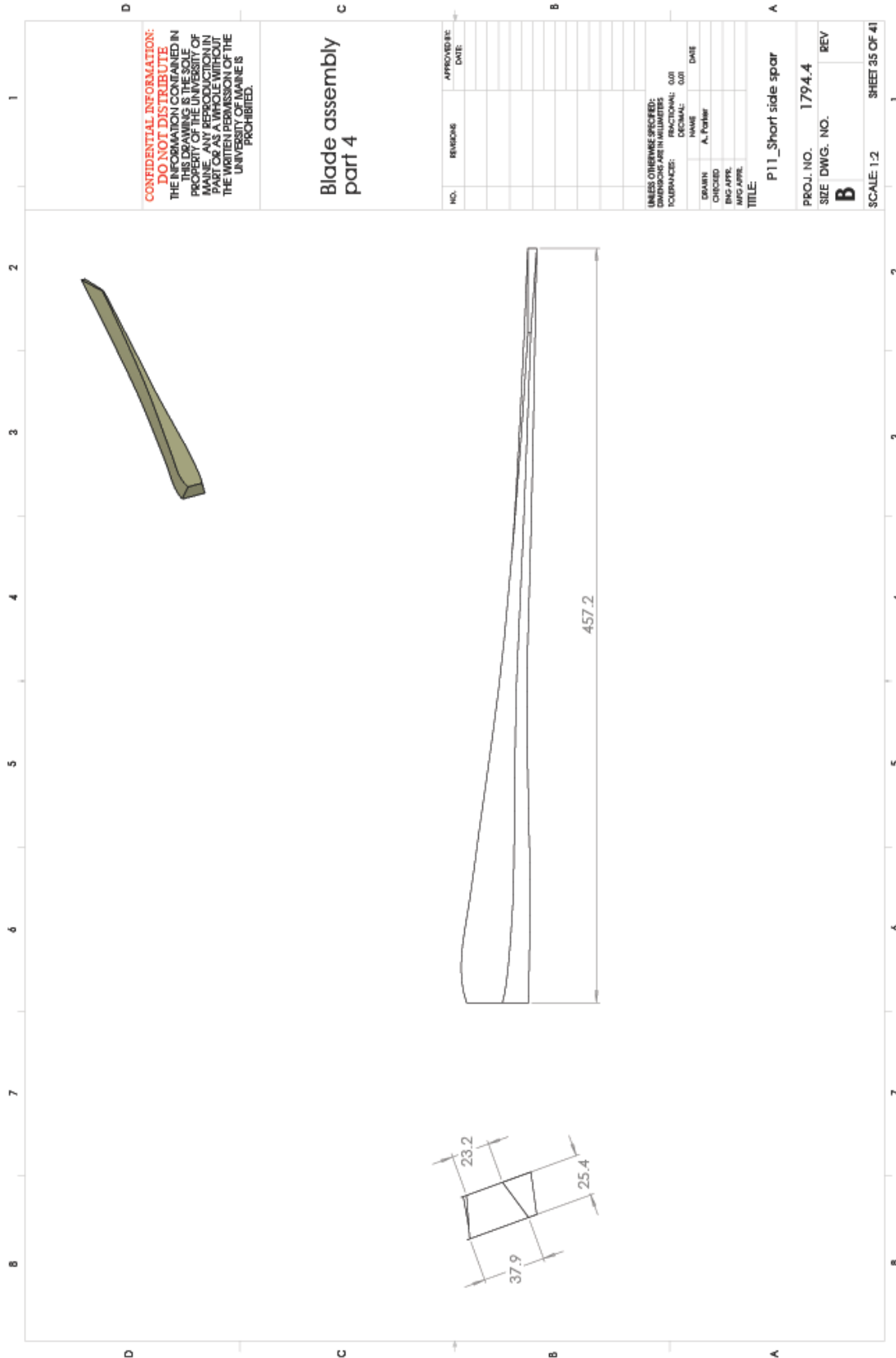
UNLESS OTHERWISE SPECIFIED:
DIMENSIONS ARE IN MILLIMETERS
TOLERANCES: FRACTIONAL: .001
DECIMAL: .001
NAME: DATE
DRAWN BY: A. Poirier
CHECKED BY: REV
MFG APP: B
TITLE: Blade Assembly

PROJ. NO. 1794.4
SHEET DWG. NO. B
REV
SCALE: 1:6 SHEET 31 OF 41



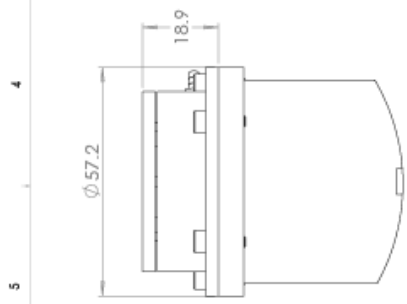








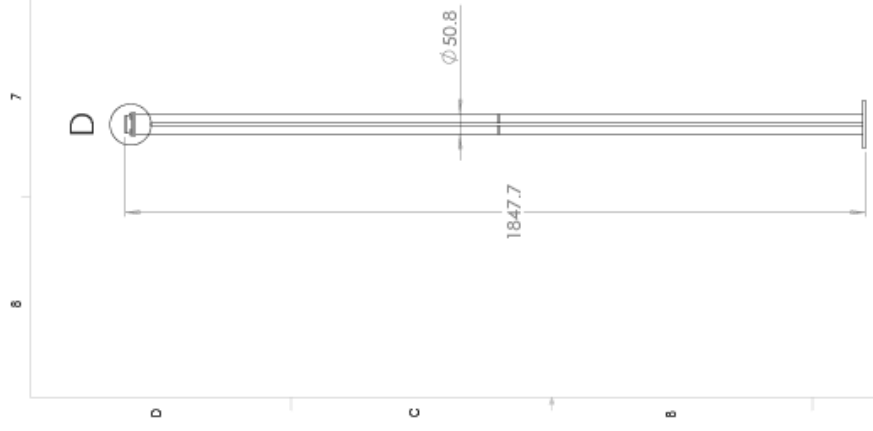
Turbine assembly
part 3



DETAIL D
SCALE 1:1

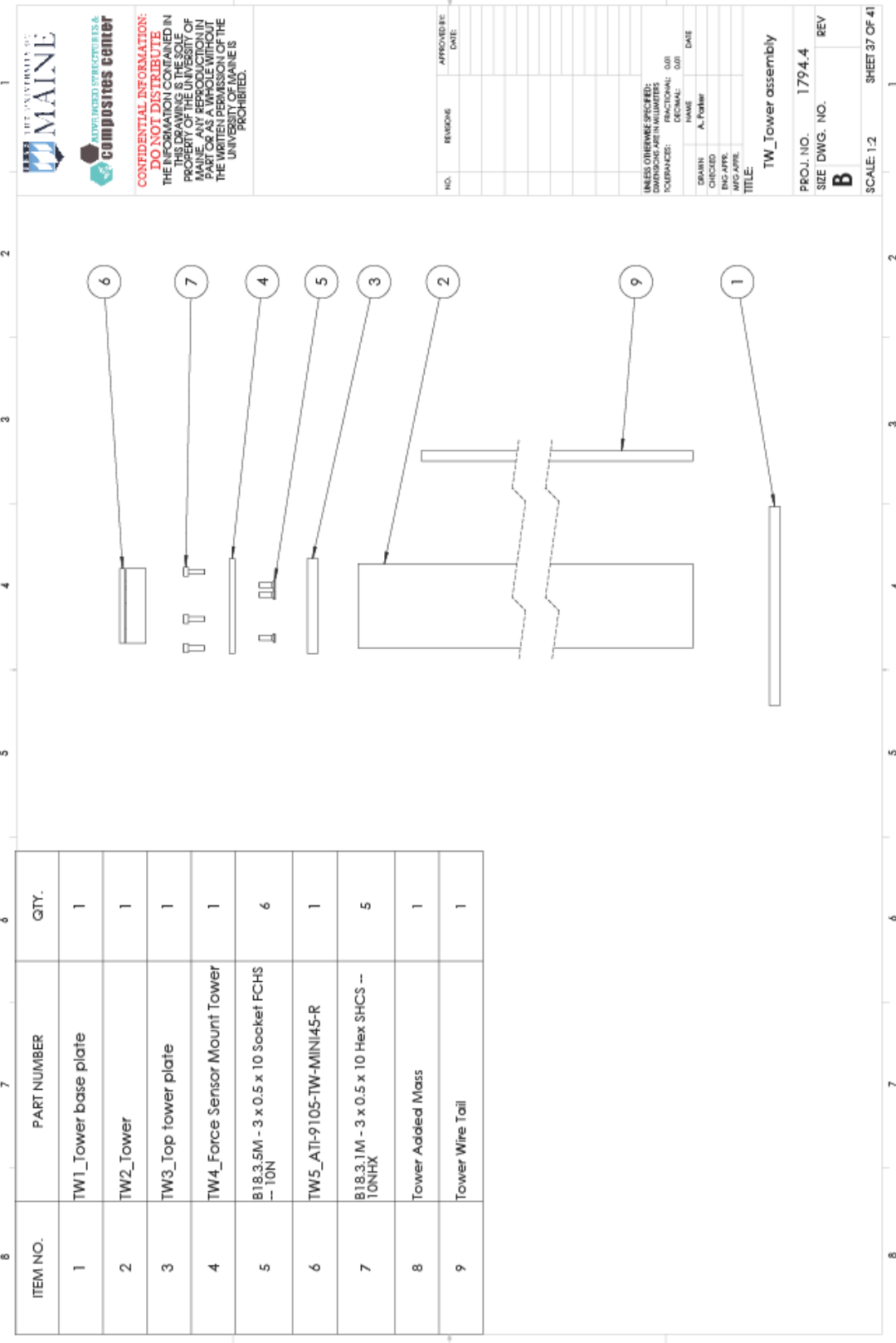


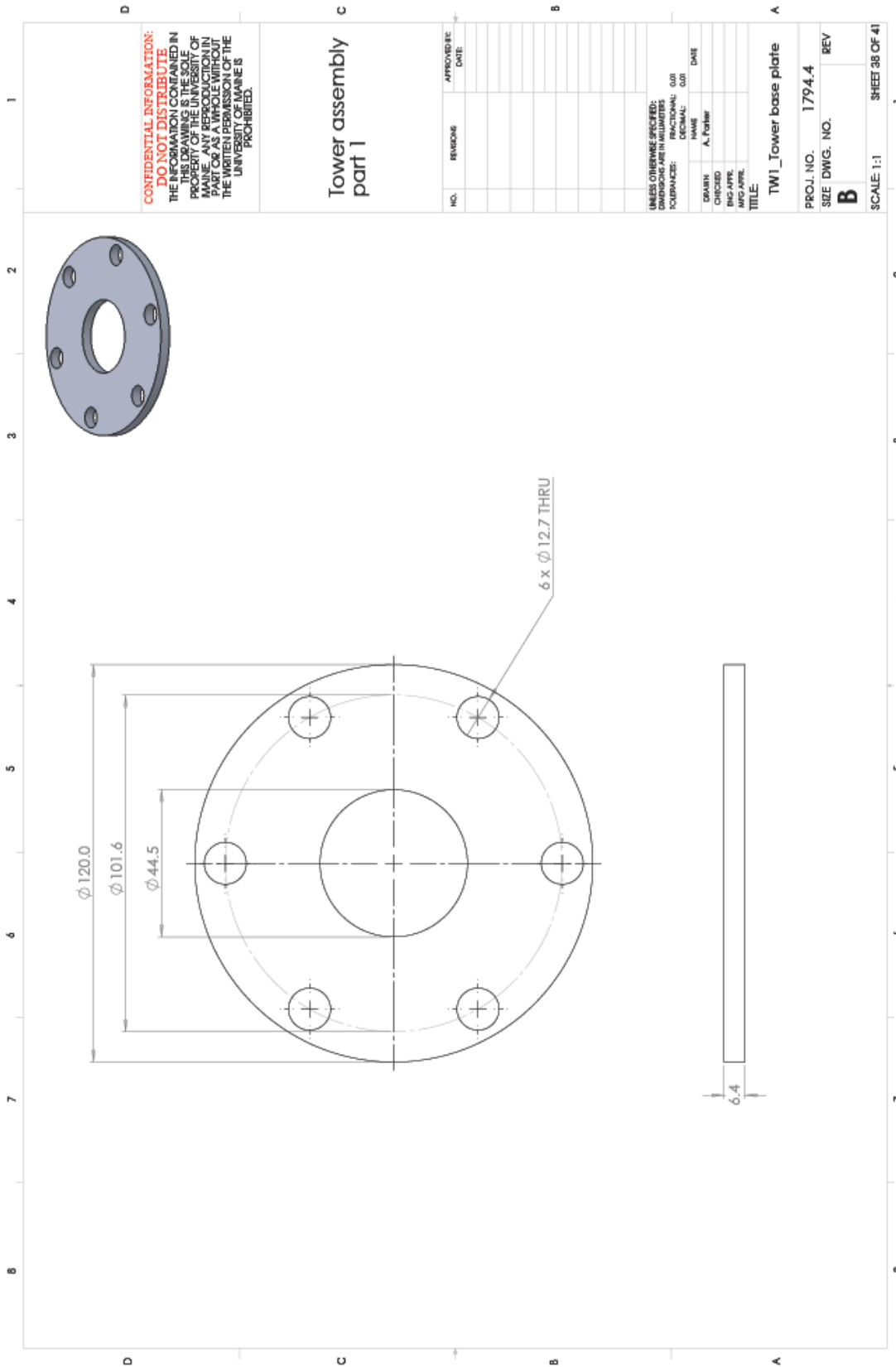
DETAIL E
SCALE 1:2

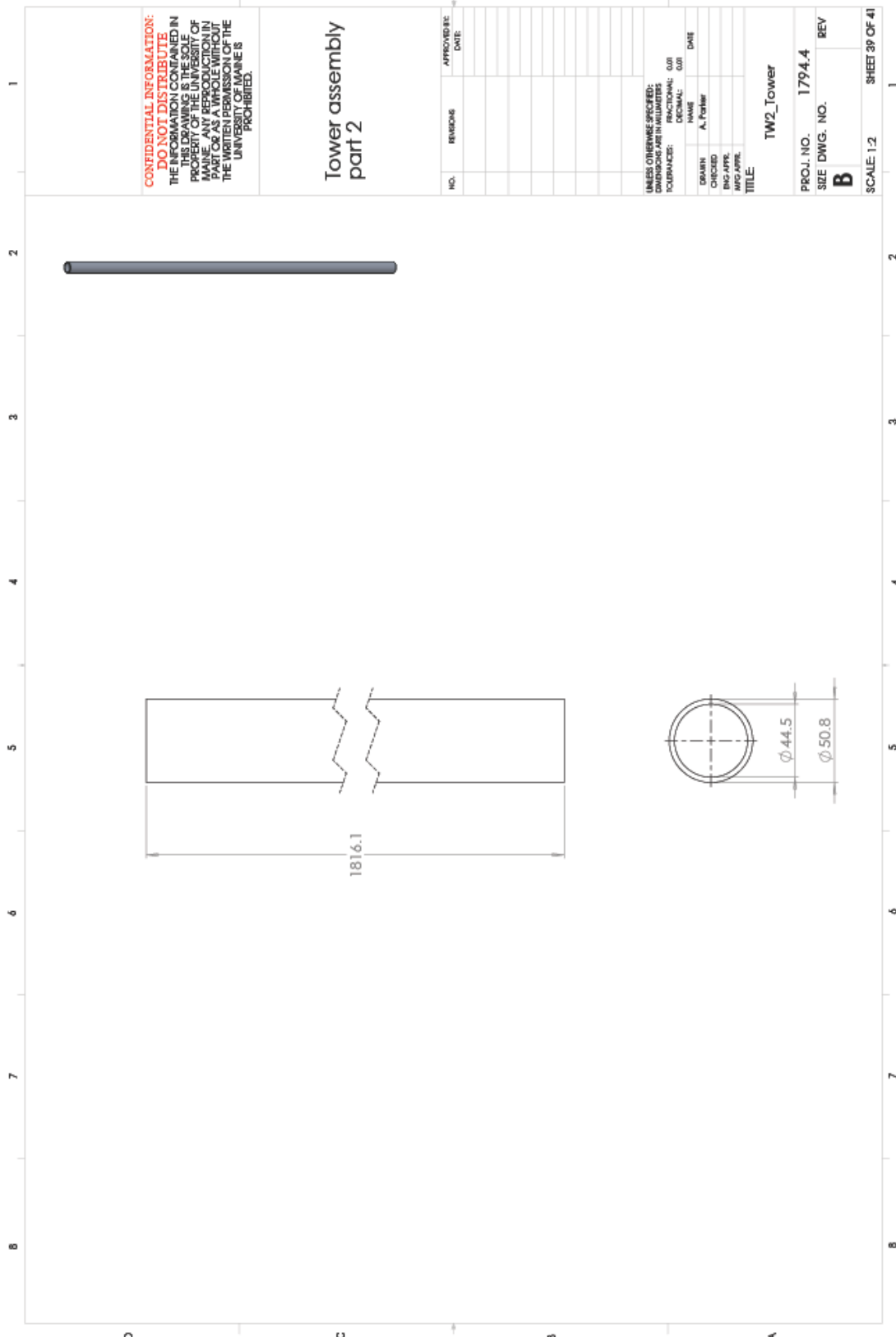


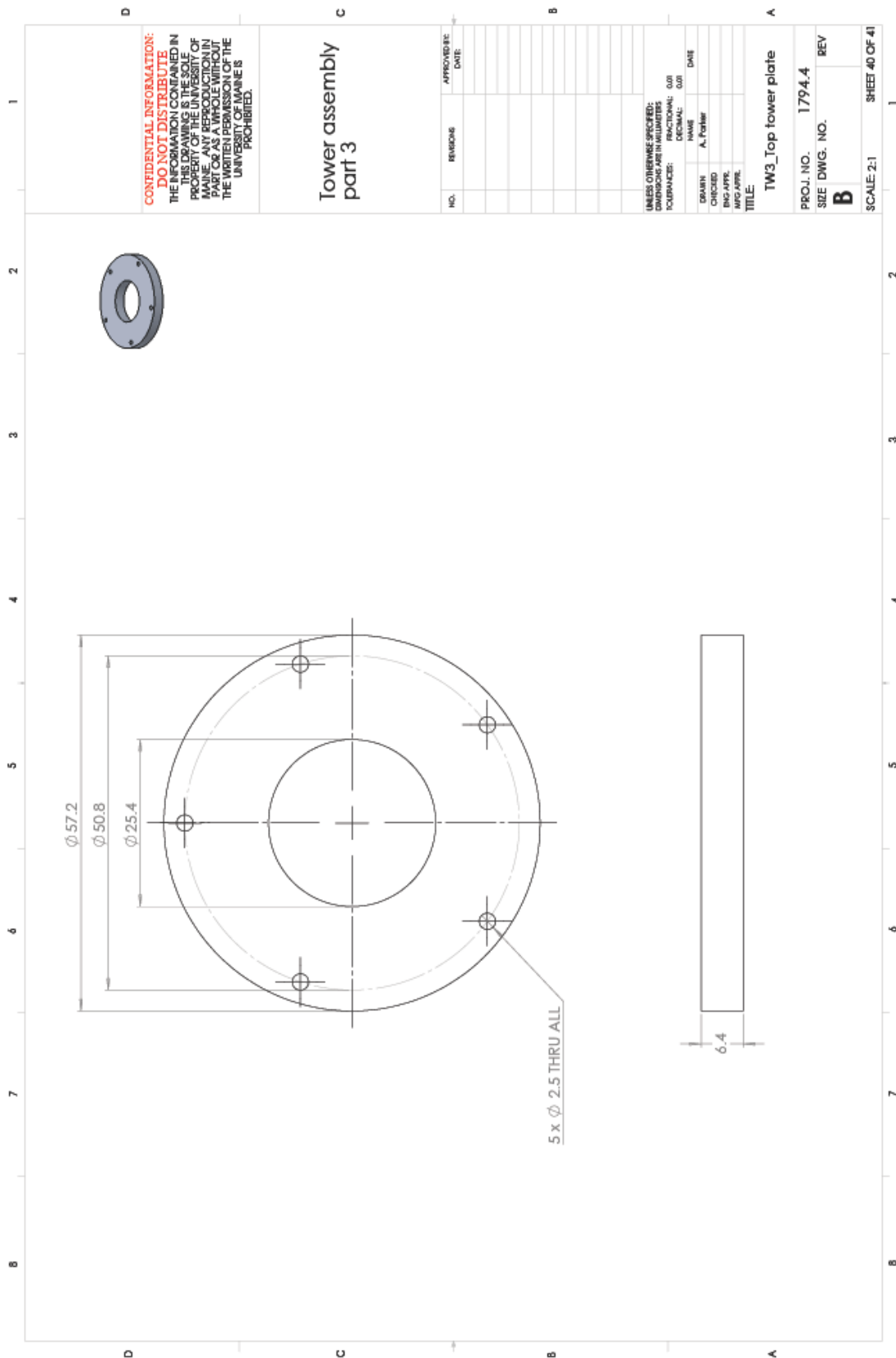
E

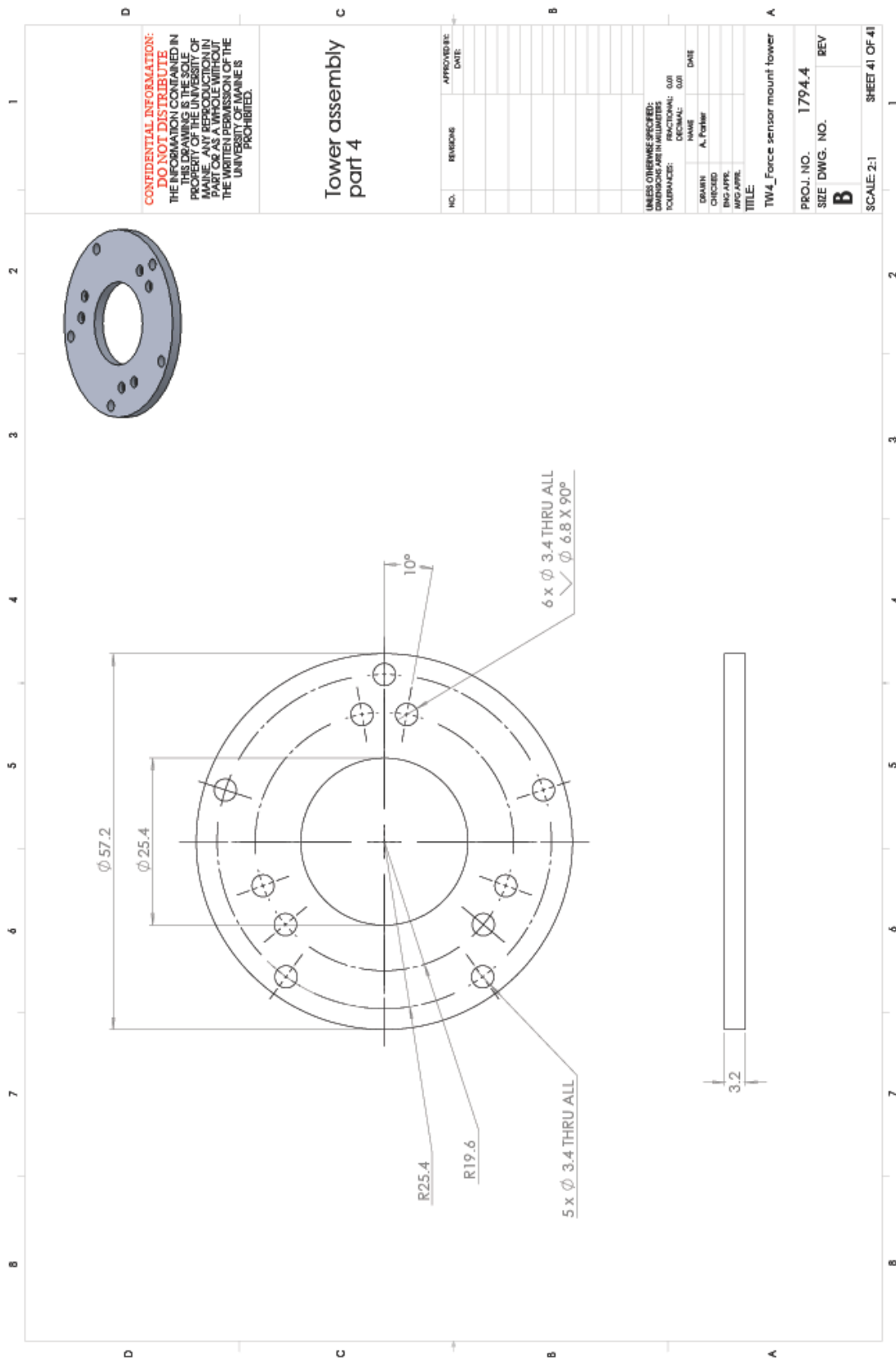
94











APPENDIX B: AIRFOIL GEOMETRY DATASETS

FFA-W3-211.dat

1.00E+00	-7.29E-04
9.76E-01	1.91E-03
9.52E-01	3.93E-03
9.28E-01	5.28E-03
9.04E-01	6.03E-03
8.80E-01	5.93E-03
8.56E-01	5.02E-03
8.32E-01	3.32E-03
8.09E-01	9.10E-04
7.86E-01	-2.15E-03
7.63E-01	-5.85E-03
7.40E-01	-1.00E-02
7.18E-01	-1.47E-02
6.96E-01	-1.97E-02
6.75E-01	-2.50E-02
6.54E-01	-3.05E-02
6.33E-01	-3.62E-02
6.13E-01	-4.19E-02
5.93E-01	-4.76E-02
5.74E-01	-5.31E-02
5.54E-01	-5.85E-02
5.35E-01	-6.37E-02
5.17E-01	-6.85E-02
4.99E-01	-7.31E-02
4.81E-01	-7.73E-02
4.63E-01	-8.10E-02
4.46E-01	-8.43E-02
4.29E-01	-8.71E-02
4.12E-01	-8.96E-02
3.96E-01	-9.16E-02
3.80E-01	-9.31E-02
3.65E-01	-9.43E-02
3.50E-01	-9.52E-02
3.35E-01	-9.58E-02
3.21E-01	-9.60E-02
3.07E-01	-9.59E-02
2.94E-01	-9.57E-02
2.81E-01	-9.52E-02
2.68E-01	-9.45E-02
2.56E-01	-9.37E-02
2.44E-01	-9.26E-02
2.33E-01	-9.15E-02
2.22E-01	-9.02E-02
2.11E-01	-8.88E-02
2.01E-01	-8.72E-02
1.91E-01	-8.56E-02
1.82E-01	-8.39E-02

1.73E-01	-8.22E-02
1.64E-01	-8.04E-02
1.55E-01	-7.85E-02
1.47E-01	-7.66E-02
1.39E-01	-7.47E-02
1.32E-01	-7.28E-02
1.25E-01	-7.08E-02
1.18E-01	-6.89E-02
1.11E-01	-6.69E-02
1.05E-01	-6.49E-02
9.90E-02	-6.30E-02
9.32E-02	-6.10E-02
8.77E-02	-5.91E-02
8.24E-02	-5.72E-02
7.73E-02	-5.53E-02
7.25E-02	-5.35E-02
6.79E-02	-5.17E-02
6.35E-02	-4.99E-02
5.92E-02	-4.82E-02
5.52E-02	-4.65E-02
5.14E-02	-4.48E-02
4.78E-02	-4.31E-02
4.43E-02	-4.14E-02
4.10E-02	-3.97E-02
3.78E-02	-3.81E-02
3.48E-02	-3.65E-02
3.20E-02	-3.50E-02
2.93E-02	-3.34E-02
2.68E-02	-3.19E-02
2.44E-02	-3.03E-02
2.21E-02	-2.89E-02
1.99E-02	-2.74E-02
1.79E-02	-2.59E-02
1.60E-02	-2.45E-02
1.42E-02	-2.31E-02
1.25E-02	-2.17E-02
1.09E-02	-2.03E-02
9.50E-03	-1.90E-02
8.15E-03	-1.76E-02
6.86E-03	-1.63E-02
5.66E-03	-1.50E-02
4.61E-03	-1.37E-02
3.72E-03	-1.24E-02
2.95E-03	-1.10E-02
2.34E-03	-9.66E-03
1.87E-03	-8.30E-03
1.52E-03	-6.97E-03
1.24E-03	-5.68E-03
9.77E-04	-4.44E-03
7.23E-04	-3.25E-03
4.80E-04	-2.12E-03

2.42E-04	-1.04E-03
0.00E+00	0.00E+00
2.31E-04	1.04E-03
4.45E-04	2.13E-03
6.51E-04	3.27E-03
8.60E-04	4.46E-03
1.07E-03	5.71E-03
1.29E-03	7.01E-03
1.55E-03	8.37E-03
1.87E-03	9.77E-03
2.32E-03	1.12E-02
2.88E-03	1.26E-02
3.53E-03	1.41E-02
4.29E-03	1.56E-02
5.17E-03	1.72E-02
6.15E-03	1.87E-02
7.18E-03	2.03E-02
8.31E-03	2.20E-02
9.55E-03	2.37E-02
1.09E-02	2.54E-02
1.24E-02	2.72E-02
1.40E-02	2.90E-02
1.56E-02	3.08E-02
1.75E-02	3.27E-02
1.94E-02	3.46E-02
2.15E-02	3.65E-02
2.37E-02	3.85E-02
2.61E-02	4.04E-02
2.86E-02	4.25E-02
3.12E-02	4.46E-02
3.41E-02	4.67E-02
3.70E-02	4.88E-02
4.02E-02	5.10E-02
4.35E-02	5.32E-02
4.71E-02	5.54E-02
5.08E-02	5.77E-02
5.47E-02	6.00E-02
5.88E-02	6.23E-02
6.31E-02	6.46E-02
6.77E-02	6.70E-02
7.24E-02	6.94E-02
7.74E-02	7.18E-02
8.27E-02	7.42E-02
8.82E-02	7.66E-02
9.40E-02	7.90E-02
1.00E-01	8.15E-02
1.06E-01	8.39E-02
1.13E-01	8.64E-02
1.20E-01	8.88E-02
1.27E-01	9.12E-02
1.35E-01	9.35E-02

1.42E-01	9.58E-02
1.51E-01	9.82E-02
1.59E-01	1.00E-01
1.68E-01	1.03E-01
1.77E-01	1.05E-01
1.87E-01	1.07E-01
1.97E-01	1.09E-01
2.07E-01	1.11E-01
2.18E-01	1.12E-01
2.29E-01	1.14E-01
2.40E-01	1.16E-01
2.52E-01	1.17E-01
2.65E-01	1.18E-01
2.77E-01	1.19E-01
2.91E-01	1.19E-01
3.04E-01	1.20E-01
3.18E-01	1.20E-01
3.32E-01	1.19E-01
3.47E-01	1.19E-01
3.62E-01	1.18E-01
3.78E-01	1.17E-01
3.94E-01	1.16E-01
4.10E-01	1.14E-01
4.27E-01	1.12E-01
4.44E-01	1.10E-01
4.62E-01	1.08E-01
4.80E-01	1.05E-01
4.98E-01	1.02E-01
5.17E-01	9.91E-02
5.36E-01	9.57E-02
5.55E-01	9.21E-02
5.75E-01	8.84E-02
5.95E-01	8.44E-02
6.15E-01	8.02E-02
6.36E-01	7.58E-02
6.57E-01	7.13E-02
6.78E-01	6.67E-02
7.00E-01	6.20E-02
7.22E-01	5.72E-02
7.44E-01	5.23E-02
7.66E-01	4.74E-02
7.89E-01	4.26E-02
8.12E-01	3.77E-02
8.35E-01	3.29E-02
8.58E-01	2.81E-02
8.81E-01	2.34E-02
9.05E-01	1.88E-02
9.29E-01	1.43E-02
9.52E-01	9.89E-03
9.76E-01	5.58E-03
1.00E+00	1.41E-03

SD7032.dat

1.00000 0.00000
0.99674 0.00048
0.98712 0.00204
0.97155 0.00485
0.95054 0.00894
0.92464 0.01420
0.89436 0.02041
0.86021 0.02731
0.82264 0.03460
0.78208 0.04199
0.73892 0.04925
0.69356 0.05620
0.64646 0.06270
0.59812 0.06861
0.54902 0.07381
0.49967 0.07816
0.45058 0.08154
0.40222 0.08385
0.35506 0.08500
0.30953 0.08493
0.26604 0.08359
0.22499 0.08096
0.18671 0.07703
0.15146 0.07182
0.11948 0.06548
0.09105 0.05809
0.06627 0.04976
0.04524 0.04078
0.02812 0.03145
0.01502 0.02206
0.00606 0.01293
0.00115 0.00448
0.00038 -0.00223
0.00532 -0.00701
0.01649 -0.01088
0.03308 -0.01403
0.05491 -0.01635
0.08180 -0.01787
0.11351 -0.01862
0.14974 -0.01867
0.19010 -0.01810
0.23420 -0.01699
0.28153 -0.01547
0.33154 -0.01363
0.38364 -0.01152
0.43724 -0.00922
0.49176 -0.00678
0.54659 -0.00430
0.60112 -0.00190

0.65469 0.00030
0.70664 0.00224
0.75634 0.00379
0.80313 0.00485
0.84635 0.00535
0.88534 0.00526
0.91942 0.00458
0.94797 0.00350
0.97054 0.00226
0.98684 0.00113
0.99670 0.00030
1.00000 -0.00000

SD7032-TTE.dat

1.0000	-0.0050
0.9988	-0.0048
0.9967	-0.0044
0.9929	-0.0041
0.9864	-0.0035
0.9784	-0.0028
0.9682	-0.0020
0.9562	-0.0012
0.9422	-0.0005
0.9263	0.0002
0.9087	0.0008
0.8894	0.0013
0.8686	0.0015
0.8461	0.0016
0.8224	0.0015
0.7972	0.0012
0.7709	0.0008
0.7435	0.0001
0.7151	-0.0007
0.6859	-0.0015
0.6560	-0.0026
0.6252	-0.0038
0.5942	-0.0050
0.5627	-0.0063
0.5310	-0.0076
0.4993	-0.0089
0.4674	-0.0103
0.4359	-0.0116
0.4045	-0.0128
0.3737	-0.0140
0.3435	-0.0151
0.3137	-0.0162
0.2849	-0.0171
0.2573	-0.0180
0.2301	-0.0187
0.2045	-0.0193
0.1800	-0.0197
0.1567	-0.0199
0.1349	-0.0199
0.1147	-0.0197
0.0957	-0.0193
0.0786	-0.0186
0.0629	-0.0177
0.0489	-0.0165
0.0367	-0.0150
0.0260	-0.0133
0.0168	-0.0113
0.0090	-0.0089
0.0033	-0.0060

0.0007	-0.0022
0.0000	0.0000
0.0007	0.0023
0.0033	0.0065
0.0090	0.0109
0.0168	0.0166
0.0260	0.0233
0.0367	0.0303
0.0489	0.0374
0.0629	0.0443
0.0786	0.0509
0.0957	0.0571
0.1147	0.0628
0.1349	0.0679
0.1567	0.0725
0.1800	0.0765
0.2045	0.0798
0.2301	0.0825
0.2573	0.0846
0.2849	0.0860
0.3137	0.0868
0.3435	0.0871
0.3737	0.0868
0.4045	0.0860
0.4359	0.0846
0.4674	0.0828
0.4993	0.0806
0.5310	0.0779
0.5627	0.0749
0.5942	0.0716
0.6252	0.0679
0.6560	0.0641
0.6859	0.0600
0.7151	0.0557
0.7435	0.0513
0.7709	0.0468
0.7972	0.0422
0.8224	0.0377
0.8461	0.0333
0.8686	0.0290
0.8894	0.0249
0.9087	0.0211
0.9263	0.0177
0.9422	0.0149
0.9562	0.0124
0.9682	0.0102
0.9784	0.0083
0.9864	0.0068
0.9929	0.0058
0.9967	0.0052
1.0000	0.005

APPENDIX C: VACUUM INFUSION OF CARBON-FIBER REINFORCED THERMOSET LAMINA

Process: Vacuum-bagging infusion

Matrix: DEREKANE 8084 Epoxy Vinyl Ester Resin

Reinforcement: Single Layer 3K Plain Weave Carbon Fiber Fabric

Fabrication of single layer carbon fiber composite laminas were conducted through a vacuum-bagging infusion process using a matrix of DEREKANE 8084 Epoxy Vinyl Ester Resin. The process included:

- Gel tests were performed to determine a mixture of Resin, Styrene, Cobalt, DMA, and Trigonox to achieve a 40 minute gel time.
- Prepping high-density foam mold surface by cleaning with acetone, then coating and polishing with three layers of Partall Paste #2.
- Carbon fiber sheets cut to correct size using template, and positioned using a light layer of spray adhesive to hold fabric to complex contours.
- Layer of peel-ply placed over fabric, overlapping by at least 1 inch on each side.
- Flow media was cut and overlapped with the feedline to allow increased flow from feedline into the part, terminating 0.5 inches from the opposite edge of the part.
- Spiral wrap feedlines were placed on either side of the part, stretching the whole length with a t-connector placed in each line near the max chord location.
- A line of butyl tape was applied along the edge of the mold with the top layer of tape left on, with pleats affixed at each corner and where the lines were to enter the bag.
- The vacuum bag was cut, dimensions calculated from mold and pleat dimensions.
- The vacuum bag was placed over the part, starting in one corner and working along the edge attaching it to the butyl tape and over the vacuum and feed line t's.
- The vacuum line was attached and sealed with butyl to the t, the other end was attached to a catch-pot which was attached to a vacuum pump. A line for the feed was attached and clamped.
- Vacuum was pulled to 30 in of Hg, and leaks were found and sealed with the assistance of a sound amplifier. Drop tests were performed until satisfactory results, and part was held under pressure for at least 2 hours.
- 2 kg of Resin was promoted in a 2 gallon bucket and placed in a water bath below the table level. Feed line was cut to the correct length.

- Catalyst was added to the resin mixture and stirred for 2 minutes. The feed line was then inserted into the resin bucket and clamped in place. The line was then unclamped and resin was allowed to flow into the part.
- The part was monitored for leaks and gel time was noted. The part was left to cure under vacuum for 12 hours.
- The part was then taken from the mold and trimmed. Assembly of the full blade followed.

APPENDIX D: TENSILE TESTING OF CARBON-FIBER REINFORCED THERMOSET LAMINA

INTRODUCTION

As part of research conducted to design a 1:70 scale 15MW floating turbine, one layer carbon fiber blade skins were manufactured using a vacuum-bagging infusion process at the Advanced Structures and Composites Center. Specimens were cut from one of the parts using a CNC Waterjet and were tested in tension in accordance with ASTM D3039. The part was infused on March 4th, 2021, and the tests were conducted by Amber Parker on December 3rd, 2021, in the Mechanical Engineering Technology Solid Mechanics Laboratory. The lab environment was at 40% humidity, and 69 degrees F. The test frame used was an MTS Criterion 43.50 test frame using a 50 kN load cell at a rate of 0.05 in/min. The properties that were computed included tensile strength, tensile modulus, and Poisson's ratio. In addition to the standard's requirements, stress vs. strain was plotted for each test, as well as force vs. load head deflection. Calculated properties using the rule of mixtures were compared with properties found through the tension testing.

MANUFACTURING OF COMPOSITE

The carbon fiber lamina consisted of one layer of 3K plain weave carbon fiber fabric infused with a matrix of Derakane 8084 epoxy vinyl ester resin as seen in Figure D.1. The pertinent manufacturer's material properties are displayed in Table D.1 and Table D.2. Additionally, the value used for fiber density was 0.00175 g/mm³.

Table D.1: 3K Plain Weave Carbon Fiber Fabric Properties. Source: “3K, plain weave carbon fiber fabric,” Fibre Glast, 2020. [Online]. [Accessed: 2021].

Fabric Property	Published Value
Areal Density (g/cm²)	0.0193
Tensile Strength (MPa)	4300
Tensile Modulus (GPa)	234

Table D.2: Derakane 8084 Epoxy Vinyl Ester Resin Properties. Source: “DERAKANE 8084 Epoxy Vinyl Ester Resin TDS,” Freeman Mfg. & Supply Co., 2006. [Online]. [Accessed: 2021].

Matrix Properties	Published Value
Density (g/cm³)	1.14
Tensile Strength (MPa)	76
Tensile Modulus (GPa)	2.90

The gel time of the resin was determined through a series of gel tests using an automated agitator that stopped when the resin had largely gelled. From those results, we determined the mixture ratios for the additives based on the resin mass were 5% Styrene, 0.3% Cobalt, 0.2% DMA for the promoting chemicals, and a catalyst of 1.25% Trigonox for a predicted gel time of 42 minutes.



Figure D.1 Partial Blade Infusion

High-density foam molds were machined to give the desired contours of the wind blade. These molds were prepped by buffing with three layers of Partall Paste #2. The carbon fiber sheets were cut and

lightly tacked in place in the mold by 3M Spray 77. Next, a layer of peel ply was used to cover the fabric, followed by flow media. Spiral tubing was inserted on either side of the part area, one for resin and the other for vacuum. Butyl tape was placed along the perimeter of the mold with pleats placed where the bag had to conform to changes in geometry. The vacuum bag was taped in place, the resin and vacuum lines were attached, and a drop test was performed at 30 in of Hg to look for leaks. Vacuum was then held on the part to consolidate for 2 hours.

Next, approximately 2 grams of resin was promoted in a 2-gallon bucket using the ratios stated previously. The catalyst was then added and mixed for 2 minutes. The feedline was then inserted into the bucket and unclamped, allowing the resin to flow into the part. The gel time was noted at 45 minutes, then left to cure under vacuum for 12 hours. The part was then removed from the mold and trimmed. The part was then treated in an oven at 80 degrees C for 30 minutes.

Eight specimens were then cut from the flat portion of the part as shown in Figure D.2.



Figure D.2 Portions of part cut on waterjet for eight specimens

CALCULATED PROPERTIES

The specimen dimensions were measured in multiple places using Mitutoyo Micrometers of 152 mm length. The average specimen properties are reported in Table D.3. Length of the specimens were measured with a metric ruler due to the length limitation of the calipers. All the lengths came out to 177.8 mm within the closest 0.1 mm.

Table D.3: Measured tension specimen properties

Specimen	Average Width (mm)	CV	Average Thickness (mm)	CV	Length (mm)	Mass (g)
T1	18.76	0.09%	0.40	2.04%	177.8	1.61
T2	18.75	0.03%	0.40	2.41%	177.8	1.57
T3	18.76	0.12%	0.40	2.04%	177.8	1.56
T4	18.73	0.13%	0.41	4.28%	177.8	1.55
T5	18.73	0.05%	0.40	1.26%	177.8	1.52
T6	18.72	0.07%	0.39	0.00%	177.8	1.50
T7	18.73	0.05%	0.39	0.00%	177.8	1.49
T8	18.74	0.37%	0.39	3.25%	177.8	1.46
Average	18.74	0.15%	0.40	2.55%	177.8	1.53

From the dimensional values, an average aerial value was calculated, and the predicted fabric weight was calculated by multiplying that value by the published aerial density, resulting in an estimate of 0.643 grams. The average total weight is 1.532 grams, meaning that the estimated resin weight is 0.889 grams. Calculations were done to find the fiber volume fraction (FVF) using the published fiber and resin densities as well as the predicted partial weights, resulting in a value of 32%. The FVF was used in the implementation of the Rule of Mixtures to find the predicted lamina properties from the combined matrix and fiber properties. Those predicted properties are shown in Table D.4.

Table D.4: Calculate predicted lamina properties

Lamina Property	Predicted Value
Tensile Strength (MPa)	1430
Tensile Modulus (GPa)	77.1
Failure Load (kN)	10.6

These values were thought to be very high for an estimate. A hypothesis as to why this discrepancy is present is that it comes from the published fabric properties, resulting in a higher predicted fiber strength than what the actual strength is.

TENSILE TESTING

The specimens were painted with a Digital Image Correlation (DIC) pattern approximately in the center portion of each specimen spanning 4 inches. A data acquisition system was used to collect crosshead displacement and load applied data at 10 Hz. Additionally, the DIC system was employed using a vertical bank of two 2.3 Megapixel Basler cameras with 16 mm Schneider-Kreuznach lenses positioned at positive and negative 20 degrees from the test specimen, collected photos as well as the corresponding applied load value at 2 Hz. The test setup can be seen in Figure D.3 below.



Figure D.3 Tension test setup on the MTS test frame with DIC

Post-processing of the DIC data was done using ARAMIS. Average strain values were computed using a rectangular area in the center of the surveyed area as seen in Figure D.4.

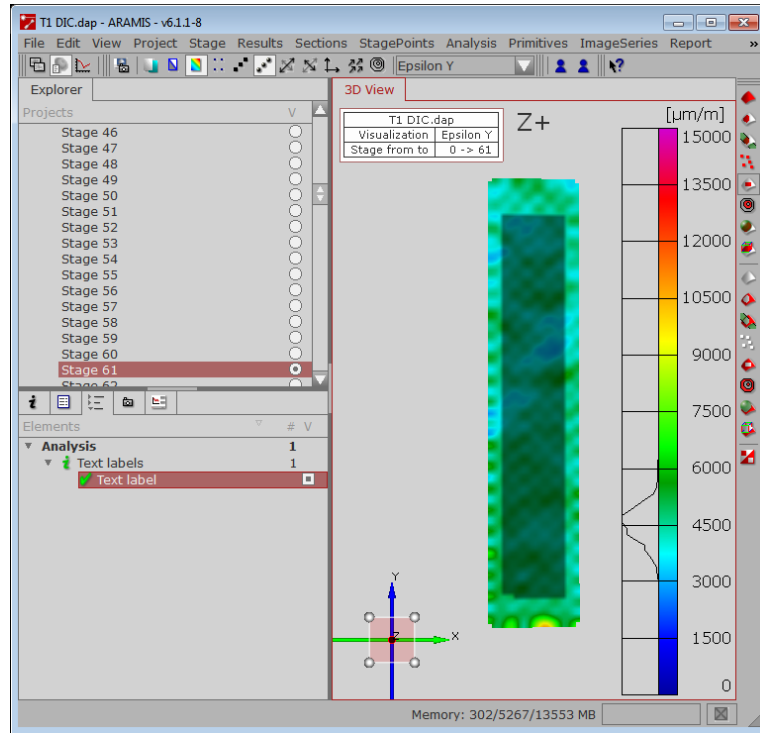


Figure D.4 ARAMIS data processing for longitudinal and lateral strain

The plot of force vs. load-head deflection for all specimens can be seen in Figure D.5. Stress and strain were calculated according to the standard and are shown for the longitudinal direction in Figure D.6, and lateral direction in Figure D.7. Values of strain could not be computed for T1 because the force readings were not saved in the DIC DAQ.

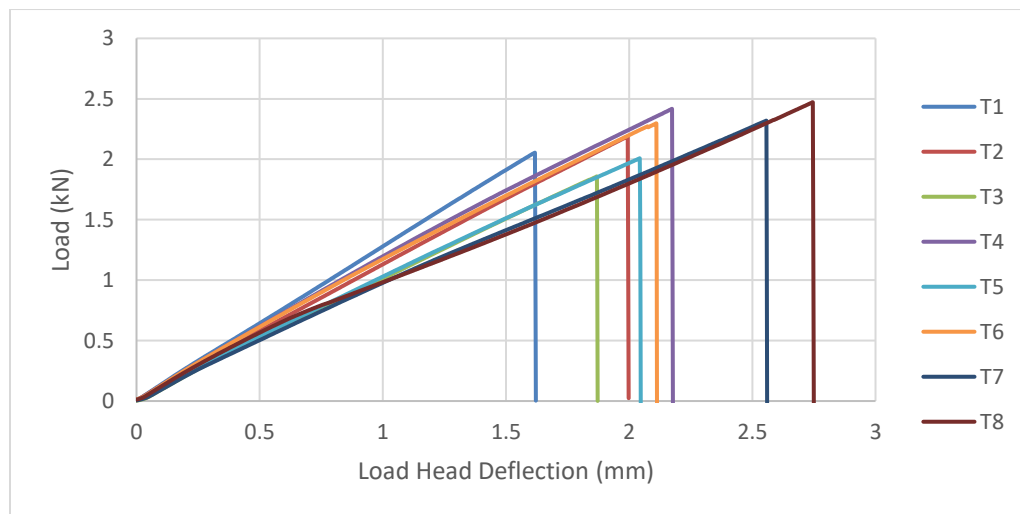


Figure D.5 Force applied to specimen vs. load-head deflection for both tension specimens

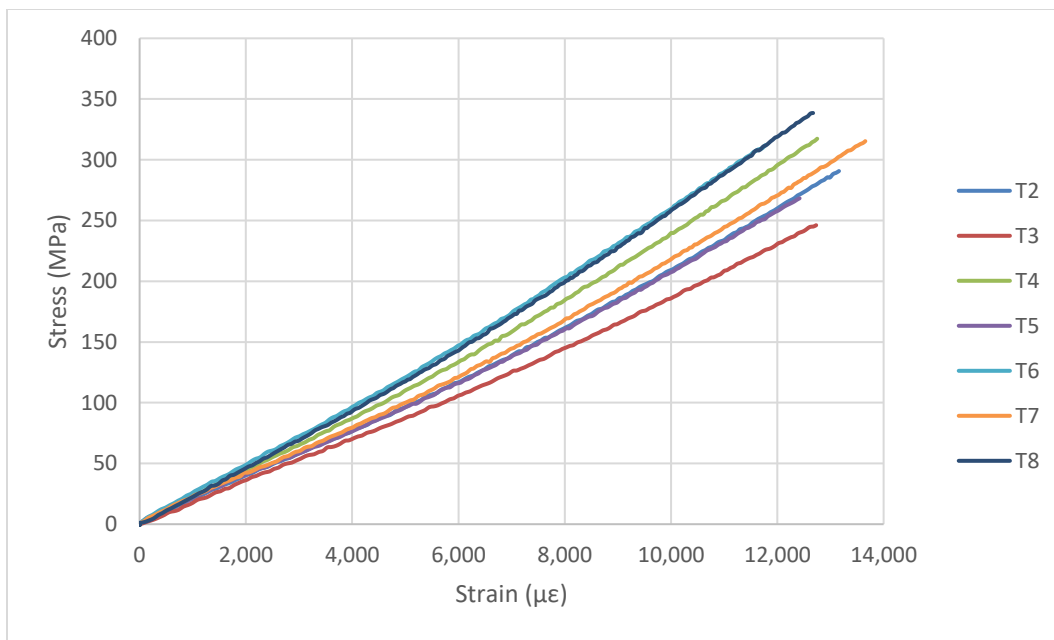


Figure D.6 Stress vs. strain in the longitudinal direction over range of data collection

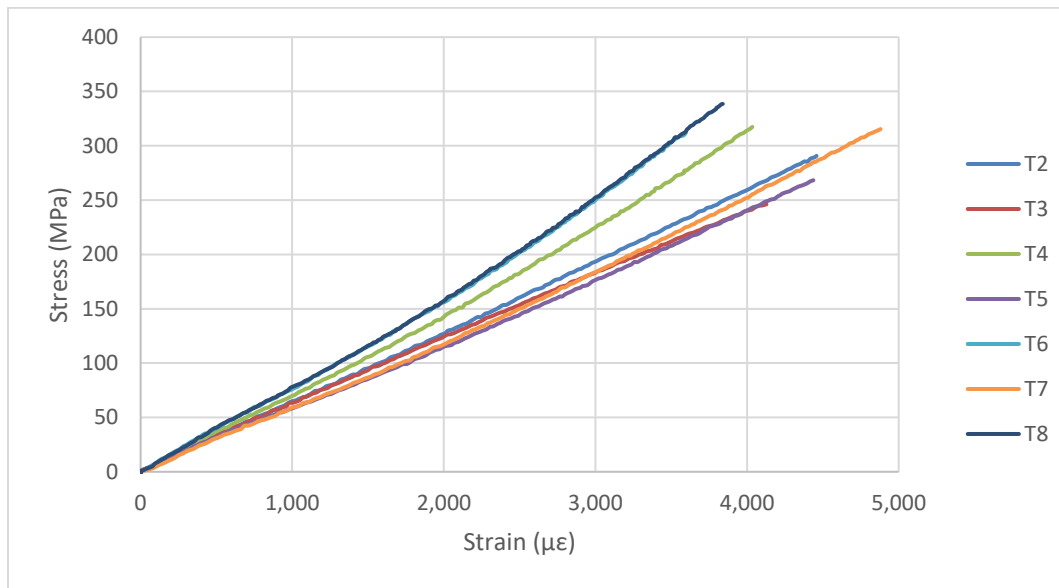


Figure D.7 Stress vs. strain in the lateral direction over range of data collection

The tensile modulus, tensile strength, and Poisson's ratio were calculated for each value. The range of strain used to calculate the modulus was as close as possible to 1000-3000 $\mu\epsilon$ in the longitudinal direction. The actual ranges of the strain used are shown in Table D.5. The tensile strength was computed using the maximum load, which corresponded with the failure load. The failure load, tensile modulus, tensile strength, and Poisson's ratio are reported in Table D.6.

Table D.5: Actual strain values used for calculations

	Lower Strain ($\mu\epsilon$)	Upper Strain ($\mu\epsilon$)
T1	1016	3038
T2	1026	2990
T3	999.7	3031
T4	1033	3041
T5	1048	2985
T6	1039	3003
T7	1021	3018
T8	1045	3054

Table D.6: Tensile Modulus, Tensile Strength and Poisson's Ratio for all specimens

	Failure Load (kN)	Tensile Strength (MPa)	Tensile modulus (GPa)	Poisson's Ratio
T1	2.05	273	n/a	-0.315
T2	2.19	292	18.9	-0.299
T3	1.86	247	17.9	-0.292
T4	2.41	317	21.1	-0.310
T5	2.01	269	17.7	-0.330
T6	2.30	313	23.0	-0.314
T7	2.32	317	18.4	-0.332
T8	2.47	339	23.3	-0.302
Average	2.20	296	20.1	-0.312
CV	9.70%	10.4%	11.9%	4.51%

All specimens had failures that occurred outside the grip area. The tension specimen failure modes were determined from the photos in Figure D.8. Table D.7 provides the failure modes for each test specimen.

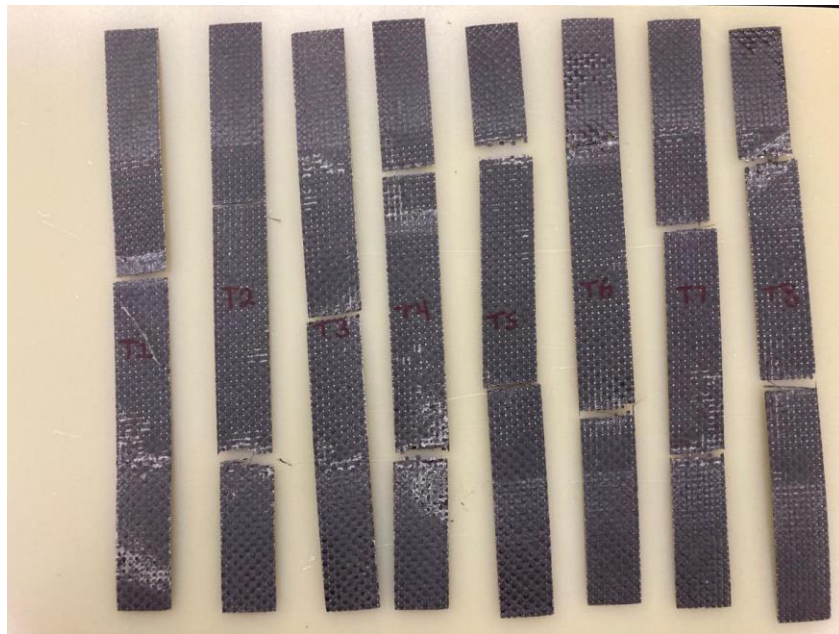


Figure D.8: Tension specimen failure modes

Table D.7: Failure modes of each test specimen

Specimen	T1	T2	T3	T4	T5	T6	T7	T8
Mode	LGM	LGV	LGM	LGV	LGV	LGV	LGV	LGV

COMPARISON

The data collected from the tensile testing as compared to the calculated response of the lamina differ by a sizable margin. The predicted lamina failure load was 10.6 kN, as opposed to the actual failure load of 2.20 kN. The predicted failure load is 382% higher than that of the experimental value. The predicted tensile strength was 1430 MPa whereas the actual tensile strength was 296 MPa. The predicted tensile strength is 383% higher than that of the experimental value. The predicted tensile modulus was 77.1 GPa whereas the actual tensile modulus was 20.1 GPa. The predicted tensile modulus is 284% higher than that of the experimental value. As discussed previously, the discrepancy seen in the predicted vs. experimental data may be due to the published fabric strength and modulus properties. If those were high, then the predicted lamina properties would be high as well.

APPENDIX E: BLADE INERTIAL CALCULATIONS

Blade_Inertia_Calculations.m

```
%Inertia Calculations
```

```
%FOCAL
```

```
%Amber Parker
```

```
%7-8-2021
```

```
clear
```

```
clc
```

```
%Length measurements in m
```

```
%Mass measurements in kg
```

Read Data for Hub and Know Hanging Mass

```
struct = TDMS_getStruct('Fixture/Fixture1_21_07_29_16_07_02.tdms',3);
```

```
Time = struct.Raw_Data.time__s__.data;
```

```
Data = struct.Raw_Data.Voltage__V__.data;
```

```
DataLength = length(Data);
```

```
Time = Time(1:DataLength);
```

```
Tinitial=Time(1);
```

```
Time=Time-Tinitial;
```

Log Decrement

```
start = 850;
```

```
stop = start+2000;
```

```
DataUsed = Data(start:stop);
```

```
avg = mean(DataUsed);
```

```
DemeanedData = Data - avg;
```

```
DemeanedDataTrim = DemeanedData(start:stop);
```

```
TimeTrim = Time(start:stop);
```

```
[P,T] = Peaks(DemeanedDataTrim,TimeTrim);
```

```
Period = mean(diff(T));
```

```
freq = 1/Period;
```

```
s=3; e=[4 6 8 10 12 14 16 18 20];
```

```
el = length(e);
```

```

for k=1:e1
Dec(k) =(1/(e(k)-s))*log(P(s)/P(e(k)));
Damp(k) =1/sqrt(1+((2*pi())/Dec(k))^2);
end

```

```
DampRatio = mean(Damp);
```

Natural Frequency

```

wd = (2*pi())/Period;
wn = wd/sqrt(1-(DampRatio^2));

```

Setup Values

```

l2 = 0.034; %distance from shaft center to mounting plate face
l1 = l2+0.1344; %distance from shaft center to hanging mass center
l3 = l2+0.0695; %distance from shaft center to hanger mass center

```

```
g = 9.81; %gravity m/s^2
```

```

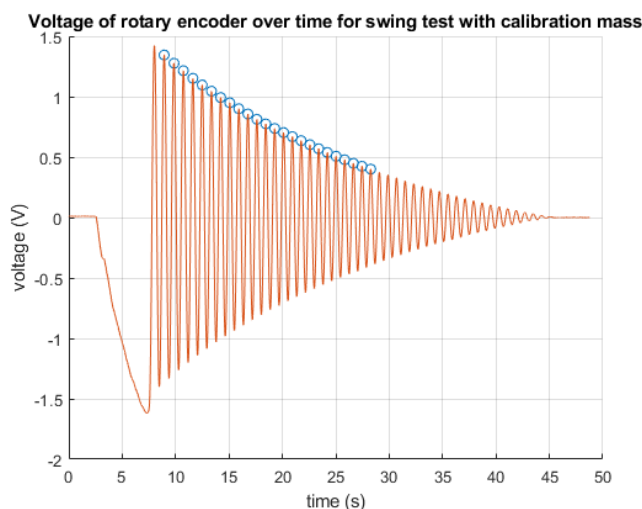
m1 = 0.06965; %hanging mass in kg
m2 = 0.00605; %mass of hanger in kg

```

```

figure
scatter(T,P)
hold on
plot(Time, DemeanedData)
grid on
title('Voltage of rotary encoder over time for swing test with calibration mass')
xlabel('time (s)')
ylabel('voltage (V)')

```



Inertia Calculation of Hub

```
Ic = (((m1+m2)*l1^2)/(wn^2))-((m1+m2)*(l1^2));
```

Read Data for Hub and Blade ***

```
struct = TDMS_getStruct('Blade1/Blade1Test1_21_07_29_16_19_05.tdms',3);
```

```
TimeB = struct.Raw_Data.time__s_.data;
```

```
DataB = struct.Raw_Data.Voltage__V_.data;
```

```
DataLength = length(DataB);
```

```
TimeB = TimeB(1:DataLength);
```

```
TinitialB=TimeB(1);
```

```
TimeB=TimeB-TinitialB;
```

Log Decrement

```
start = 1000;
```

```
stop = start+6000;
```

```
DataUsedB = DataB(start:stop);
```

```
avgB = mean(DataUsedB);
```

```
DemeanedDataB = DataB - avgB;
```

```
DemeanedDataTrimB = DemeanedDataB(start:stop);
```

```
TimeTrimB = TimeB(start:stop);
```

```
[PB,TB] = Peaksfine(DemeanedDataTrimB,TimeTrimB);
```

```
PeriodB = mean(diff(TB));
```

```
freqB = 1/PeriodB;
```

```
s=2; e=[3 5 8 10 12 14 16 18 20];
```

```
el = length(e);
```

```
for k=1:el
```

```
DecB(k) =(1/(e(k)-s))*log(PB(s)/PB(e(k)));
```

```
DampB(k)=1/sqrt(1+((2*pi())/DecB(k))^2);
```

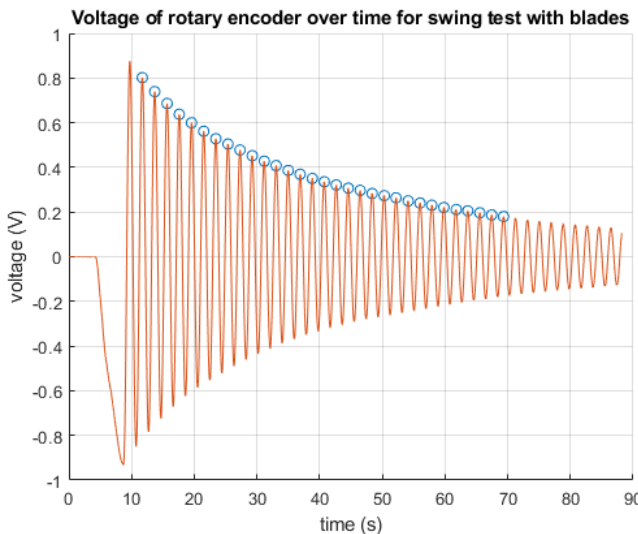
```
end
```

```
DampRatioB = mean(DampB);
```

```

figure
scatter(TB,PB)
hold on
plot(TimeB, DemeanedDataB)
grid on
title('Voltage of rotary encoder over time for swing test with blades')
xlabel('time (s)')
ylabel('voltage (V)')

```



Natural Frequency

```

wdB = (2*pi())/PeriodB;
wnB = wdB/sqrt(1-(DampRatioB^2));

```

Setup Values

```

l4 = l2+0.537; %distance from shaft center to blade CG
l5 = 0.0792; %hub radius
l6 = l5 + 0.537; %distance from shaft center to blade CG

```

$m_B = 0.2364$; %Mass of blade

Inertia Calculation of Blade

$I_g = ((m_B * g * l4) / (w_n B^2)) - (I_c + m_B * (l4^2))$; %About cg

$I_r = I_g + m_B * ((l4 - l2)^2)$; %Parallel Axis about root of blade

$I_s = I_g + m_B * ((l6)^2)$; %Parallel Axis about shaft center

```

function [p,t] = Peaks(data,time)
%Peaks: Finds peaks in a sine function and corresponding data point
% data = Voltage (v)
% time = Time (s)
[P,T] = findpeaks(data,time,'MinPeakDistance',0.5);
n = length(data);
na = length(T);
a=1;

for i=1:n-1
    if a<=na
        if time(i)==T(a)
            p(a)=data(i);
            t(a)=time(i);
            a=a+1;
        end
    end
end
end

```

```

function [p,t] = Peaksfine(data,time)
%Peaksfine: Finds peaks in a sine function and corresponding data point
% data = Voltage (v)
% time = Time (s)
[P,T] = findpeaks(data,time,'MinPeakDistance',1.5);
%Differs from Peaks by spacing value input into findpeaks
n = length(data);
na = length(T);
a=1;

for i=1:n-1
    if a<=na
        if time(i)==T(a)
            p(a)=data(i);
            t(a)=time(i);
            a=a+1;
        end
    end
end
end

```

APPENDIX F: BLADE SCAN PROCEDURE

FOCAL Partnering with the AMC

Equipment: Quantum m FARO arm

Original procedure tested on 2/7/22

Fixturing: A fixture was machined by the AMC to align the turbine blade with the 0-90 degree axis of the blade, corresponding to the flat outer faces. As seen in the Figure F.1.

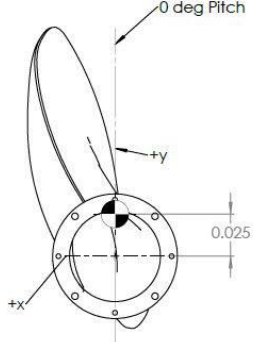


Figure F.1: Blade Alignment

Mounting: The blade was mounted with the front of the blade facing away from the TV and the trailing edge pointing away from the FARO arm, as shown in Figure F.2. Two M4 dowel pins were inserted for positioning, and the blade was bolted down with four M2.5 screws.



Figure F.2: Blade Mounting

Datums: The point indicator was used on the FARO arm to indicate the surface of the cylindrical part of the blade flange at six points using a cylindrical setting. Next, the top surface of the mounting block was

indicated using four points using the planar setting. The outer circle of the flange where it contacts the mounting block upper face was indicated at four points using the circular setting. The front-most positioning pin was then indicated with four points to locate the dowel hole using the hole setting. These four datums were then combined to locate the coordinate system on the mounting surface with the origin at the center of the cylindrical flange. The coordinate system was as shown in the photo above, with the +x axis towards the tv on the wall, the +z axis pointing towards the FARO arm, and the +y axis following the axis of rotation of the blade pointing towards the ceiling.

Surface Scan: The FARO arm was then set to use the laser scanner. The surface scan setting was used to scan first the front of the blade from ~ 6 inches away, being careful not to vibrate the blade while scanning. Kyle stood on a ladder to reach the tip of the blade, being careful that all of the joints of the arm were within their operational limits. After the front side, the backside was scanned using the same method, seen in Figure F.3. The screen was monitored in order to make sure that there were no gaps in the scanned surface and that the scan was completed as close to the leading and trailing edges as possible.

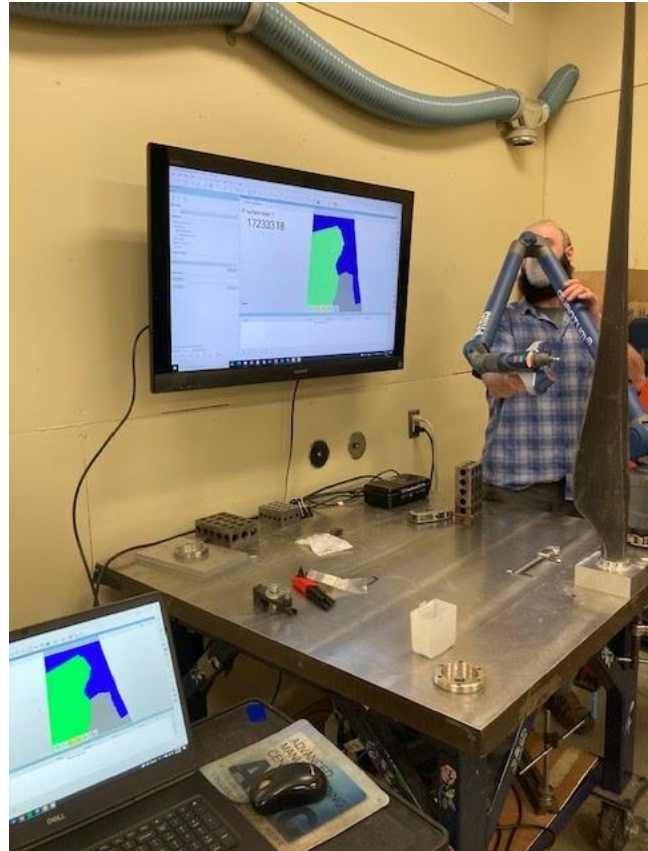


Figure F.3: Scanning of Blade

Comparison: After the scan was complete, the dataset was saved as a surface and was generated in relation to the coordinate system previously established. The scan is predicted to be accurate to within 0.01 inches and can pick up the roughness of the surface. The first comparison was made by comparing

the location of the SolidWorks model blade surface to that of the scanned surface in 3D space. This gave offset values for the front surface in relation to the scan, and the back surface in relation to the scan. The data can also show if there is any excess twist present in the blade.

Note: for blade 7, there was an overall tip offset in the +x direction, so a comparison of the back surface showed a + difference, and the front surface comparison resulted in a - difference.

A second scan comparison was made in comparing the form or shape of the SolidWorks model as compared to the scan. This was to show deviation in airfoil shape due to assembly. This was done by using the surface match feature that superimposes the scan surface onto the SolidWorks model with the goal of creating the closest match possible. This shows areas that are stretched due to spars, or warped due to assembly or infusion.

Report: A report was generated of both surface comparisons for both the front and back of the blade for each. The deviation near the tip was called out for each graph, and the color gradient is shown for the surface with the corresponding values provided. The point cloud data of the surface scan was also obtained to be processed in Matlab to pull out airfoil slices and compare them with the SolidWorks geometry.

APPENDIX G: FIGURE REPUBLICATION PERMISSIONS

4/13/2022

Amber Parker

University of Maine Advanced Structures and Composites Center

Dear Christopher Allen: I am completing a Master's Thesis at the University of Maine entitled "DEVELOPMENT AND TESTING OF A 1:70 SCALE MODEL WIND TURBINE OF THE IEA REFERENCE 15 MW FLOATING OFFSHORE SYSTEM." I would like your permission to reprint in my thesis a figure from the following: Allen, C., et. al. 2020 Definition of the UMaine VolturnUS-S reference platform developed for the IEA Wind 15-megawatt offshore reference wind turbine, National Renewable Energy Lab. (No. NREL/TP-5000-76773)



The figure to be reproduced is:

The requested permission extends to any future revisions and editions of my thesis. These rights will in no way restrict republication of the material in any other form by you or by others authorized by you. Your signing of this letter will also confirm that you own the copyright to the above- described material.

If these arrangements meet with your approval, please sign this letter where indicated below and return a scanned copy to me by email. Thank you very much.

Sincerely,

Amber Parker

Amber F. D. Parker

PERMISSION GRANTED FOR THE USE REQUESTED ABOVE:

Christopher Allen  Digitally signed by Christopher Allen
DN: cn=Christopher Allen, o=University of Maine,
ou=Advanced Structures and Composites Center,
email=christopher.allen@maine.edu, c=US
Date: 2022.04.13 13:04:27 -04'00'

Christopher Allen

Date: 4/13/2022

BIOGRAPHY OF THE AUTHOR

Amber Frances Delaney Parker was raised in Livermore, Maine where she lived with her parents Richard and Sarah Delaney. She attended school at Spruce Mountain in Jay, Maine where she discovered the field of engineering through FIRST Robotics, and renewable energy through advanced studies in environmental science.

After graduating from Spruce Mountain High School in 2016 as class salutatorian, Amber attended the University of Maine where she pursued a Bachelor of Science degree in Mechanical Engineering with a minor in Ecology and Environmental Science. In May 2020, Amber completed her Bachelor's degree and minor with summacum laude honors.

Amber worked as an undergraduate research assistant for Dr. Justin Lapp in the UMaine Solar Thermal Energy Laboratory as well as at the UMaine Advanced Manufacturing Center. In addition to her academic pursuits, she also enjoys spending time with her family, outdoor activities, gardening, fiber arts, cooking, flying with her husband, and studying theology. She looks forward to where her professional and family life will take her in the future. Amber is a candidate for the Master of Science degree in Mechanical Engineering with concentrations in Offshore Wind Energy and Aerospace from the University of Maine in May 2022.